

Bentonite Re-saturation – limited Access to Water and high Temperature Gradients

Supported by:



Federal Ministry
for Economic Affairs
and Energy

on the basis of a decision
by the German Bundestag

Bentonite Re-saturation – limited Access to Water and high Temperature Gradients

Klaus-Peter Kröhn

August 2019

Remark:

This R&D report was prepared under reference No. 02E10548 and 02E11102 with the Federal Ministry of Economic Affairs and Energy (BMWi).

The work was conducted by the Gesellschaft für Anlagen- und Reaktorsicherheit (GRS) gGmbH.

The author is responsible for the content of the report.

Key-Words:

Bentonite buffer, Final repository, Temperature gradient, Water uptake

Acknowledgements

Funding of the two experiments “Re-saturation under limited access to water” and “Final state of re-saturation under a thermal gradient” within the projects WiGru-6 (FKZ 02 E 10548) and WiGru-7 (FKZ 02 E 111 02) by the German Federal Ministry for Economic Affairs and Energy (BMWi) is gratefully acknowledged. Many thanks are also due to the GRS Geotechnical Laboratory, particularly to Karsten Hellwald for his engagement in construction and running the tests within both experiments until his retirement, and to Bernd Zehle and Michael Kröhn for their skilful, creative and competent technical support later on, especially in devising the eventually successful set-up for the test under limited access to water.

Abstract

Two water uptake experiments with compacted MX-80 bentonite have been performed: an isothermal experiment with limited access of confined pre-compacted bentonite to water and a non-isothermal experiment aiming at the final state of hydration against a temperature gradient. In both cases, the experimental effort was quite high and quite a variety of different set-ups have been tried in order to achieve reasonable results. Since the key results have been published earlier¹ this report focusses more on the different test concepts which are explained in detail, and on the reasons why they failed. It proved to be unavoidable, though, to come up with more insight and understanding of the results while writing this work. One or two new aspects and conclusions are therefore reported here as well.

¹ /NOS 18/

Table of content

	Acknowledgements	I
	Abstract	II
1	Introduction	1
1.1	Motivation for the report	1
1.2	Experiment 1: limited access of bentonite to water	1
1.3	Experiment 2: final hydration state under a thermal gradient.....	2
2	Re-saturation under limited access to water	5
2.1	Thoughts on hydraulic interplay of rock and buffer	5
2.2	Impediment of flow by a natural low permeable material	10
2.2.1	Principle of the test	10
2.2.2	Materials	13
2.2.3	First tests	17
2.2.4	Test over 5 weeks.....	18
2.2.5	Test over 12 weeks.....	19
2.3	Impediment of flow by an artificial low permeable material.....	19
2.4	Re-saturation via a rising water table	20
2.4.1	Principle of the test	20
2.4.2	Technical requirements.....	21
2.4.3	Tests with one cell – part I	24
2.4.4	Tests with three cells.....	25
2.4.5	Tests with one cell – part II.....	26
2.5	Direct water injection.....	26
2.5.1	Principle of the test	26
2.5.2	One final problem.....	27
2.5.3	Test program	32
2.5.4	Modelling prerequisites	33
2.5.5	Results from varying the inflow rate	35
2.5.6	Results from varying the running time	38
3	Final state of re-saturation under a thermal gradient.....	45
3.1	Idea of the test	45

3.2	Expected evolution.....	45
3.3	Test set-up.....	46
3.4	Procedure	49
3.5	Characteristic values.....	50
3.6	Temperature distribution	52
3.7	Results.....	53
3.7.1	Dynamics of the water content distribution	53
3.7.2	Mean water content at end of test.....	61
3.7.3	Water uptake dynamics.....	62
3.7.4	Total water uptake	68
3.7.5	Dry density.....	70
3.7.6	Checking consistency of water uptake data	71
4	Conclusions and recommendations.....	75
4.1	Re-saturation under limited access to water.....	75
4.2	Final state of re-saturation under a thermal gradient	76
	References	79
	Table of figures.....	83
	List of tables.....	85
A	Appendix: Analysis of data	87
A.1	Measured data.....	87
A.2	Derived data	87
A.3	Compilation of derived dataFußn	91
B	Appendix: Revisiting data from earlier uptake experiments.....	93
B.1	Final porosity	93
B.2	Degree of saturation in the narrow zone of peak water content.....	96

1 Introduction

1.1 Motivation for the report

Two water uptake experiments with compacted MX-80 bentonite have been performed: an isothermal experiment with limited access of the bentonite to water and a non-isothermal experiment aiming at the final state of hydration against a temperature gradient. The first experiment began in autumn 2012, the second one even earlier in autumn 2008 and both were terminated in spring 2018. The results of both experiments are reported in short in /NOS 18/.

The technical challenges involved proved to be much higher than anticipated in both cases. Several conceptual approaches to these tests were tried but failed. They are described here in detail in order to document the problems that came with specific test designs. The present report thus represents an extended version of previously published results with focus on the description of the difficulties encountered during the respective tests.

As it turned out, writing about the experiments in greater detail provoked some new thoughts and some new interpretations of already existing data. These are of course reported here as well

1.2 Experiment 1: limited access of bentonite to water

The dynamics of water uptake in terms of the evolution of the water content distribution inside the bentonite have already been extensively tested in the laboratory e.g. /BÖR 84/, /KRÖ 04/, /FRA 17/. All these experiments have at least the potential to show the water uptake dynamics in great detail. However, they all allowed unimpeded access to water (UA) for the bentonite meaning that the water uptake rates are exclusively controlled by the ability of the bentonite to take up water.

Under in-situ conditions, by contrast, comparatively low flow from the rock can be found. In fact, a potential host rock for a nuclear waste repository qualifies for that purpose by showing as little water flow as possible. The related flow rates indicate that such a host rock will initially not provide as much water as the bentonite would take up under UA-

conditions /KRÖ 18/. The same applies to smaller fractures with comparatively low transmissivity. In this case a limited water supply rate (LWSR) can be envisaged. Detection of a detailed transient water content profile under in-situ conditions is not possible, though, due to the spatial requirements of the measuring equipment. The water uptake dynamics of a bentonite buffer under LWSR-conditions were thus not really known.

This knowledge gap was noticed while contributing to the Buffer-Rock Interaction Experiment (BRIE) /FRA 17/ at the Hard Rock Laboratory at Äspö in Sweden in the framework of the Task Force on Groundwater Flow and Transport of solutes (TF GWFTS) /VID 17/ as well as the Task Force on Engineered Barriers (TF EBS). As with comparable in-situ experiments where the uptake was monitored during the test, relative humidity could only be measured at three different positions over a distance of 15 cm in the radial direction.

Thus, a supplemental laboratory experiment was conceived at GRS. The intended purpose was to gain insight into the water uptake dynamics of pre-compacted and confined bentonite in the vicinity of the bentonite-rock contact that develop at a limited water supply.

1.3 Experiment 2: final hydration state under a thermal gradient

As of 2008, there had been several non-isothermal water uptake tests from which the steady-state conditions at the end of re-saturation could not clearly be derived. Characteristic for the state of knowledge at that time were the two laboratory experiments performed by CEA and by CIEMAT that were investigated in “Task 1 – Laboratory experiments”² in the framework of the TF EBS. The results from CEA indicated an even distribution of the water content at steady-state /GAT 05/. Unfortunately, the test was terminated before reaching these conditions. The test of CIEMAT did not show changes in the water content after a year, having seemingly reached steady-state. However, the water content showed a clear trend from full saturation in the bentonite at the cold end to an unsaturated state at the hot end /VIL 05/. Also, not entirely clear in this respect were the results from the running FEBEX mock-up test /SAN 06/.

² In 2008 “Task 1” was still called „Benchmark 1“

The established THM-models for re-saturation predict generally full saturation all over the bentonite at steady-state backed up by other experiment like the canister retrieval test /KRI 15/ which indeed showed full saturation in parts. This prediction, however, is inherent in the approach. Also, during development of the experimental code VIPER which is based on an entirely different set of physical assumptions than the THM-models /KRÖ 11/ this question had not been addressed. Other than the THM-models, though, the theoretical approach for VIPER suggested steady-state conditions with an uneven water content distribution as reported by CIEMAT. A laboratory experiment was thus devised to settle the question of the steady-state water content distribution after water uptake against a thermal gradient.

2 Re-saturation under limited access to water

2.1 Thoughts on hydraulic interplay of rock and buffer

After excavating a drift or drilling a borehole, the rock surface is exposed to the atmosphere. Evaporation enhanced by ventilation causes drying of the rock before the waste canisters and the buffer are installed. The moisture front retreats into the host rock so that evaporating water migrates by means of vapour diffusion from the water-air interface towards the rock wall before it reaches a drift or a borehole (see Fig. 2.1). The rate at which the moisture leaves the host rock is highest at the beginning. It decreases with time because resistance against vapour flow increases with distance between moisture front and rock wall.

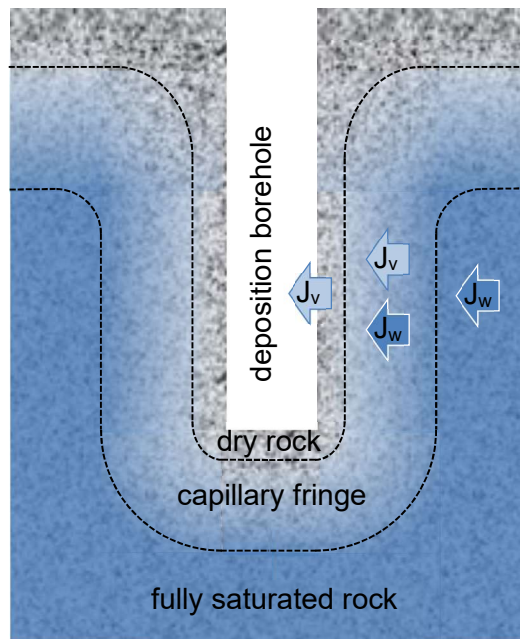


Fig. 2.1 Flow situation after drilling a deposition hole

The drying process is countered by groundwater flow which is driven by the hydraulic pressure in the water as well as by the capillary pressure at the water-air interface towards tunnel and borehole wall. The system thus converges towards a balance between advective water flow from the rock and evaporation at which the moisture front comes to a standstill. Where in the rock this happens depends considerably on the permeability. The transition between the completely dry and the completely water-saturated zone is a gradual one since the initially sharp moisture front is widened by capillary forces. The

thickness of this transition zone depends on the variability of the pore channel diameters.

In the following the buffer is assumed to consist of pre-compacted air-dry bentonite. Since waster canisters and buffer cannot be installed instantaneously some preceding drying of the rock must be expected. This condition is depicted Fig. 2.2. It is thus that the buffer will initially not be in contact with a fully water-saturated host rock. The rock is possibly only partially saturated or even completely dry. As a consequence, the initial phase of water uptake by the buffer can be a rather complex interplay of several processes.

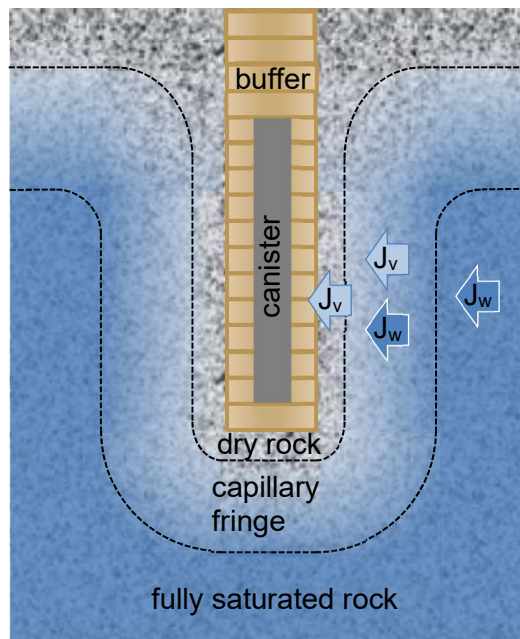


Fig. 2.2 Flow situation immediately after emplacement of canister and buffer

The bentonite buffer takes up liquid as well as vaporous water depending on what the pore channels in the partially saturated host rock provide at the buffer-rock interface. If the rock at the bentonite-rock contact zone was completely dry prior to the installation of the buffer, the initial water-uptake of the bentonite takes obviously place via vapour flow only. How long it takes the liquid water to reach the bentonite depends on the movement of the moisture front in the rock.

However, it is not clear in which direction the moisture front initially migrates after buffer installation. The vapour is still provided by evaporation at the moisture front, as men-

tioned above, but it is not clear if the vapour uptake rate of the buffer exceeds the vapour flow rate at the preceding drying conditions. In the long run, though, the ability of the buffer to draw water from the rock decreases with the increasing water content at the bentonite-rock contact. Eventually the rock here will thus be fully water saturated again.

If the rock was partially saturated at the buffer-rock interface, some of the pore channels are filled with water so that this water comes into direct contact with the bentonite. The water is then drawn into the buffer by suction. Data from /VID 17/ let expect an initial suction in the order of 100 MPa. According to /VID 17/ the only retention curve for granitic rock that is based on measurements stems from /FIN 95/. Later also data from /FRA 17/ became available. They indicate that such a capillary pressure in the rock can be reached only for very low degrees of saturation³. However, the uncertainty in the retention curve in this range is rather high and the curve itself might look different for other crystalline rocks /KRÖ 17/. It is therefore conceivable that this capillary pressure is not reached in the rock at all.

However, high suction on a partially filled flow channel might simply draw laterally air from larger pores with larger pore throats and thus lower capillary forces as schematically depicted in Fig. 2.3. In case of a more or less fully saturated rock, the suction might exert tensile stresses on the groundwater to the extent that the pore pressure falls below the saturated vapour pressure which would interrupt the flow towards the buffer (see Fig. 2.4). In both cases, liquid-water flow across the bentonite-rock interface might therefore become intermittent because groundwater flow needs to replenish the volume of water that has been either quickly sucked up (partially water-filled flow channels) or instantaneously filled with vapour (fully saturated case). In the meantime, uptake of vapour would continue, though.

Subsequent water-uptake by the bentonite becomes continuously slower because the increasing water content in the bentonite at the buffer-rock interface lowers the suction. The periods of water-drawing thus lengthen, the interruptions become shorter.

³ This means also that liquid water reaches the buffer via small pore channels first.

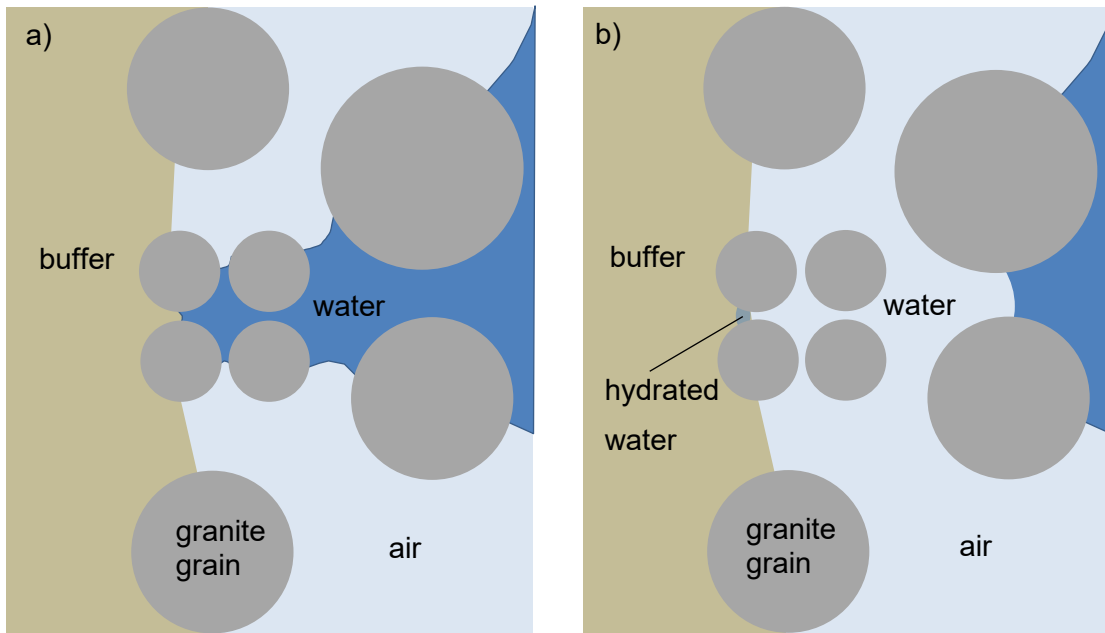


Fig. 2.3 Water reaching the buffer; a) moment of contact, b) shortly afterwards

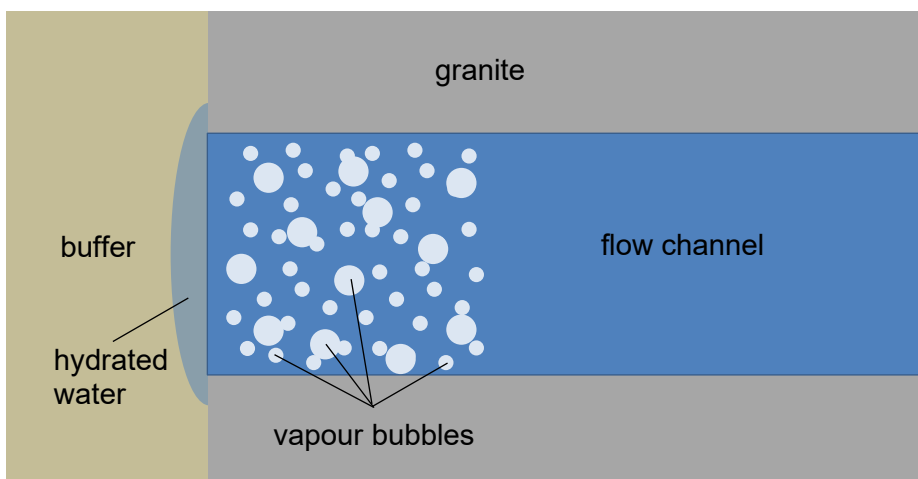


Fig. 2.4 Water in a fully saturated granite under extremely low pressure

During phases without uptake of liquid water, hydrated water in the buffer is still subject to moisture-redistribution. This redistribution tends to equalize the water content in the buffer. Consequently, the water content in the bentonite at the buffer-rock interface is lowered by this process. However, the bentonite can still take up vaporous water. Uptake experiments with vapour-saturated air have shown that compacted bentonite can quickly take up comparatively large amounts of water. After 4 days in an uptake test with vapour the water content had risen from 10 % up to 17 % at the inflow side while an increased water content could be detected up to a depth of 3 cm into the sample /KRÖ 04/. Since

vapour flow has also to be expected in the rock under partially saturated conditions this process would counteract the lowering of the water content in the buffer due to moisture redistribution.

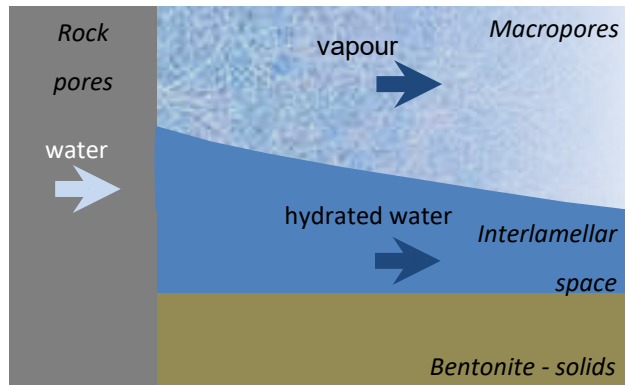


Fig. 2.5 Water re-distribution in the buffer at a limited water supply rate

After a certain period of time – if not instantaneously – the water uptake will become continuous. But the flow rate might not be high enough to meet the demand of the bentonite so that the water supply for the bentonite would still have to be called restricted. In this situation the processes of water-uptake and moisture redistribution have an opposed effect on the water content at the inlet. As a result, it is expected that the water content in the bentonite close to the buffer-rock interface does not rise as fast as under unlimited water supply.

Due to the continuous decrease in suction caused by the increasing water content the situation changes once more when the rock begins to provide potentially more water than the bentonite is able to take up. The bentonite experiences no restrictions in the water supply anymore and the buffer starts to act as an increasingly effective obstacle to the water flow from the rock.

What these considerations basically add up to is that under the expected repository conditions, the buffer will have a restricted water supply during a first phase of re-saturation. This is not the situation that has been tested in the laboratory time and again where always more water was available for re-saturation than was required by the bentonite. Moreover, the phase of restricted water supply is physically a rather complex one. It thus appears to be advisable to investigate the uptake behaviour of the compacted bentonite

under restricted water supply to improve predictions about buffer re-saturation as well as to test the present conceptual understanding of the processes involved.

At the Hard Rock Laboratory at Äspö this phenomenon has been investigated in-situ in the framework of the Buffer-Rock Interaction Experiment (BRIE) where a test borehole of about 3 m depth and a diameter of 30 cm has been filled with bentonite. The borehole was instrumented with several humidity sensors but for technical reasons they were placed only at three different positions in the radial direction.

Since the details of the water content dynamics under LWSR-conditions had been unknown at that time, a re-saturation experiment supplementing the BRIE in this respect has been proposed in the beginning of 2012 and was granted in August 2012 in the framework of the project WiGru-7 /NOS 18/. The initially proposed experimental set-up, however, proved not be appropriate, calling for alternatives. The different attempts, the related work and the outcome of all these tests are described in the following subsections.

2.2 Impediment of flow by a natural low permeable material

2.2.1 Principle of the test

A one-dimensional test set-up similar to earlier water uptake experiments (/KRÖ 04/) was chosen. MX-80 bentonite was compacted in a cylindrical steel cell in layers of about 1 cm thickness to a density of about 1450 kg/m³ (air dry material) in order to provide a maximum of homogeneity. The resulting bentonite specimen had a diameter of 50 mm and a length of 40 mm.

In the spirit of a supplementary test to the BRIE, the impediment of flow was intended to be realised by a piece of granite. Granitic bore cores with a diameter of 61.7 mm from the BRIE site were sawed into discs. It had been tried extensively to determine a reasonable length of the granite disc by calculating the time required for water to reach the bentonite sample /KRÖ 17/. This sort of modelling requires data on relative permeability and capillary pressure (equations of state) for granitic rock that were not available in

abundance. The calculated breakthrough times were therefore varying over two orders of magnitude /KRÖ 17/⁴ so that eventually a length of 2 cm was adopted for technical reasons. Such a disc was placed between water and bentonite to provide a resistance against water flow.

The rock was exposed to the well-defined Äspö-solution (see section 2.2.2 for details) under isothermal conditions. After a pre-defined period of time the bentonite was squeezed out of the cell and cut into thin slices of a few millimetres. These slices were then weighed, dried in an oven at 105 °C for 24 hours and weighed again to obtain momentary distributions of water content and dry density. Also weighed and dried was the piece of granite to get the average degree of saturation.

The whole test procedure was to be repeated for different periods of time to get an impression of the evolution of the water content. Priority in the test design had the high resolution of the obtained water content profiles as well as the conceptual straightforwardness of the test setup.

In the early phase of planning the experiment, it was anticipated that the bentonite could take up water vapour and liquid water simultaneously under unsaturated flow conditions in the rock. Since it appeared to be technically not feasible to obtain the required detail of information about the transient saturation in the rock, two supplemental tests were envisaged instead. In one variant the Äspö-solution was replaced by water-saturated air to study the effect of uptake via water vapour. In the second variant the granite disc was to be fully water-saturated from the beginning on to investigate the effect of flow resistance of the rock. The principal of the three test setups is illustrated in Fig. 2.6. All tests were to be repeated in order to provide an accuracy check on the measurement.

The design of a test cell meeting all these requirements is depicted in Fig. 2.7. Basically, it consists of a hollow cylinder containing the bentonite, a holder for the granite disc and two head ends. A separate holder for the granite was chosen because the diameter of

⁴ Two conclusions from this calculation exercise appear to be worth mentioning again: 1. Transfer of equations of state between different granitic materials can be strongly misleading. 2. From this follows that in the context of unsaturated flow direct measurements on the material in question is preferable over theoretical considerations.

the granite discs differed from the diameter of the bentonite samples that could be produced with standard equipment and procedures at the GRS lab. The bentonite was envisaged to be compacted directly in the hollow cylinder. At the faces of the bentonite a sinter plate was placed to enable equally distributed entry of water and exit of gas. To avoid clogging of the pores of the sinter plates by the swelling bentonite a filter paper was placed directly on the faces of the bentonite sample.

The inlet was then connected to a burette that provided the water and at the same time the means of monitoring the water uptake. A pressure gauge was foreseen to be installed at the opposite end of the cell to check for an expected compression of air in the pore space of the bentonite.

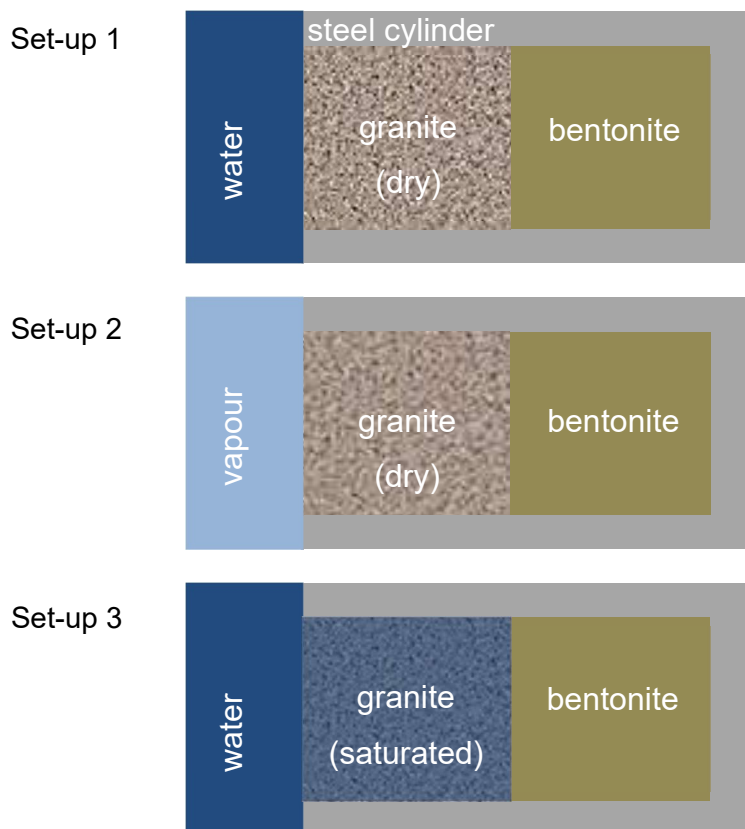


Fig. 2.6 Principle of the three test set-ups

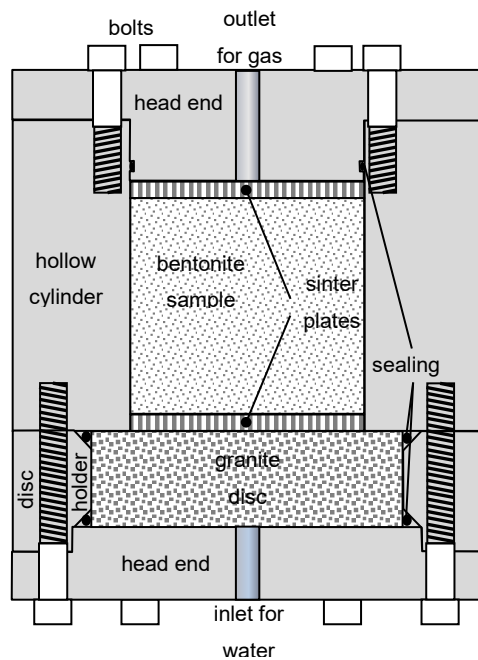


Fig. 2.7 Sketch of a test cell

2.2.2 Materials

Granite

Seven granitic discs with a length of 20 mm that seemed to be of comparable mineralogy by visual inspection were cut from a bore core and characterized with respect to volume, porosity, density and gas permeability.

To determine the porosity the granite discs were firstly dried at 105 °C for 24 hours and then weighed. Next, they were emplaced in a desiccator that was connected to a vacuum pump. Also connected to the desiccator but shut off by a stop cock was a reservoir containing Äspö-solution. After evacuating for 2 days the pump was disconnected and the stop cock for the solution carefully opened to saturate the granite discs. Afterwards they were weighed again providing the porosity by the weight difference to the dried sample. This procedure was repeated two times. Volume and bulk dry density of the granite discs are compiled in Tab. 2.1, the porosity values from the three measurement campaigns as well as maximum, minimum, mean and deviation from mean in Tab. 2.2.

Tab. 2.1 Volume and bulk dry density of the seven granite discs

	disc 1	disc 2	disc 3	disc 4	disc 5	disc 6	disc 7
Volume [cm ³]	59.3068	58.2637	59.0088	58.1147	59.0088	59.3068	55.7305
Bulk dry density [g/cm ³]	2.776	2.792	2.781	2.777	2.769	2.765	2.817

At all discs except disc 5 the porosity decreases from campaign 1 to campaign 2. But between campaigns 2 and 3 the determined porosity values increases in three discs and decreases in four discs. While the reason for the first observation remained unclear the second one indicates the order of magnitude of the inherent uncertainties related to this determination method. To quantify and compare these errors they are ad hoc defined as the maximum deviation of the single values from the mean. The resulting error thus amounts to ± 0.1 % porosity. In terms of absolute values this appears to be quite low. It has to be mentioned, though, that the determined mean porosities vary only between 0.29 % and 0.74 %.

Tab. 2.2 porosity: measured, maximum, minimum, mean and deviations

porosity [%]	disc 1	disc 2	disc 3	disc 4	disc 5	disc 6	disc 7
campaign							
1	0.41	0.40	0.59	0.43	0.39	0.74	0.76
2	0.25	0.24	0.24	0.31	0.49	0.68	0.72
3	0.30	0.22	0.22	0.50	0.44	0.59	0.76
max. value	0.41	0.40	0.59	0.50	0.49	0.74	0.76
min. value	0.25	0.22	0.22	0.31	0.39	0.59	0.72
mean	0.32	0.29	0.35	0.41	0.44	0.67	0.74
Deviations from mean	0.08	0.11	0.24	0.09	0.05	0.07	0.01
	-0.07	-0.06	-0.13	-0.10	-0.05	-0.08	-0.02

The first porosity value for disc 3 is remarkably high in comparison to the subsequent two values. This has to be taken into account looking at the resulting mean value and particularly at the deviation from the mean (cf. Fig. 2.8).

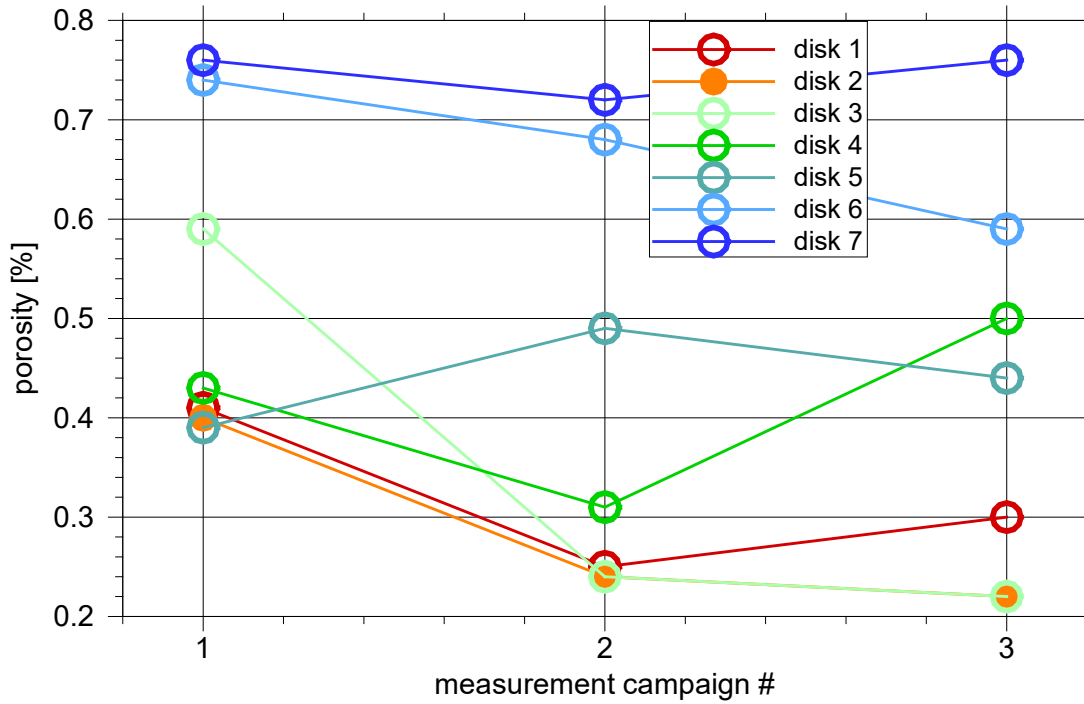


Fig. 2.8 Granite porosities determined by sample and pore water weight

Furthermore, the gas permeability of the dried granite discs was determined. This was done for two reasons. Firstly, the gas permeability was used as input for the calculations concerning the possible duration of the experiments (see /KRÖ 17/ Appendix C). Secondly, the data for the seven discs was supposed to provide some insight into the homogeneity of the bore core from which the discs had been cut.

The tests were performed with nitrogen. Evaluation was based on Darcy's law for compressible fluids:

$$k_g = \frac{2 \cdot q_g \cdot \mu_g \cdot l \cdot p_0}{A \cdot (p_1^2 - p_0^2)} \quad (2.1)$$

where the symbols mean

- | | | |
|---------|----------------------|--------------|
| k_g | permeability to gas | m^2 |
| q_g | flow rate of the gas | m^3/s |
| μ_g | viscosity of the gas | $Pa \cdot s$ |
| l | sample length | m |

A	cross-section areas	m^2
p_0	atmospheric pressure	Pa
p_1	injection pressure	Pa

The resulting gas permeabilities are depicted in Fig. 2.9 as a function of the inverse mean absolute gas pressure in the samples in a form that allows for a Klinkenberg-correction. A data fit by eyes suggests for the corrected gas permeability a bandwidth from $4 \cdot 10^{-20} \text{ m}^2$ to $2 \cdot 10^{-19} \text{ m}^2$ where the results from the 6 samples scatter around a value of about $9 \cdot 10^{-20} \text{ m}^2$.

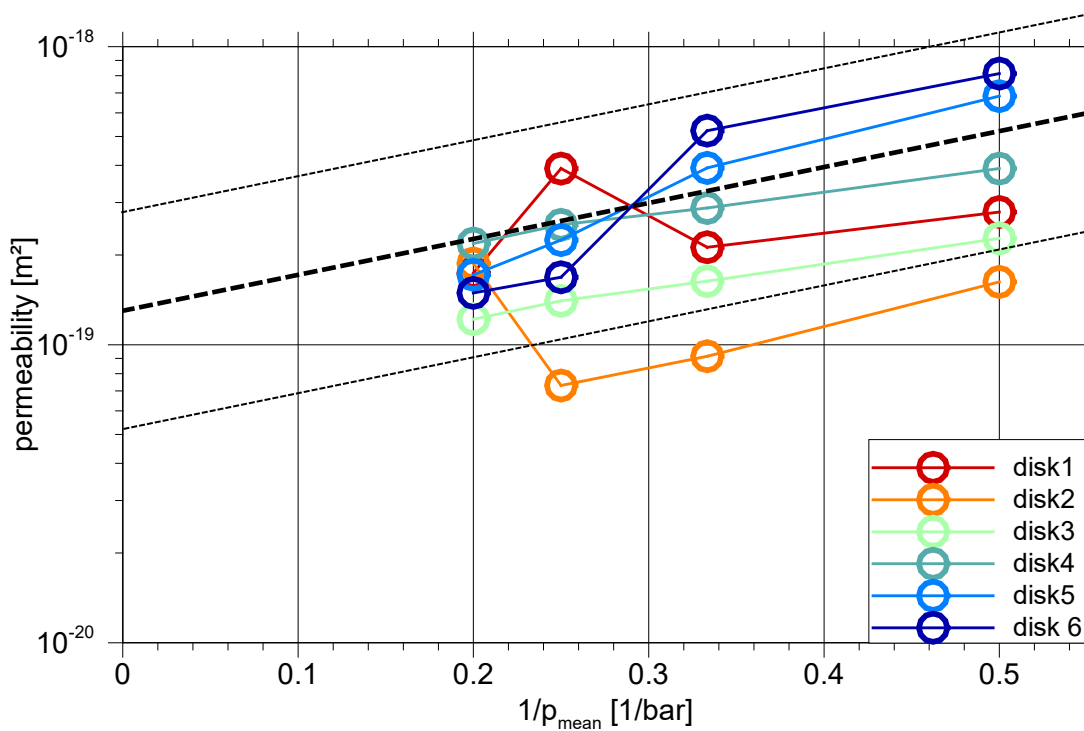


Fig. 2.9 Gas permeability as a function of the gas pressure

Note: The six granite discs had been taken from a part of a bore core which appeared visually to be homogeneous. However, the porosity varied by a factor of 2 over this short distance, the permeability even by something like a factor of 5. The data for a seventh disc taken from an adjacent but slightly suspicious part of the same core deviated even more. The granite at Äspö thus shows a considerable inhomogeneity even on a centimetre to decimetre-scale.

Bentonite

MX-80 bentonite was compacted in a cylindrical steel cell in layers of about 1 cm thickness to a density of the air-dry material of about 1450 kg/m³ and emplaced in the test cell at air-dry conditions.

Solution

The recipe for mixing a solution that is representative for the groundwater at Äspö is given in Tab. 2.3.

Tab. 2.3 Composition of synthetic Äspö-solution (e.g. /KRÖ 04/)

Na	K	Ca	Mg	Cl	SO ₄
mmol/l	mmol/l	mmol/l	mmol/l	mmol/l	mmol/l
79.67	0.25	17.06	3.33	113.92	3.40

2.2.3 First tests

After designing and producing the 6 test cells a first uptake test was performed. It turned out, though, that there had been severe leakage. A considerable amount of water had left the burettes but could not be found in the granite discs or in the bentonite.

The experiment was therefore suspended to identify the reason for this discrepancy. Even though the samples had been carefully installed, an uptake test according to set-up 1 was repeated with a plastic dummy replacing the bentonite. Since the water loss prevailed, tightness of the supply tubes was then in question even if this appeared to be rather unlikely. The test set-up was then successively simplified even further until the faulty component was identified. It turned out that glass turncocks between burette and inflow tubes were leaking at rates that are unnoticeable over a few days but add up considerably over a period of weeks. A modified test set-up took care of that problem.

2.2.4 Test over 5 weeks

Having assured tightness of the conduit system, a full test with all 6 test cells over five weeks was performed. The water content of the sliced bentonite samples as well as of the granite discs were measured by heating. Since the granite discs were left intact only a mean water content could be derived.

Despite the comparatively long testing period none of the bentonite specimen showed an appreciable water uptake of the bentonite. The determined amount of water in the granite discs in combination with the (later determined) porosities allowed calculating the mean degree of saturation in the discs. The results are compiled in Tab. 2.4.

Tab. 2.4 Mean degree of saturation in the granite discs after 5 weeks

test set-up (see Fig. 2.6)	1		2		3	
granite disc	1	2	3	4	5	6
degree of saturation [%]	63	41	20	28	202	113

In the two cells used for test set-up 1, where liquid water was connected to an initially dry granite disc, the discs were found to be unsaturated while the water content in the bentonite had apparently been remaining at initial conditions. An uneven water saturation profile along the disc axis that did not reach the end of the granite disc even after 5 weeks of testing would explain these findings.

In test set-up 2, the initially dry granite discs were brought into contact with water saturated air⁵. They should therefore have been dry at the end of the test. Instead, a mean degree of saturation of 20 % and 28 %, respectively, was determined. Even taking the comparatively large uncertainties of the measurements into account⁶ there must have been a significant amount of liquid water in the granite discs at the end of the test. Condensation as a probable reason for this observation is assumed. However, it is not clear if it occurred as a consequence of slight temperature variations in the tempera-

⁵ The air was pumped through wash bottles filled with Äspö-solution and subsequently lead across the surface of the granite discs.

⁶ The accuracy of the scale used for weighing amounted ± 0.01 g. This error margin resulted in an error for discs 3 and 4 of ± 14 % and 17 %, respectively, in the degree of saturation. This error decreases with increasing saturation and reduces to about 2 % at full saturation.

ture-controlled room, if it is a case of capillary condensation in the small pores of the granite or a combination of both. It should be noted, though, that the bentonite had apparently not been able to mobilise and suck up this water again.

Quite conspicuous are the degrees of saturation calculated for the granite discs in test set-up 3 where liquid water was connected to a fully saturated disc. Both values are above 100 %. Particularly disc 5 with a saturation of 202 % indicates that the pore space might have been partly clogged by precipitating solutes during the final heating. It remains totally unclear why the bentonite had not taken up any of this water. No increase of the gas pressure could be observed.

2.2.5 Test over 12 weeks

In a last attempt to get the bentonite wetted in this set-up, a test over 12 weeks was performed. However, it produced essentially the same results as the previous test over 5 weeks meaning that the granite discs were hydraulically too tight to allow for water uptake in a reasonable period of time. As in the previous test no increase of the gas pressure was noticeable.

2.3 Impediment of flow by an artificial low permeable material

To reduce testing time an alternative material was sought to replace the granite. A few hydraulically tight glass sinter plates that had been in stock at the laboratory were characterised for this purpose with quite some effort. The lowest permeability was found to be in the range of 10^{-16} m². Hydraulic properties also varied significantly but as a larger amount of sinter plates could easily be acquired a suitable set was expected to be available in the end.

A test with two samples was performed over a period of three weeks. Unfortunately, a space of 2 mm thickness between bentonite and sinter plates remained open unnoticed so that the bentonite could swell into this space. Direct interpretation of the test by looking at the water content at this interface was thereby compromised.

In order to come up at least with an indication of the effectiveness of the sinter plate impediment the re-saturation test was modelled with code VIPER /KRÖ 11/ which assumes

confined conditions for the bentonite. The resulting error with respect to the actual test was therefore assumed to be minimal at the sample side opposite of the water inlet. A comparison of the calculated and the measured water content showed no significant difference thus implying that even the low permeable glass sinter plates posed no serious impediment for water uptake of the bentonite.

The tedious search for a suitable material that would impede flow effectively at reasonable testing times was then abandoned because of the time that had already been spent in vain. As a consequence, the concept of flow impediment by a low permeable material was dismissed.

2.4 Re-saturation via a rising water table

2.4.1 Principle of the test

A new test design was worked out in the hope that it would still allow for successfully completing the experiment within the given time of the project. However, no new test cells were to be constructed in order to go easy on the already low project resources.

The idea of a series of tests with different running times was maintained as well as the cutting and drying of the bentonite samples to derive water content distributions. The principal difference of the new design to the earlier tests was to replace the flow impeding materials (granite discs or sinter plates) by a directly controlled water flow. The advantage of the new approach lay of course in the simple and well-posed boundary conditions for the bentonite which had previously to be determined laboriously from the conditions in the flow impeding material. However, this advantage had to be paid for by intricacies concerning very low flow rates and by assurance of an equally distributed water inflow over the bentonite surface. The test principle is depicted in Fig. 2.10.

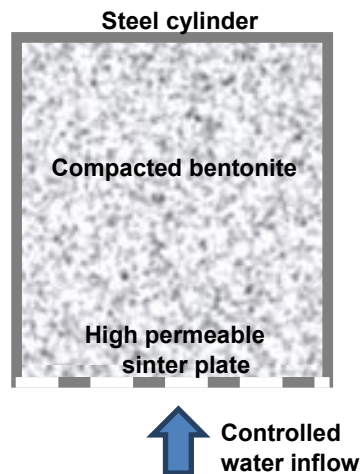


Fig. 2.10 Principle of the test via a rising water table

2.4.2 Technical requirements

The highest water uptake rate of a partially saturated compacted bentonite can be observed at the first moment of contact between bentonite and water. Subsequent water uptake takes place at an exponentially decreasing rate. A rough estimate from data by /KRÖ 04/ for the initial uptake rate of compacted bentonite with a dry density of 1500 kg/m^3 under unlimited access to water (UA)-conditions amounts to a flow density of approximately $1020 \text{ ml}/(\text{m}^2 \text{ h})$ /KRÖ 18/. This value relates to a flow rate of 2 ml/h over the face of a cylindrical sample with a diameter of 50 mm . After about 75 days this rate had gone down to about 0.01 ml/h in this experiment.

In order to provide for a limited water supply rate (LWSR) a target inflow rate of several tens of $\mu\text{l/h}$ was aimed at for the test in order to be significantly lower than the initial uptake rate. An appropriate syringe pump producing a minimal flow rate of 0.01 ml/h was found to be provided by medical technology⁷. Due to an error at the time of ordering a wrong pump had been ordered with a minimum flow rate of 0.1 ml/h . This went unnoticed for some time and led to an attempt to correct this error by modifying the setup. When this did not work the pump was replaced with the desired model.

⁷ Perfusor® compact S, B. Braun Melsungen AG, 34209 Melsungen, Deutschland, www.bbraun.de

A simple dripping on the top of the sample was not feasible because it would have led to a quite local re-saturation instead of an equal distribution over the sample face. Instead, the test cell was to be positioned over a (horizontal) water table in a water-filled bowl in such a way that the circular face would be aligned horizontally (see Fig. 2.11). Water from the syringe pump would then drop into the bowl and raise the water table accordingly.

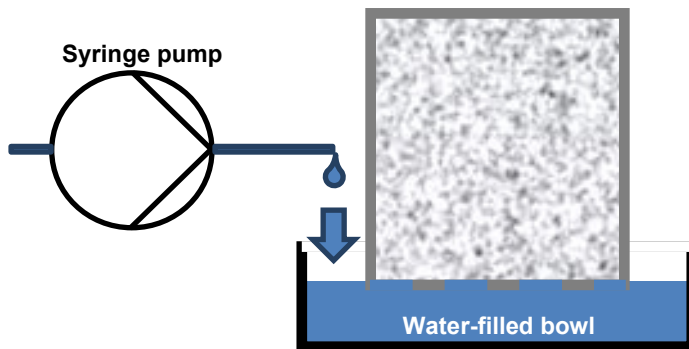


Fig. 2.11 Principle of re-saturation via rising water table

Note that this set-up connects the bentonite not permanently with water. The water table rises continuously until it reaches the bentonite. At contact, the bentonite takes up some water but also lowers the water table by this action, thereby disconnecting water and bentonite sample again. Water uptake was thus in principle discontinuous. Over the envisioned test periods of weeks this effect was considered to be of secondary importance, though.

Two conditions of the test combined quite unfortunately: firstly, the bentonite sample needed to be kept fully confined in a steel cell due to the swelling induced by the increasing water content. A swelling pressure of at least 2 MPa was expected. It was therefore not possible to determine visually the starting time of the test, i.e. the time of the first water-bentonite contact. Secondly, the rate at which water was entering the bowl had to be that of the pre-determined inflow rate Q for the bentonite, in other words, the water table was rising very slowly before the water reached the sample. These factors were bound to cause a high uncertainty with respect to the exact starting time of the test.

A set-up was therefore conceived that allowed for permanently measuring of the weight of the test cell as depicted in Fig. 2.12. The set-up realised in the laboratory is shown in

Fig. 2.13. The idea was here that the weight of the test cell starts to change only when water was taken up by the bentonite thereby indicating the beginning of the test. The cell was hanging in a steel frame which was placed on a scale. The bowl with the water was completely disconnected from this frame and supported by a plate-like holder with threaded rods as feet which were standing beside the scale. This set-up was intended to prevent the water that was added by the pump from being weighed as well.

The flexible tube connecting pump and water bowl posed a certain problem. In order to minimise evaporation from the water bowl, the diameter of the bowl had been chosen to be only little larger than that of the test cell. The tube could thus easily get too close to the test cell where water would be drawn upwards by adhesion between tube and cell. This would have compromised the flatness of the water table in the vicinity of the cell and lead to uncontrolled water uptake by the bentonite. A hypodermic needle was therefore connected to the loose end of the flexible tube and taped to the wall of the water bowl. However, positioning water bowl and test cell remained to be delicate.

As in the original test set-up the gas pressure evolving during re-saturation was checked by a manometer.

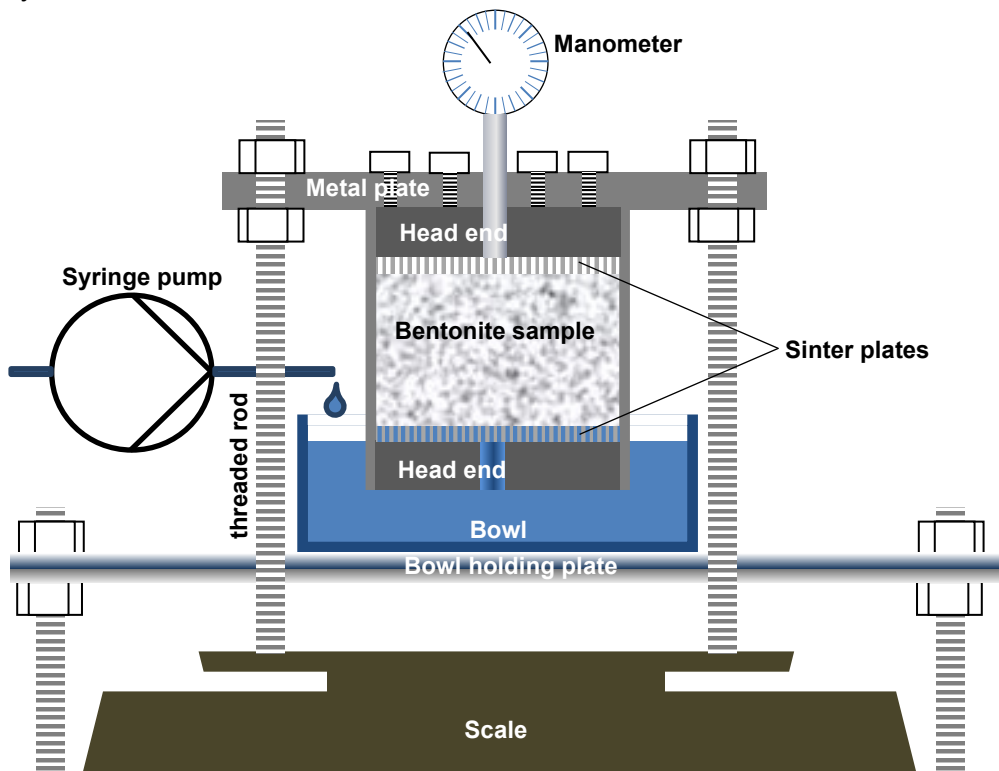


Fig. 2.12 Weighing arrangement for determination of the beginning of the test

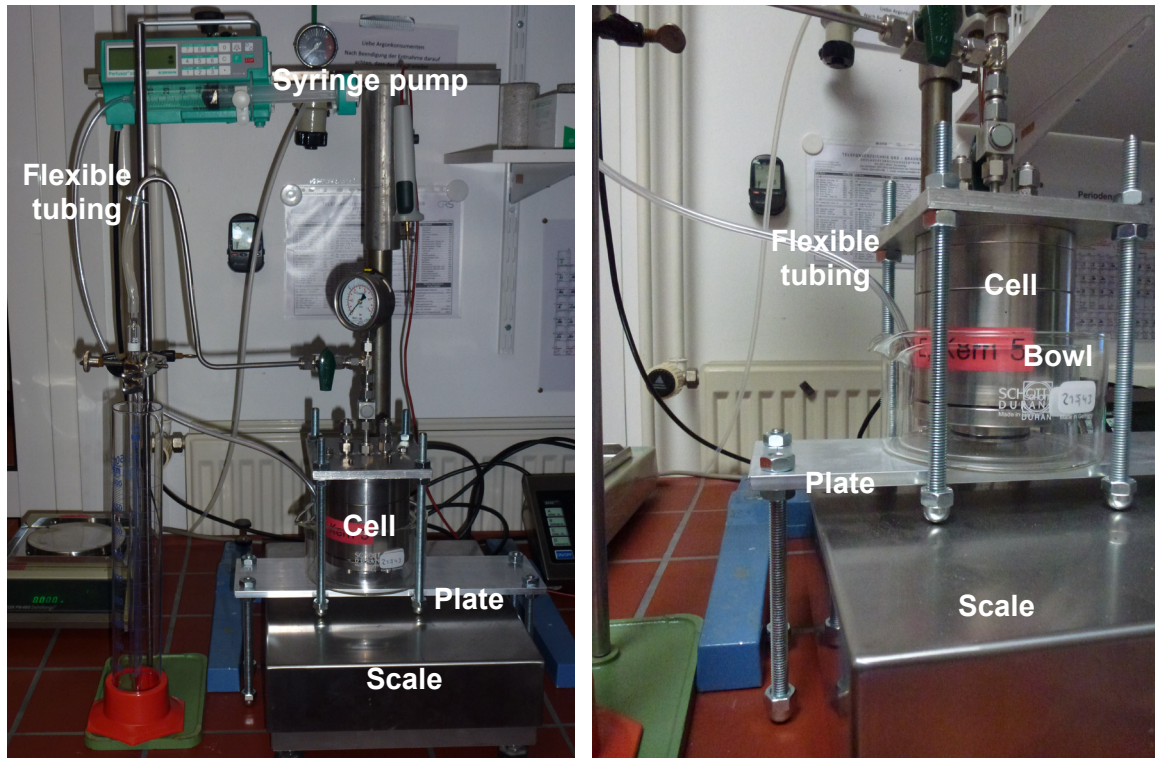


Fig. 2.13 Whole test set-up (left) and close-up of the test cell and water bowl

2.4.3 Tests with one cell – part I

In a first test with the new set-up the water table was rising as planned after switching on the pump. However, the inflow rate had been set to a value that let the water table clearly rise even after reaching the bottom of the bentonite sample. The weight was measured continuously and recorded.

Totally unexpected was the protocol of the changing weight of the sample that showed a continuous decrease of weight after starting the test and still even after the water had contact with the bentonite. The reason for that was not immediately clear. A rough calculation showed then that the effect of buoyancy on the cell could explain this observation not only qualitatively but also quantitatively.

For further tests the bottom of the bentonite was scribed outside the cell, marking the target position of the water table in order to reduce the uncertainty of the starting time as depicted in Fig. 2.14. It has to be noted, though, that measuring errors in the setting of the marking and the adhesion of water at the outer cell wall during the test were still considered to be a significant source of uncertainty.

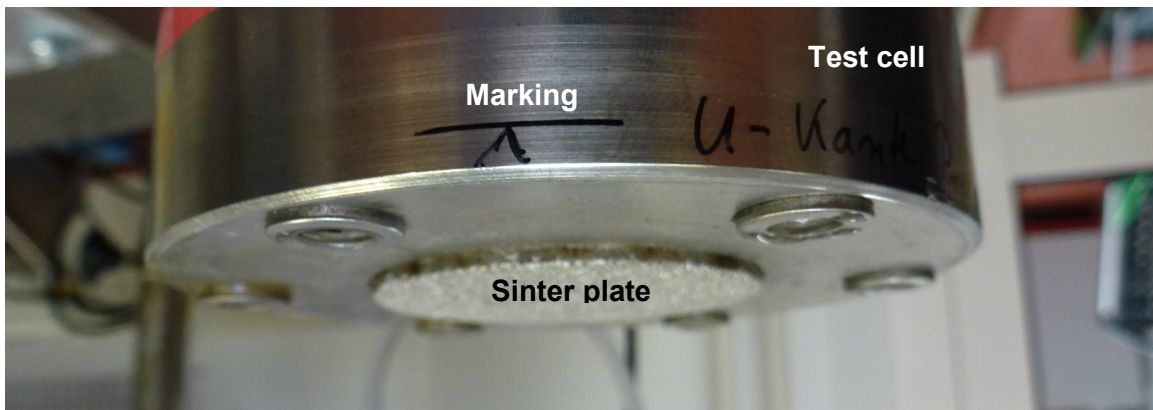


Fig. 2.14 Marking of the bottom of the bentonite sample at the outside of the cell

2.4.4 Tests with three cells

After noticing the error with the wrong specifications of the pump a variation of the test set-up was tried in order to avoid additional costs for a second pump and with the prospect of accelerating the performance of the whole test series. To reduce the inflow rate, the water flow produced by the pump was trifurcated using a four-way cock that was connected to the pump and to three test cells. This set-up proved to be not manageable, though.

The tubing for the water supply formed a system of syphons that were connected at the top. After switching on the pump, the distribution of water over the three tubes passing the four-way cock could not be ensured to be entirely equal. Consequently, gravity exerted a stronger pull at the tube with the highest share of water thereby drawing the water from the other two tubes since the tubes formed a system of communicating vessels. Starting with dry tubes thus lead to just one line carrying water.

It was then tried to start with an initially fully water-filled tubing. However, the syphon system ended up with one line drawing water from the other two, even before the pump

was started. In hindsight it is assumed that slight differences in the height of the water bowls lead to differences in the weight of the three water columns in the tubes so that the system of communicating vessel immediately drew water from two ends of the system in favour of the third one. As this test variant did not work either, the tests with three cells were abandoned and acquisition of the originally envisioned pump had become unavoidable.

2.4.5 Tests with one cell – part II

Deploying the new pump with lower minimal flow rate in order to provide LWSR-conditions for the bentonite, the tests with just one cell were resumed. It was noticed, though, that the scale readings were implausible, suggesting a loss of water from the bowl. An influence of evaporation of water from the bowl on the weight was suspected.

In order to check this idea, the test was repeated several times with an empty cell monitoring the weight of the water bowl. For this purpose, the cell was closed at the bottom to avoid evaporation into the empty space that had held the bentonite sample. Weighing indicated a considerable evaporation rate in the order of 0.05 to 0.15 ml/h. This rate, however, proved to be quite variable. It could not be excluded that the evaporation rate was influenced by other experiments performed in the same room. They involved large amounts of water and may have interfered by changing the relative humidity in the room despite climate control. In the end, the tests with a rising water table were abandoned as a whole because of the amount of unexpected difficulties that were encountered.

2.5 Direct water injection

2.5.1 Principle of the test

The final and eventually successful test design meant to go for a direct injection into the test cell. In principle this could be done again with the original test cell introducing minor changes in the set-up.

First of all, the cell had to be turned around in order to enable an as even as possible distribution of the inflowing water across the sample face. This was to be insured by in-

jecting the water from below while assuring an upright position of the cell and by the grooves in the head end connecting to the sinter plate next to the bentonite sample.

Determination of the starting time was no problem in this case. The free volume in the cell below the bentonite sample could be measured quite accurately and from this, the time until filling this space could be calculated precisely enough. The principle of the test and the actual set-up in the laboratory are depicted in Fig. 2.15 and Fig. 2.16, respectively.

2.5.2 One final problem

A lot of effort went into aligning the test cell strictly vertical in order to have an equal wetting of the lower face of the bentonite sample. After dismantling the first test, areas of dark and light grey were visible at this surface (see Fig. 2.17) nevertheless. Taking the shading as an indication of the water content (see /FRA 17/ and /DES 17/), a strongly uneven distribution of the water content had to be concluded.

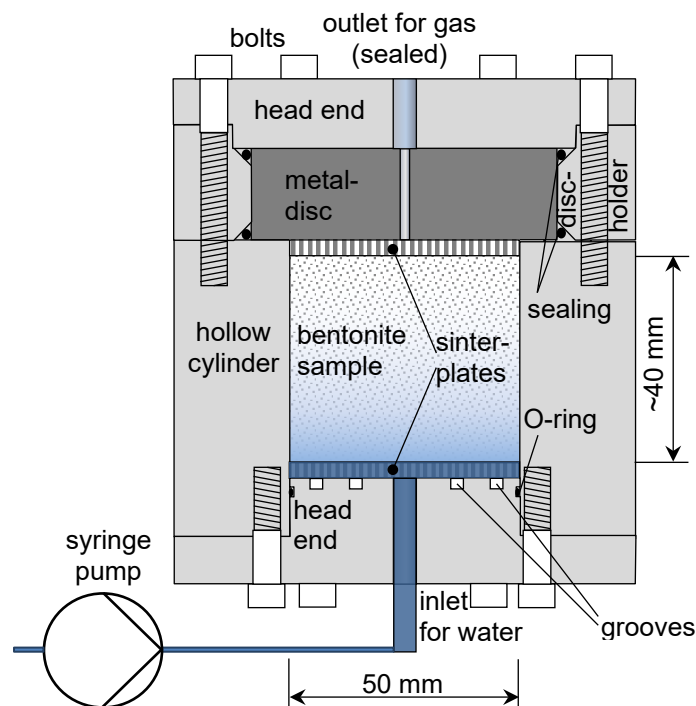


Fig. 2.15 Principle of the final test configuration



Fig. 2.16 Final test configuration in the laboratory

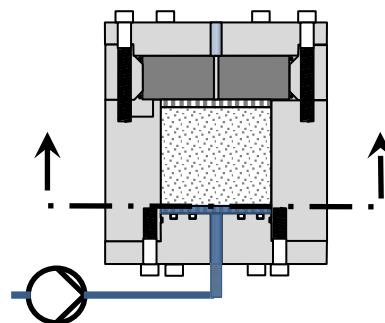


Fig. 2.17 View of the cell from below after removing head end and sinter plate

The test was repeated in order to check if this uneven distribution had developed by chance or if there was a systematic flaw in the test. The second time, a series of photos was taken from the surfaces of the slices that were cut off from the sample to determine the water content. This series is depicted in Fig. 2.18 giving an impression of the spatial distribution of the water content inside the sample. The white colouring at the sample surface stems from remains of the filter paper that was used to keep the bentonite from swelling into the sinter plate.

The pictures from Fig. 2.18 confirmed the observation from the previous test. However, they confirm also the rather sharp transition from dark grey to light grey in Fig. 2.17. Assuming that the spreading of water is caused by diffusion-like processes and assuming further a linear relation between grey shade and water content as suggested by /DES 17/ a much smoother transition would have been expected. Since this linear relationship has not been confirmed under the stringent conditions of a laboratory, yet, it is suspected that the grey shades are not linearly related to the water content.

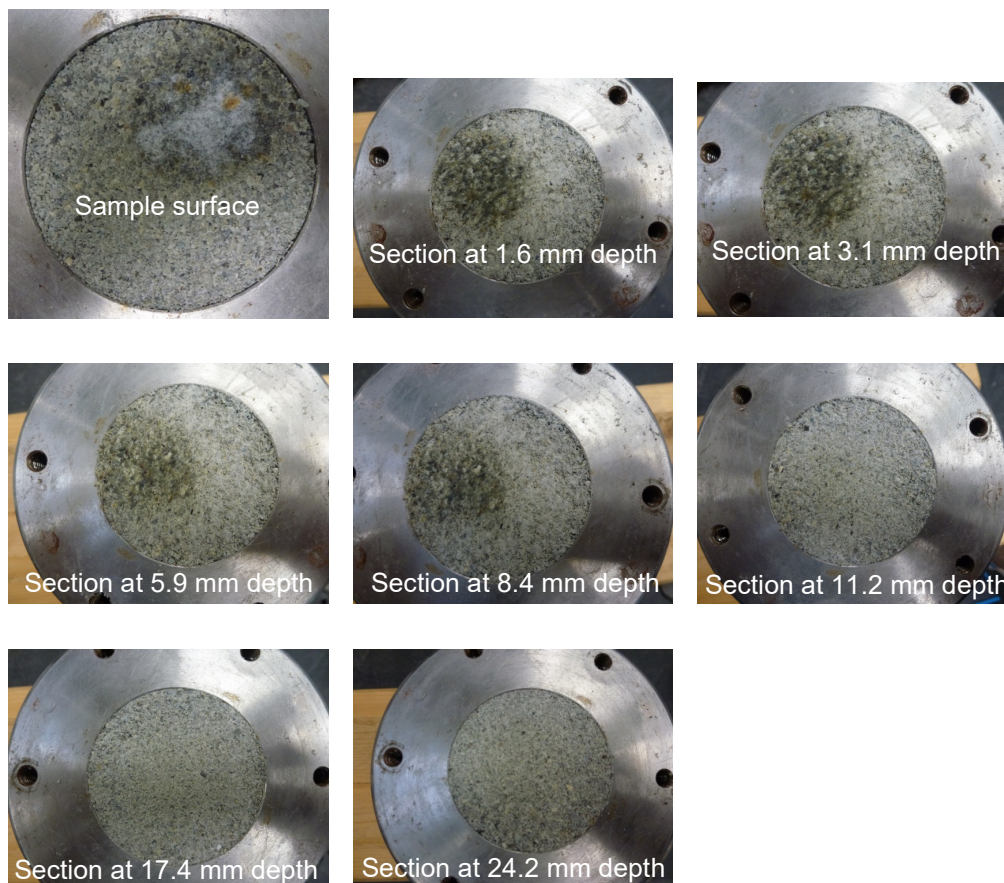


Fig. 2.18 Visual inspection of water content distributions inside the sample

Giving the set-up more thought, it was suspected that the pores of a common sinter plate were small enough to exert a significant capillary pressure when in contact with water. This notion could be confirmed by a simple test with a sinter plate slightly immerse in water in a Petri dish. After a short period of time wetness on the top of the previously dry sinter plate could be demonstrated by the wetting of a filter paper that was placed on the surface of the sinter plate.

Taking into account a certain roughness of the surface of a sinter plate it was assumed then that this roughness would counteract the effort for an even wetting of the bentonite. At a point sticking out of the surface of the sinter plate, water could be sucked up locally slightly earlier than in the vicinity leading to the observed uneven wetting pattern.

In order to avoid this effect alternative sinter plates were sought. A very coarse sinter plate made from comparatively large bronze spheres (see Fig. 2.19) was used further on instead of the stainless steel sinter plates. Note that the pattern of circles and straight lines visible on the surface of the bronze sinter plate are artefacts from the system of water distributing grooves on the inside of the head end.



Fig. 2.19 Eventually used bronze sinter plate; total and close-up

Fig. 2.20 shows the resulting water content distribution for a test with bronze sinter plates over 7 weeks by a series of photographs in the same manner as in Fig. 2.18. The grey shades are more or less the same over a specific cross-section demonstrating that

the bronze sinter plates had large enough pore diameters to reduce the capillary suction sufficiently.

With this last modification of the set-up, the intended tests could eventually be performed.

Note: The pictures shown in Fig. 2.20 suggest the sharp transition in the grey shades to occur between a depth of 12.2 and less than 24.6 mm. Correlating this depth with the water content data derived later from this particular test (see the cyan coloured line in Fig. 2.25 in section 2.5.5) suggests that the transition relates to a water content of 26 – 29 %. This range of water contents is particularly intriguing for two reasons: (1) This range coincides nicely with a relative humidity of about 95 % where basically all measured isotherms/retention curves for MX-80 show a change in trend towards an exponential increase of the water content /KRÖ 11/. (2) According to /KAH 86/ the water content of about 28 % marks the completion of the third hydrate layer between the clay lamellae. For further interpretation of pictures of wetted bentonite, it is therefore strongly advised to derive a relationship between grey shades and water content from well-defined laboratory tests.

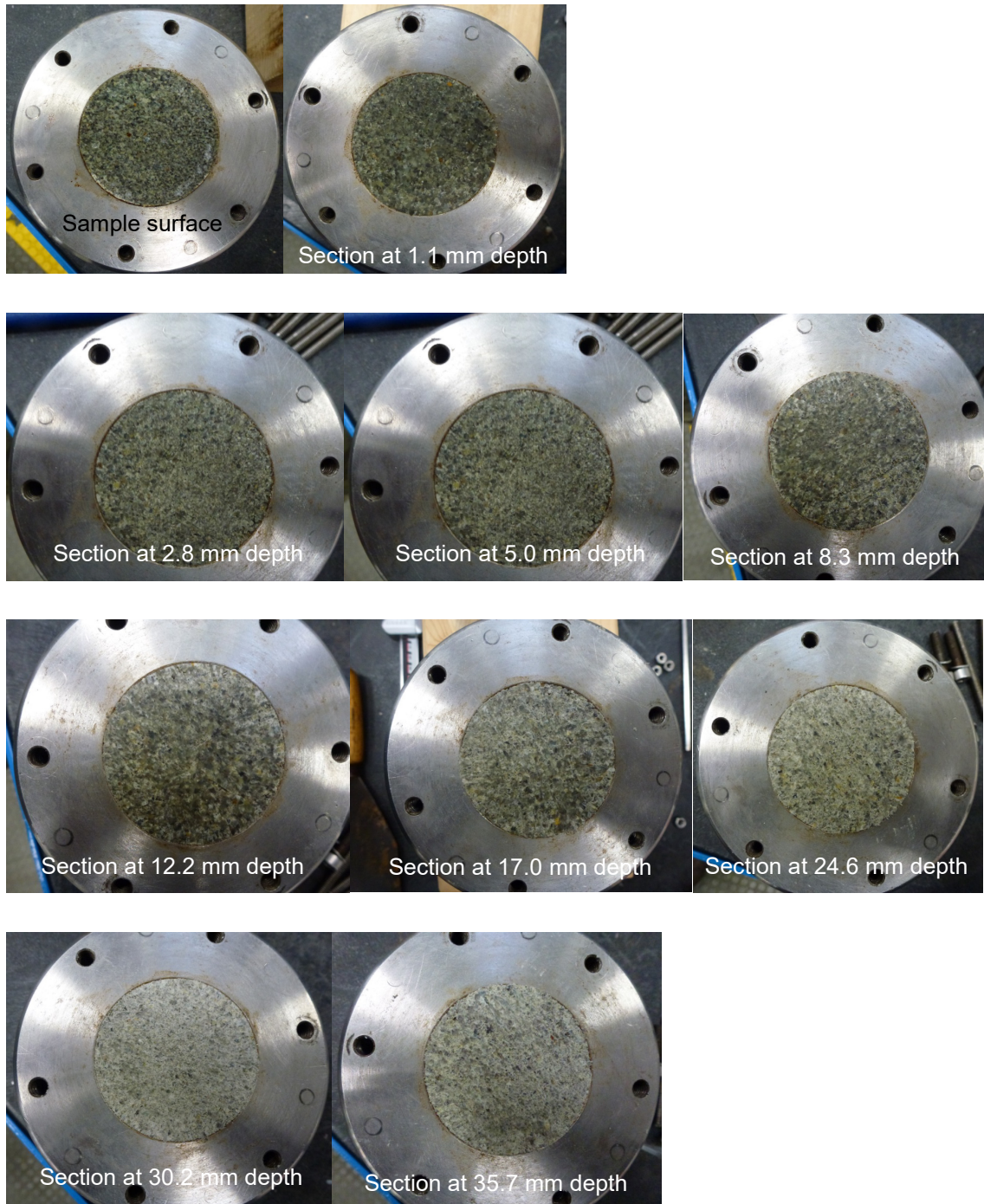


Fig. 2.20 Water content distributions inside the sample using bronze sinter plates

2.5.3 Test program

Two series of water uptake tests were performed. In one series the duration of the individual tests was fixed to approximately one week and the inflow rate was varied between

0.01 and 0.05 ml/h. For comparison, also a test with an inflow rate of 0.05 ml/h over two weeks is included here. In the second series the inflow rate was set to 0.02 ml/h and the test duration was varied amounting to 1, 2, 3, 4, 7, and 9 weeks, respectively. The tests were performed with MX-80 bentonite at a target air-dry density of 1450 kg/m³ being wetted in the test by a solution typical for the groundwater at the Äspö HRL.

Two samples of MX-80 bentonite were tested for the initial water content. The raw data are compiled in Tab. 2.5 indicating an initial water content of about 12.7 %

Tab. 2.5 Data for determination of the initial water content

Testing date	10.04.2017	17.05.2017
Weight before drying [g]	46.51	38.06
Weight after drying [g]	41.22	33.79
Difference [g]	5.29	4.27
Water content [-]	0.1283	0.1264

2.5.4 Modelling prerequisites

In parallel, the concept of the extended vapour diffusion (EVD) model for water uptake by compacted bentonite under confined conditions /KRÖ 11/ had been advanced on a theoretical basis to cope with LWSR-conditions. Appropriate formulations were derived /KRÖ 17/ and implemented in the referring code VIPER before the first test results had been obtained. The combination of theoretical considerations, realisation in a code and experimental inspection allowed for checking the new model concept qualitatively as well as quantitatively and thereby for qualifying the advanced code VIPER.

All input parameters were kept constant for all models except for the test specific and thus slightly varying data. Test specific data are compiled in Tab. 2.6 and input data valid for all models in Tab. 2.7. Among the material data in Tab. 2.7 there is the entry “final porosity” meaning the porosity at the end of re-saturation. The choice of this parameter is discussed in detail in Appendix B.

Tab. 2.6 Test specific input data

Target duration [w]	Inflow rate [ml/h]	Actual duration [d]	Density [kg/m ³]
1	1	6.39	1393
1	2	5.47	1507
1	3	5.59	1480
1	4	7.0	1499
1	5	6.93	1466
2	5	13.0	1519
2	2	12.65	1444
3	2	18.7	1395
4	2	26.12	1422
7	2	41.43	1441
9	2	63.85	1464

Tab. 2.7 Input data valid for all numerical models

Geometry	
Cross-section area [m ²]	19.63e-4
Number of elements	100
Time step [s]	10
Pore space	
Tortuosity [%]	65
Interlamellar space	
Tortuosity [%]	40
Critical water content w_{crit} [%]	17
Diffusion coefficient [m ² /s]	$7.5 \cdot 10^{-10}$ ($w < w_{crit}$)
Diffusion coefficient [m ² /s]	$12.0 \cdot 10^{-10}$ ($w > w_{crit}$)
Initial conditions	
Initial water content [%]	12.7
Final conditions	
Final porosity [%]	9
Boundary conditions	
Inflow rates [ml/h]	0.01 0.02 0.03 0.04 0.05
[kg/(m ² s)]	$1.41 \cdot 10^{-6}$ $2.83 \cdot 10^{-6}$ $4.24 \cdot 10^{-6}$ $5.66 \cdot 10^{-6}$ $7.07 \cdot 10^{-6}$
Miscellaneous	
Grain density [kg/m ³]	2780
Water density [kg/m ³]	1000
Isotherm	according to /DUE 04/, /DUE 07/, described in /KRO 11/

2.5.5 Results from varying the inflow rate

The results of the laboratory tests varying the inflow rate while keeping the test duration at close to 1 week are depicted in Fig. 2.21. The dashed lines indicate the size of the slice for which the value is representative. The overall characteristics of these water content curves appear to be consistent with a diffusion-like water migration process. The highest value along with the highest gradient can be found at the inflow boundary and it decreases exponentially with distance from this boundary. Contrary to water uptake under UA-conditions where the water content at the inflow boundary shows its maximum value from the beginning on, the present measurements show water content distributions whose boundary values increase with the inflow rate.

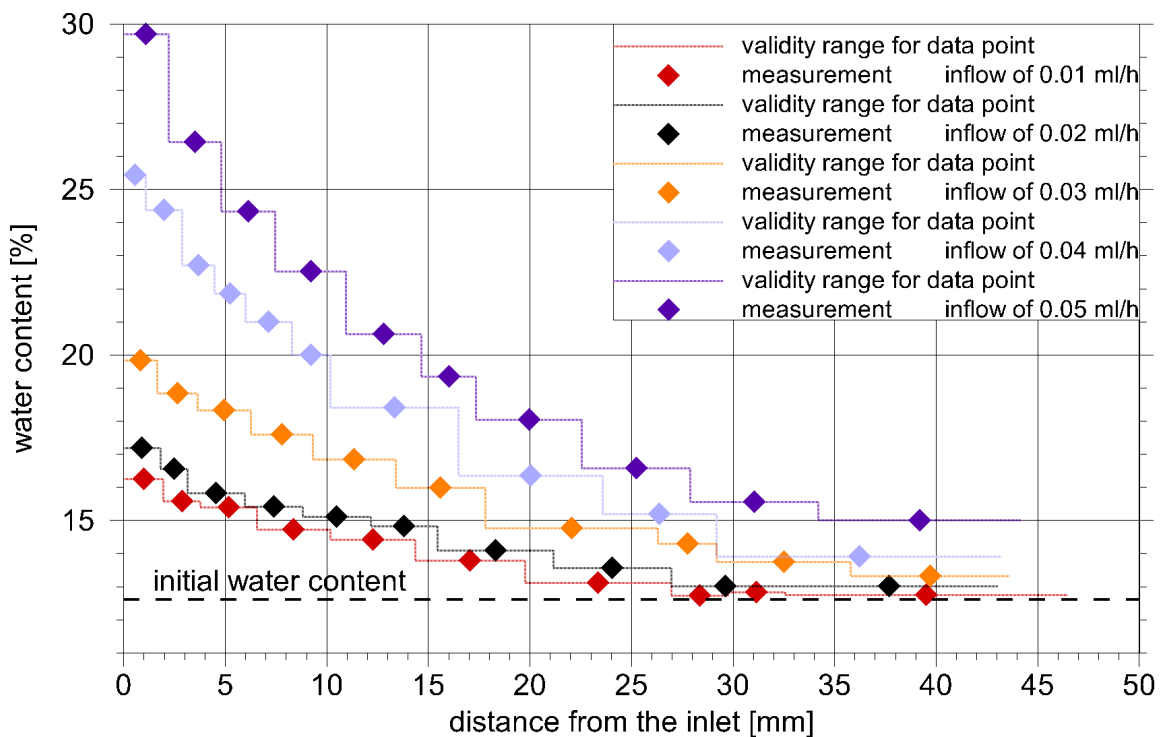


Fig. 2.21 Measured water content distributions varying the inflow rate

In Fig. 2.22 the measured data are overlain with the results of the related model calculations. They are plotted at a different scale to allow for a comparison with subsequent figures. All simulations were done with the same parameter set. By and large, the calculated water content curves match the measurements satisfyingly well even if the match for single tests shows in some cases potential for a better fit. As an ensemble, though, the calculated water contents fit the measured data fairly well thereby confirming the

assumptions of the EVD-concept in general and the considerations about the specific aspects of uptake under LWSR-conditions in particular.

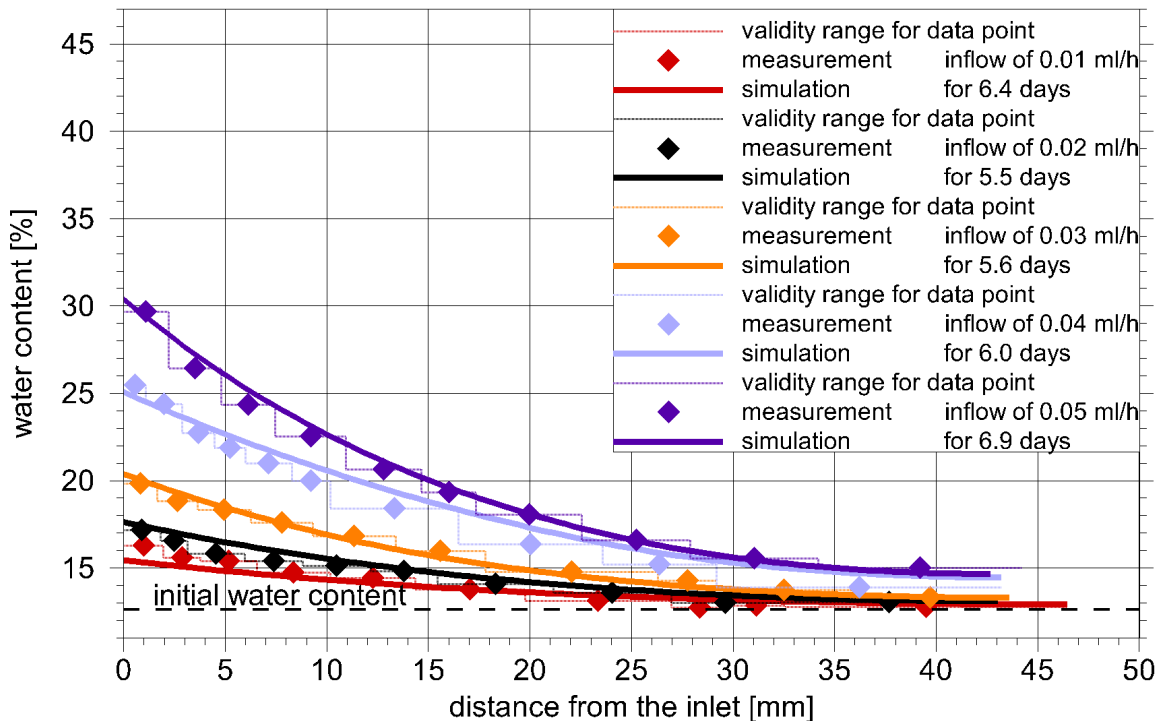


Fig. 2.22 Measured and calculated water content distributions varying the inflow rate

Dry density data can also be derived from the data for the water content. The results in terms of dry density distributions are shown in Fig. 2.23. Apparently, the data for dry density are more sensitive to errors in the slice thickness than the data for water content. Nevertheless, there appears to be a reduction of dry density within the first ten millimetres with its maximum directly at the boundary. Otherwise, the dry density is more or less constant. A black line is inserted in Fig. 2.23 for orientation.

It was tried ad hoc to dampen the errors from slice preparation by taking an average over the value itself and its neighbours at each location. The result is depicted in Fig. 2.24 confirming the trends suspected in the previous section with more clarity.

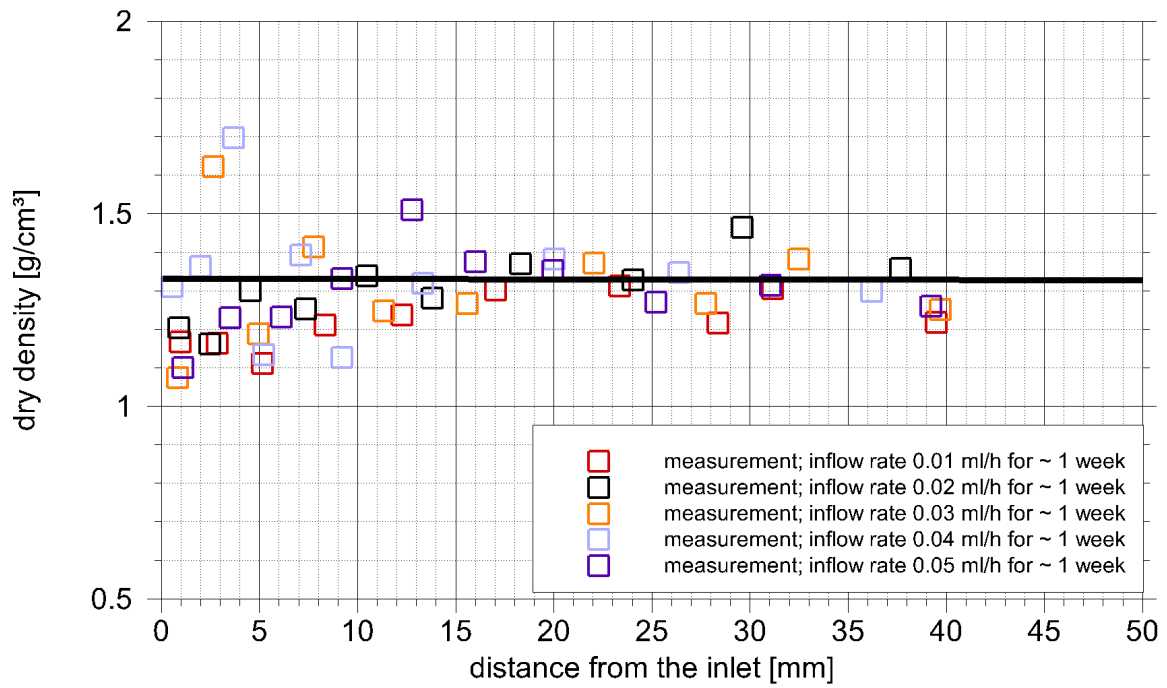


Fig. 2.23 Measured distributions of dry density varying the inflow rate

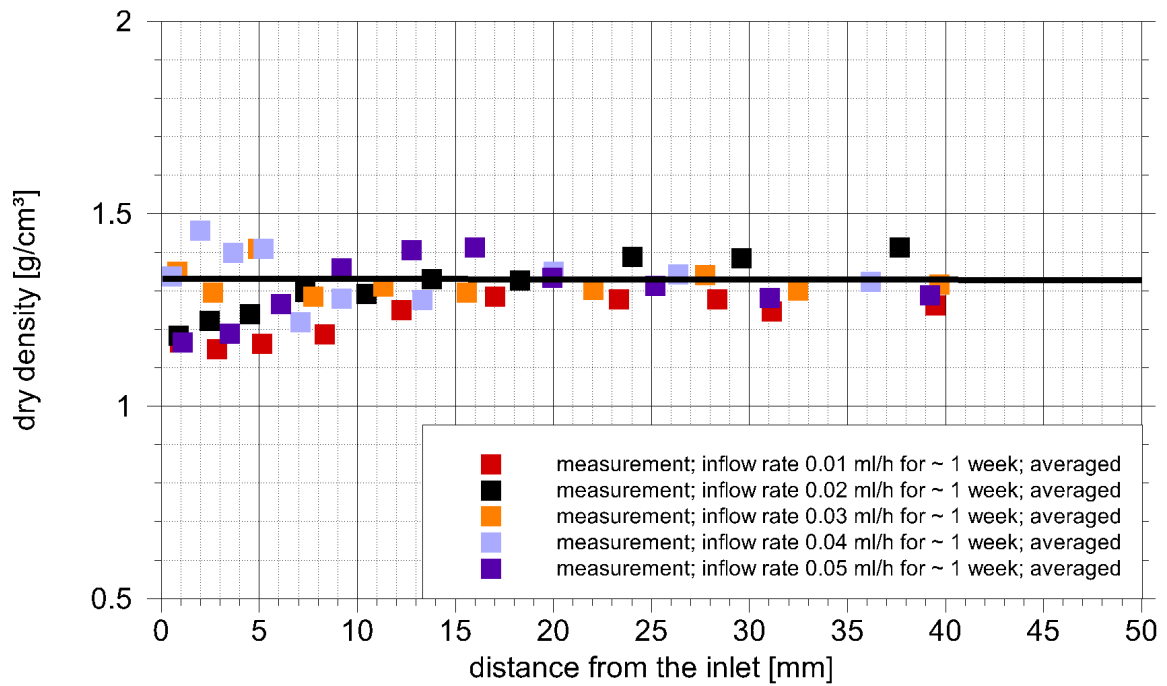


Fig. 2.24 Averaged distributions of dry density varying the inflow rate

2.5.6 Results from varying the running time

The water content distributions resulting from an inflow rate of 0.02 ml/h for varying periods of time are depicted in Fig. 2.25. For the tests lasting up to four weeks basically an upwards shift of the water content curve can be seen. Apparently, the diffusive water flux along the sample axis distributes the inflowing water more or less equally over the whole sample length. Accumulation of water at the inflow boundary to a narrow fully saturated zone as observed under UA-conditions is therefore not possible during this period of time.

However, already after four weeks there is a slightly too high value at the inflow boundary that does not quite fit the trend of the earlier water content distributions. Considering the data scatter that comes with the measurements of the shorter running tests, this could certainly be accounted for as scatter in case of the 4 weeks lasting test as well. This particular feature is repeated and more pronounced, though, in the distributions for the 7 and the 9 weeks running tests.

After 7 weeks test duration the full saturation of the interlamellar space is slightly exceeded. This value is defined here as the maximum water content after re-saturation by vapour saturated air exclusively, or in other words, as the maximum interlayer water content corresponding to uptake from vaporous air. For orientation the related value range is indicated in Fig. 2.25 for the two longest lasting tests by the lower pink bar⁸. This high water content can be explained either by liquid water in the pore space, by local swelling or by both phenomena.

Seeing only the curve for 7 weeks the evidence is therefore not conclusive. Continuing the test for another two weeks under LWSR-conditions, however, produces a pronounced peak at the boundary. This peak is even higher than the maximum water content at filling the interlamellar space as well as the pore space completely with water. The maximum water content according to the initial water content is indicated in Fig. 2.25 by a pink bar as well. From the measured peak at the boundary, the effect of

⁸ This critical water content is actually fixed for each sample but it depends on the dry density which has been subject to a slight scatter. The related uncertainty is therefore expressed by a bar rather than a line.

local swelling at a high degree of saturation within the confined bentonite sample can be concluded.

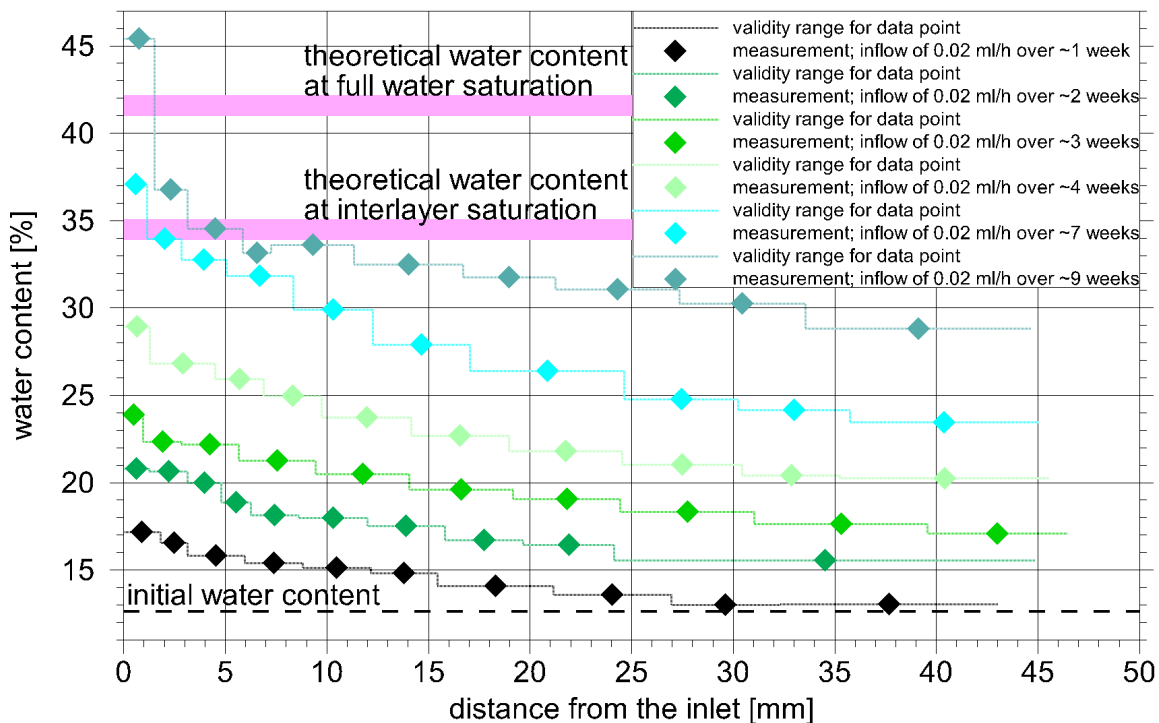


Fig. 2.25 Measured water content varying running time of the tests at 0.02 ml/h

Corroborating the conclusion about forming a fully saturated zone in the tests is the fact that the test over 9 weeks had actually to be terminated because the syringe pump stopped working automatically after sensing a pressure build-up in the inflow tube. An increase of flow resistance is in line with experiments performed under UA-conditions where it has been tried to force water into a bentonite sample by applying a hydraulic pressure. In a matter of minutes this had not been possible anymore even building up a pressure of 6 bar at the inflow boundary /PUS 01/.

A similar observation had been done during the first orientating tests where a test had been running 2 weeks at 0.05 ml/h. The results together with those of the test of one week duration are depicted in Fig. 2.26. Again, the results from one week running time are in line with the theoretical approach for uptake under LWSR-conditions while the curve for two weeks shows a peak exceeding the theoretical water content at full water saturation at the inflow boundary. Apparently due to the higher inflow rate it takes just two weeks for an inflow rate of 0.05 ml/h instead of 9 weeks in case of 0.02 ml/h.

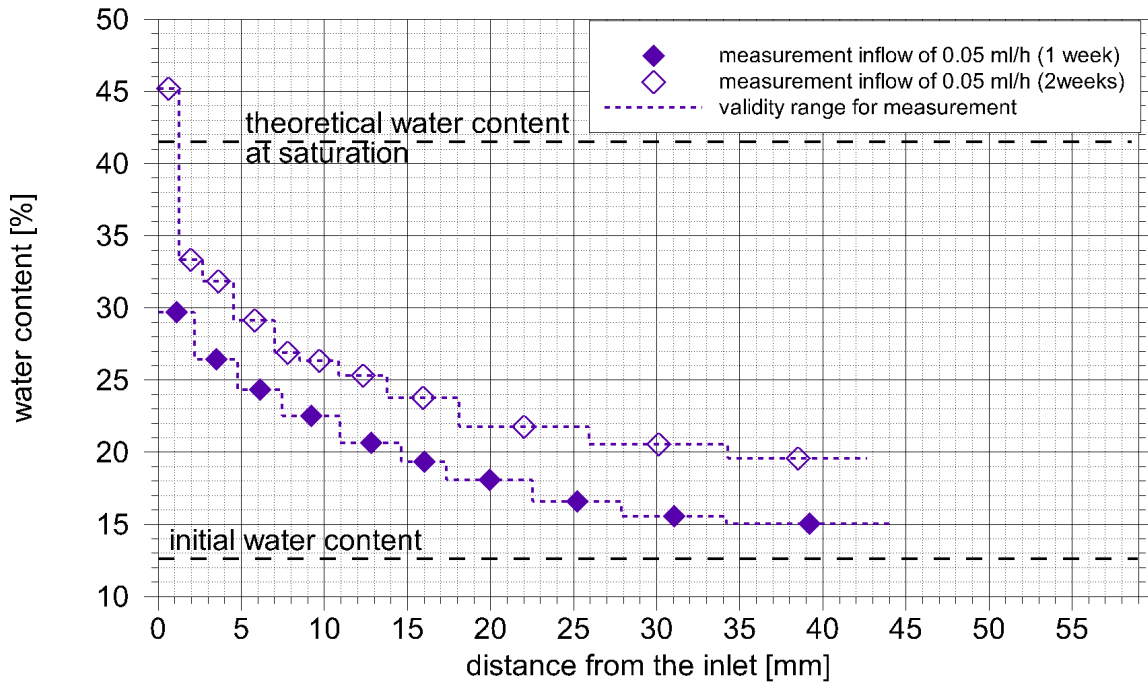


Fig. 2.26 Measured water content varying running time of the tests at 0.05 ml/h

Further insight comes from the comparison of the measured data with the results of the model calculations as the model calculations reflect the theoretical approach to water distribution in the bentonite under LWSR-conditions. The approach postulates a steady increase of the water content at the inflow side of the bentonite with time which can be observed in the measurements as well as the model (see Fig. 2.27), again confirming the theoretical considerations concerning uptake under LWSR-conditions.

This increase continues until the theoretical maximum water content according to the initial dry density is reached. At this point, an instantaneous switch from LWSR- to UA-conditions is assumed /KRÖ 17/. The data depicted in Fig. 2.25, however, indicate rather a transition period. This becomes even clearer in the comparison of measurements and simulations depicted in Fig. 2.27. However, quantifying the extent of such a transition period is rather hard to conclude from the comparatively low number of the tests in combination with the data scatter.

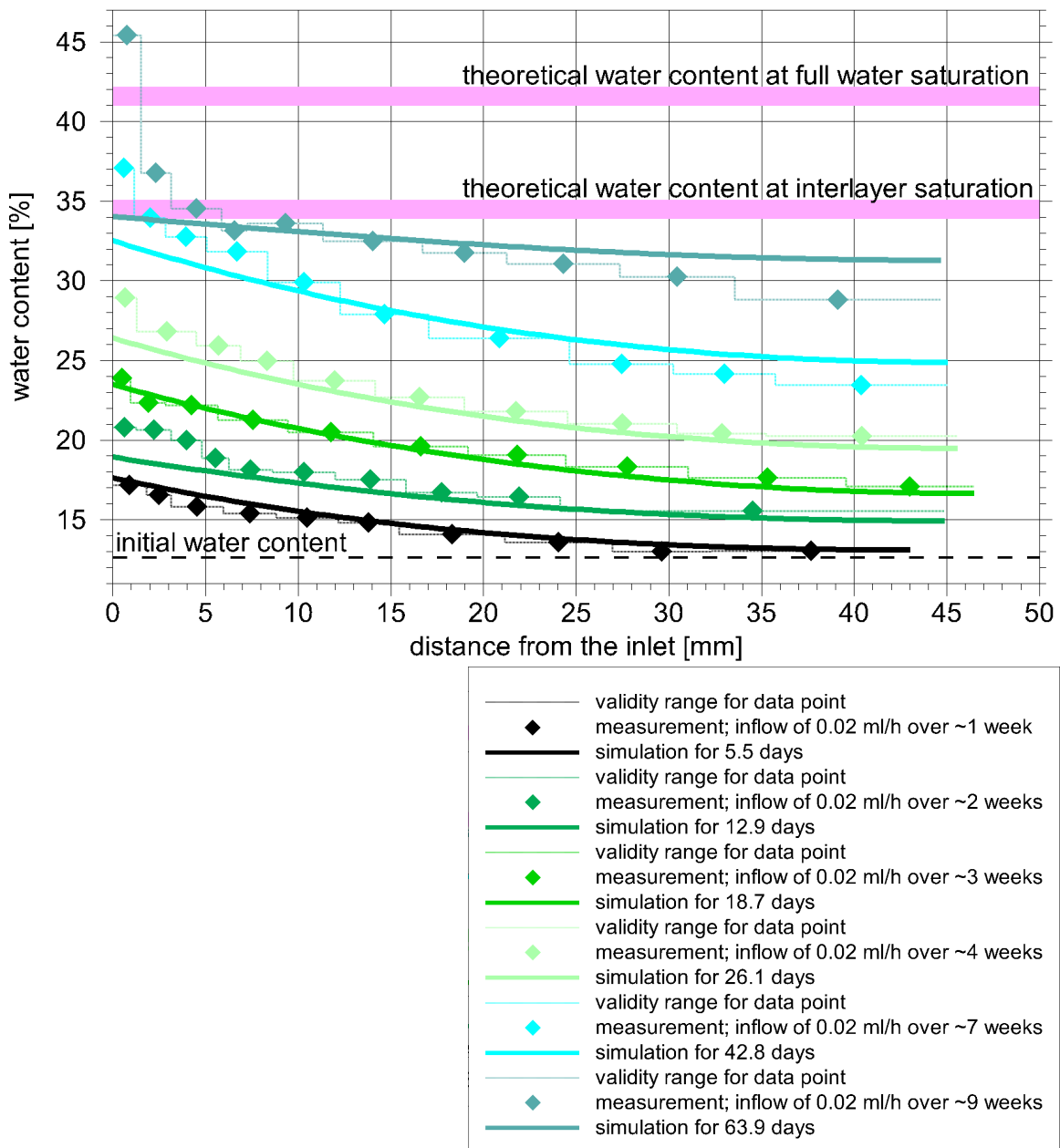


Fig. 2.27 Measured and calculated water content distributions varying running time

The related measured and averaged dry density distributions are shown in Fig. 2.28 and Fig. 2.29, respectively. The trend in these data appears to be quite similar to the one revealed by Fig. 2.23 and Fig. 2.24, respectively, and is apparently also independent of the running time. This is particularly remarkable as it applies also to the longest running test of 9 weeks duration after which time a change from LWSR- to UA-conditions is suspected.

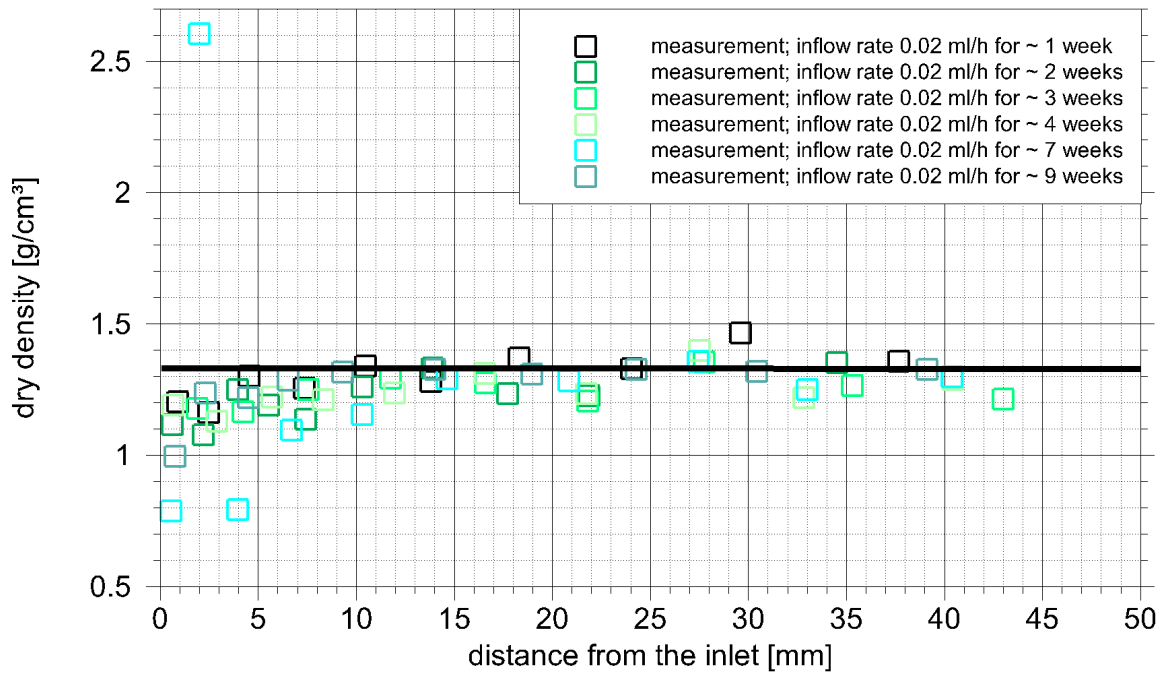


Fig. 2.28 Measured distributions of dry density varying the running time

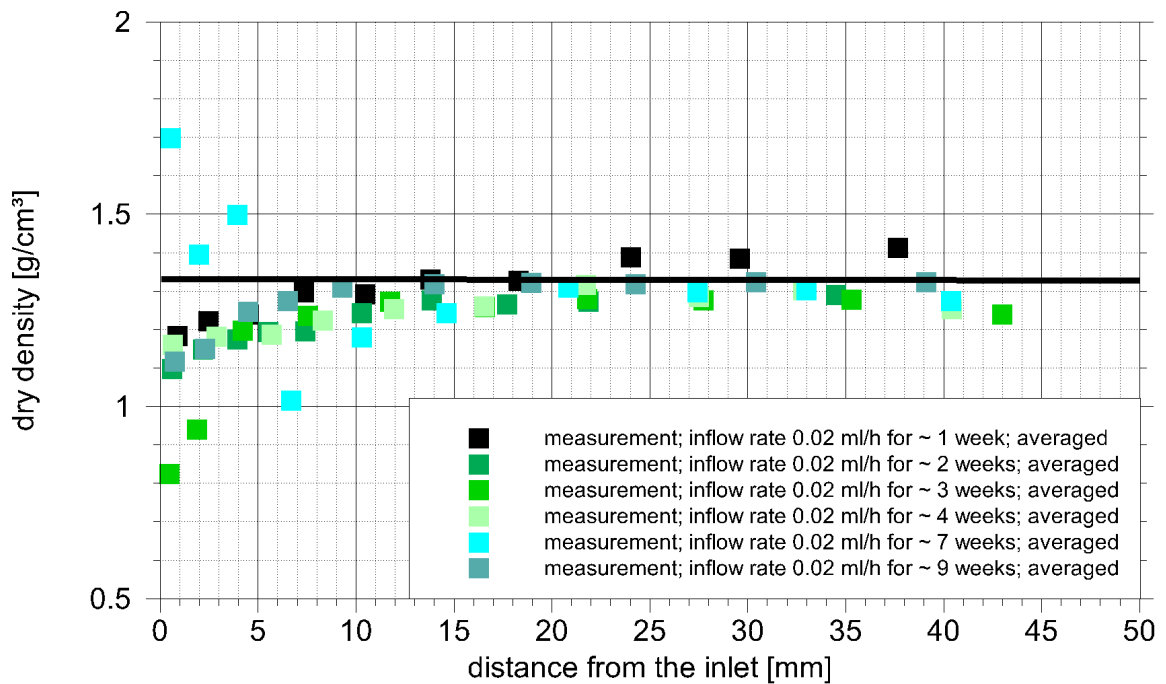


Fig. 2.29 Averaged distributions of dry density varying the running time

Within the uncertainties that come with the scatter of the data, two conclusions can be drawn from Fig. 2.24 and Fig. 2.29, respectively:

- A representative curve of the dry density over distance from the inflow boundary would show a somewhat linear increase within the first 10 mm. Beyond that, the dry density would be constant.
- After one week, the reduction appears to be independent of the inflow rate.

3 Final state of re-saturation under a thermal gradient

3.1 Idea of the test

The simple principle of isothermal uptake experiments performed earlier /KRÖ 04/ was considered to be an applicable method for the present non-isothermal experiment as well. In order to avoid irregular flow paths and leakage, direct instrumentation of the sample with humidity and temperature sensors was waived here again. Each of the cylindrical samples was hydraulically loaded at one planar side with water cooled to 20 °C. At the opposite side the sample was heated to 95 °C. A constant temperature gradient along the sample axis was aimed at.

Four test cells were used in parallel and under the same physical conditions to perform tests with different running times. While running, the water uptake and the temperature distribution along the outside of the test cells were measured. At the end of each test, water content and dry density distributions were determined by cutting the sample and subsequently weighing and drying the resulting bentonite discs. The use of several tests cells allows then to minimise the overall duration of the experiment by starting the long-term tests right at the beginning while doing short-term tests in parallel.

3.2 Expected evolution

For a limited period of time after starting a test the impact of water uptake and heating on the water content distribution were expected to be independent from each other. Forming a fully saturated zone at the water inlet was anticipated to happen basically instantaneous, followed by a diffusion-like spreading of the water into the sample beyond that zone. Starting from the heated end, drying and a related moisture migration towards the cool end were presumed.

However, after some time into the test the wetting front from the cool side and the drying front from the heated side were to meet so that both effects would add up. What happened afterwards and in particular the final steady-state conditions were anticipated to be the outcome of the experiment.

3.3 Test set-up

In order to minimise the influence of the expected rapid cooling after dismantling of a test – particularly at the heated side – it was decided to abandon the idea of using a metal cylinder for housing the samples. Instead, a series of plastic rings made of PEEK was used that allowed for a quick cutting of the samples in between them⁹. To ensure water and vapour tightness of the cell interior, the rings had grooves to accommodate O-rings and were pressed against each other by mechanical clamping. A sketch of the test cell is given in Fig. 3.1. A photograph of a cell is depicted in Fig. 3.2.

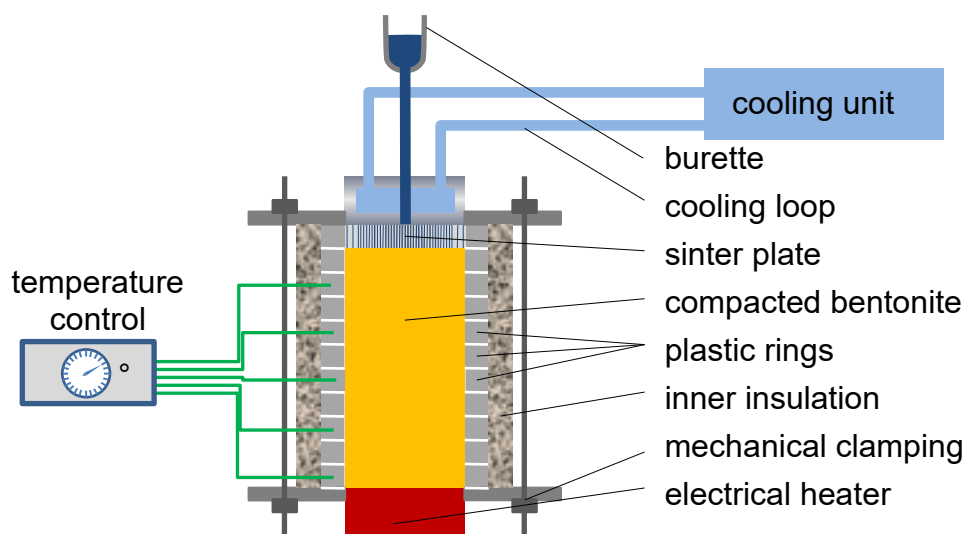


Fig. 3.1 Sketch of the test cell

A cooling unit provided a temperature of 20 °C at the top of the test cells. Water for the uptake of the bentonite was supplied from a burette. It was distributed by grooves in the head piece (see Fig. 3.3) as well as by a sinter plate to ensure an equally distributed water flux into the sample. The thermal gradient was basically kept constant along the axis of the test cells due to generous padding with glass wool. Two layers of insulation were actually applied, one layer to equalise the cell surface and a thicker one around that. To control the temperature in the cell, each ring had a small borehole for placing

⁹ The original idea of cutting the samples with a wire had to be dismissed, though, as the bentonite turned out to be too stiff for that. The wire was thus replaced by a simple scraper.

temperature sensors close to the samples. The insulation is illustrated by two photographs in Fig. 3.4, the full set-up by Fig. 3.5.

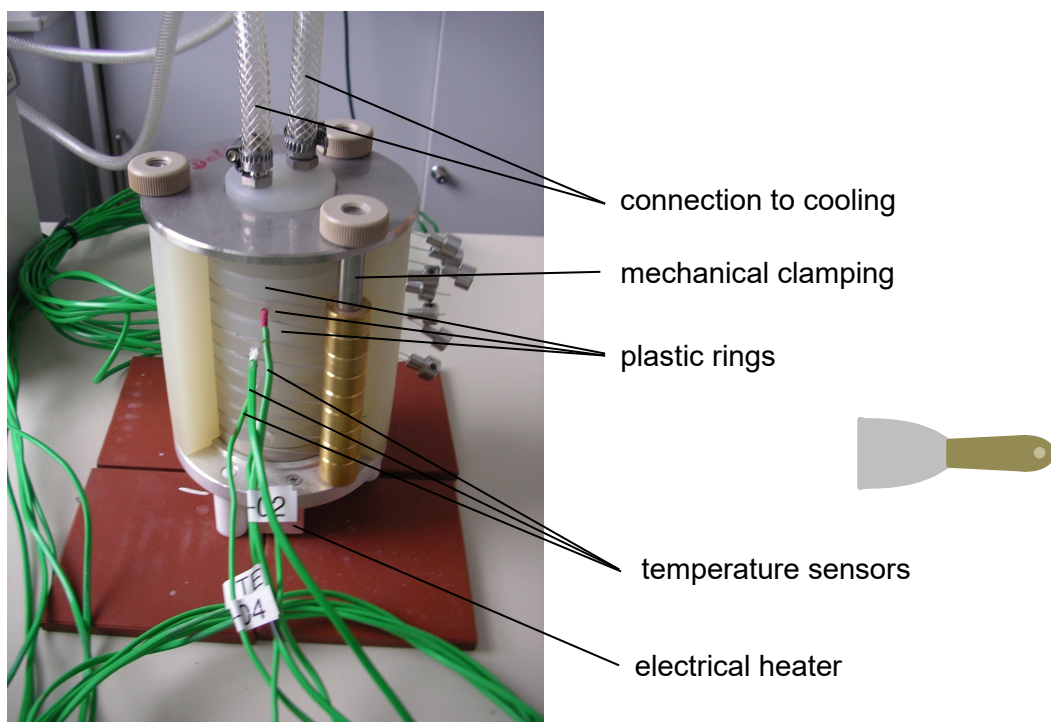


Fig. 3.2 Photo of the test cell without thermal insulation¹⁰

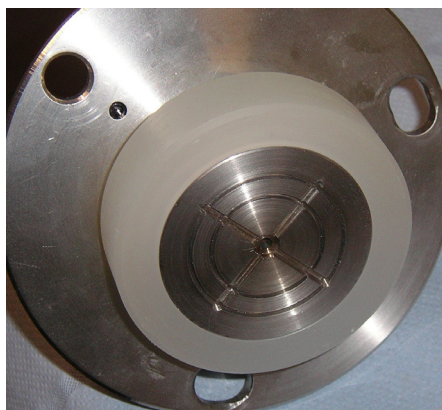


Fig. 3.3 View from below the head piece

¹⁰ Inlet for the burette not yet installed

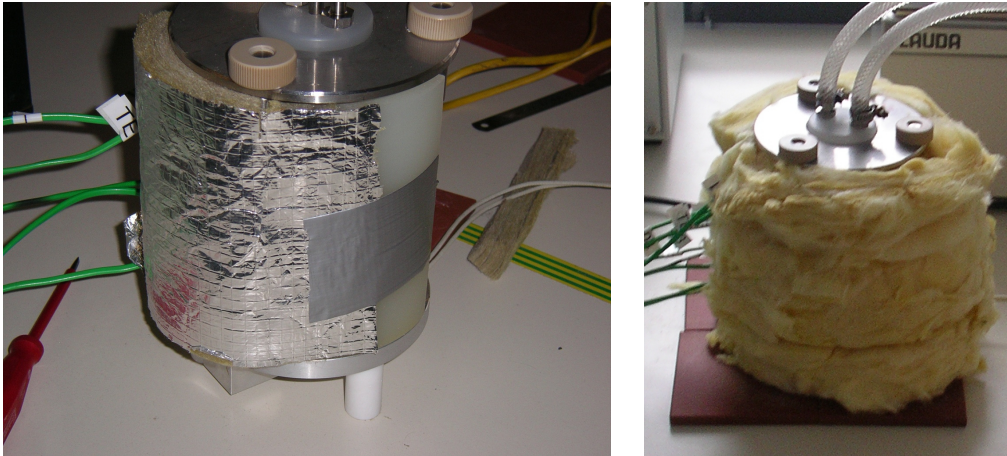


Fig. 3.4 Test cell with inner and outer thermal insulation¹¹

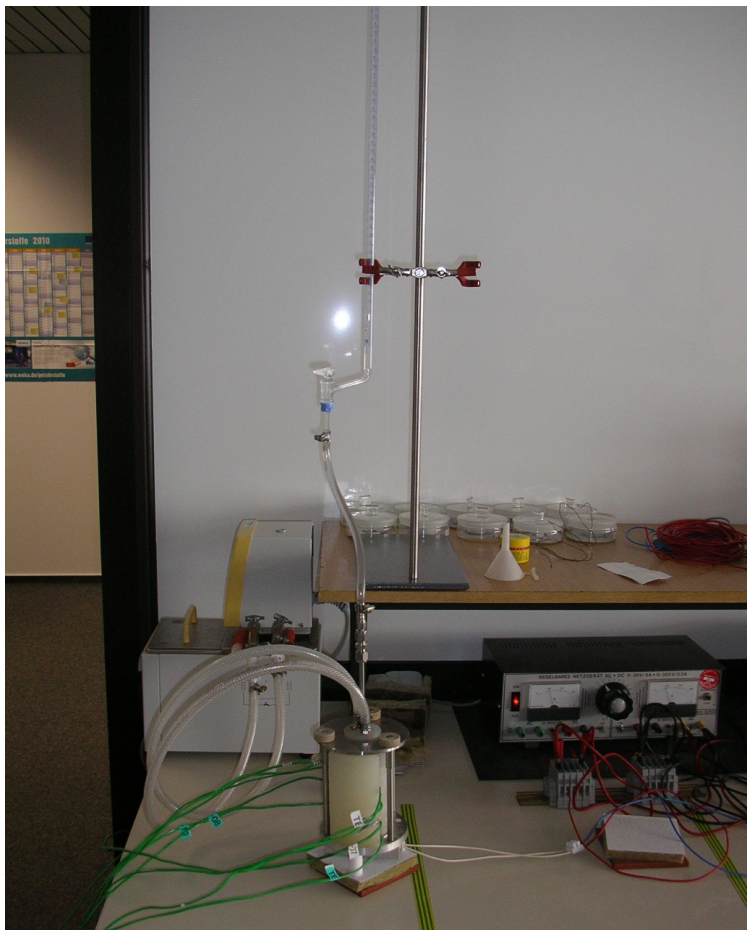


Fig. 3.5 Complete test set-up

¹¹ Inlet for the burette not yet installed

At an advanced stage of the experiment leakage had to be suspected due to an insufficient clamping. The components of the clamping were thus inspected and particularly the plastic nuts exchanged for stiffer metal ones. This change is referred to in the following as the switch from the original to the strengthened cell design.

3.4 Procedure

Two halves of a bentonite sample were compacted separately outside the test cell to cylindrical blocks of a target dry density of 1430 kg/m^3 . The blocks were carefully but quickly installed in the cell in order to avoid swelling after unloading from the compacting press, leaving an annulus to the rings after installation of about $1/10 \text{ mm}$. Then, the thermocouples were attached, insulation applied to the cell, and heating and cooling system as well as the burette for the water supply were connected. After switching on heating and cooling, the valve at the burette was opened and thereby inflow into the cell commenced. Note that it took about 6 hours to reach a temperature of $90 \text{ }^\circ\text{C}$ at the heated side of the bentonite.

After a pre-determined period of time the test was terminated and dismantled. The mechanical clamping was removed, and the sample cut at the edges of each ring producing slices with a clearly defined diameter. Due to swelling they had to be pressed out of the related ring manually as demonstrated in Fig. 3.6 before they could be weighed and dried. From a second weighing after drying, dry density and water content at the end of the test could be derived for a specific sample section.



Fig. 3.6 Pressing a bentonite disc out of a ring after cutting

To distinguish the tests from each other, each test is labelled in curly bracket by the referring test duration where “D” stands for days and “W” for weeks. Where tests had been repeated the sequence is defined by a following lowercase letter such as {2 D a} or {16 W b}.

3.5 Characteristic values

All in all, 26 tests have been performed with the original cell design and 7 tests with the strengthened cells. Characteristic values for the experiment were determined as the mean over all 33 tests. The resulting data are compiled in Tab. 3.1 together with the referring maximum and minimum values as well as the standard deviation. The data allow conclusions concerning the uncertainties introduced by the manufacturing process and thus help to identify samples with uncharacteristic deviations that may lead to misleading results.

Tab. 3.1 Characteristic values for the Experiment

Quantity	Unit	Maximum	Minimum	Mean	Standard deviation
Sample height	[cm]	9.70	9.45	9.54	0.06
Sample diameter	[cm]	5.00	4.94	4.99	0.01
Sample volume	[cm ³]	189.70	183.04	186.5	1.27
Dry mass	[g]	287.24	244.35	268.1	7.67
Initial mass (air dry)	[g]	306.44	271.12	295.8	5.86
Initial water content	[%]	18.87	2.22	10.6	2.26
Dry density	[g/cm ³]	1.546	1.335	1.435	0.038
Initial density	[g/cm ³]	1.643	1.481	1.586	0.028
Dry porosity	[-]	0.520	0.444	0.484	0.014
Initial porosity	[-]	0.410	0.262	0.333	0.023
Water uptake capacity	[g]	95.88	82.46	90.26	2.58
max. water content	[%]	38.94	28.71	33.78	1.88

The overall dimension of the samples was apparently quite nicely reproducible. The same applies essentially also to the majority of samples with respect to the other quantities. In some cases, however, a specific value shows a serious deviation from the mean of all data.

Some initial procedural inaccuracies have apparently lead to problems with the samples {1 D a}, {1 D c}, and {2 D a} whose dry mass amounts to 287.2 g, 244.4 g, and 249.9 g, respectively, thus showing significant deviations of the dry mass from the mean of 268.1 ± 7.67 g. Moreover, the initial water content of tests {1 D a} and {2 D a} differs by more 75 % from the mean value. The results of these three tests are therefore presented in the following but apparent deviations from the other tests will not be discussed. The characteristic values without these three tests are compiled in Tab. 3.2. Note that the standard deviation for the initial water content, the porosities and the water uptake capacity have dropped considerably by this measure from 2.26 to 0.40 %, 1.4 to 0.7 %, and 2.58 to 0.43 g, respectively.

Tab. 3.2 Characteristic values after removal of tests {1 D a}, {1 D c}, and {2 D a}

Quantity	Unit	Maximum	Minimum	Mean	Standard deviation
Sample height	[cm]	9.70	9.45	9.54	0.06
Sample diameter	[cm]	5.00	4.99	4.99	0.00
Sample volume	[cm ³]	189.70	184.81	186.74	1.11
Dry mass	[g]	280.81	263.34	268.5	3.62
Initial mass (air dry)	[g]	306.44	291.15	296.86	3.56
Initial water content	[-]	11.23	9.13	10.56	0.40
Dry density	[g/cm ³]	1.505	1.407	1.438	0.021
Initial density	[g/cm ³]	1.643	1.555	1.590	0.020
Dry porosity	[-]	0.494	0.458	0.483	0.007
Initial porosity	[-]	0.346	0.313	0.331	0.008
Water uptake capacity	[g]	92.76	85.52	90.16	0.43
max. water content	[%]	35.10	30.46	33.59	0.99

Where results are plotted over time, this is done in the dimension of days. Longer periods of time are more comprehensible if referring to weeks, though. In Tab. 3.3 the individual tests are therefore listed together with their running times in both dimensions to ease comprehension.

Tab. 3.3 Test labels, cell design, and running times

label	running time [days]	running time [weeks]	cell design	comments
{1 D a}	1		original	compromised
{1 D b}			original	
{1 D c}			original	compromised
{1 D d}			original	
{2 D a}	2		original	compromised
{2 D b}			original	
{2 D c}			original	
{4 D a}	4		original	
{4 D b}			original	
{7 D a}	7	1	original	
{7 D b}			original	
{2 W a}	14	2	original	
{2 W b}			original	
{4 W a}	28	4	original	
{4 W b}			original	
{8 W a}	56	8	original	
{8 W b}			original	
{8 W c}			strengthened	
{16 W a}	112	16	original	
{16 W b}			original	
{16 W c}			strengthened	
{32 W a}	224	32	original	
{32 W b}			strengthened	
{64 W}	448	64	original	
{72 W}	504	72	original	
{96 W}	678	96	strengthened	
{104 W a}	727	104	original	
{104 W b}	729		strengthened	
{134 W}	939	134	original	
{154 W}	1079	154	original	
{156 W}	1092	156	strengthened	
{160 W}	1120	160	strengthened	
{173 W}	1212	173	original	

3.6 Temperature distribution

At perfect thermal insulation of the cell, the temperature gradient would have been constant, showing a linear temperature decrease from the heater to the water inlet. The short-term tests of up to 8 weeks duration were chosen to check the efficiency of the thermal insulation by overlaying the results from thermocouples at the same location. The results are shown in Fig. 3.7.

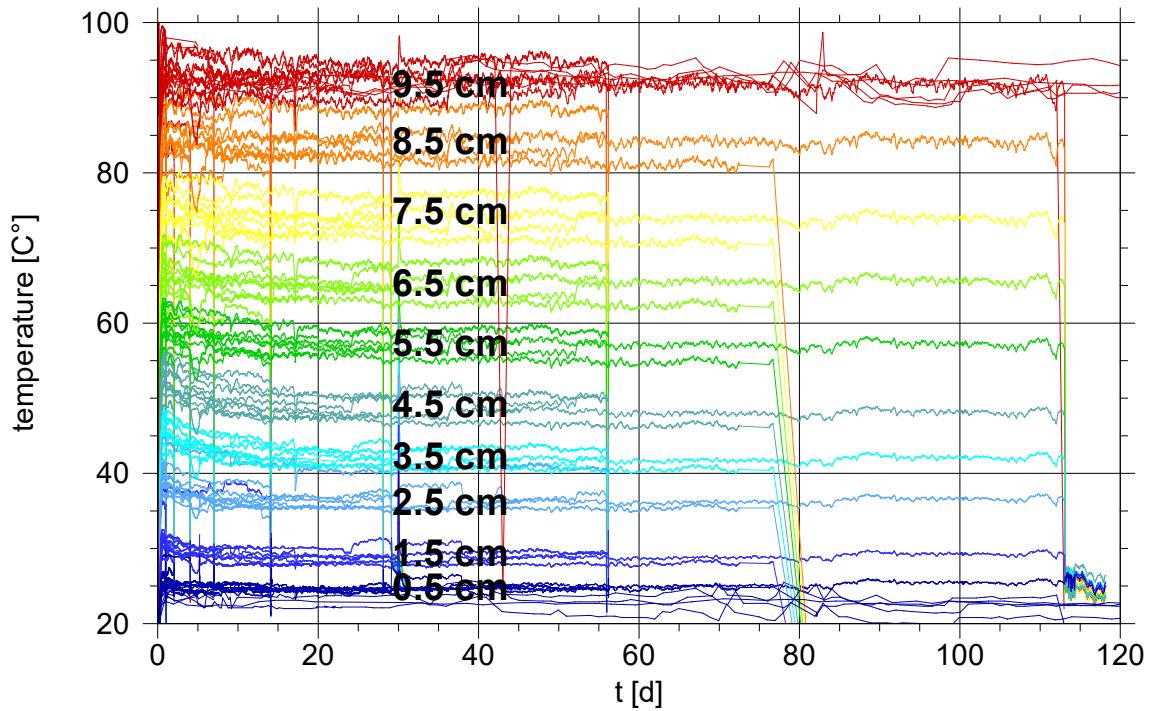


Fig. 3.7 Temperatures from the short-term tests at specific locations

Each individual temperature evolution appears to be sufficiently stable while there is a certain spread between temperatures at the same position. However, the ensemble of data indicates that the desired linear temperature change within the sample has been largely accomplished. The longer running tests thus went without a full set of sensors.

3.7 Results

3.7.1 Dynamics of the water content distribution

Visualisation of the results

All water content distributions measured with the original test set-up are shown together in Fig. 3.8. They are constructed by linear connections of the single water content values that are representative for the referring bentonite discs and are assigned to the bary-center of these discs.

Some distributions in Fig. 3.8 are plotted in dashed lines to indicate problematic tests that are not taken into further consideration. This concerns tests {1 D a}, {1 D c}, and {2 D a} because of non-conformance with the average samples characteristics (see section 3.5) and tests {64 W}, {134 W}, {154 W}, and {173 W} because the position of the wetting front is not consistent with less long running tests and thus suggest leakage during the test (see section 3.7.6). However, tests {72 W}, and {104 W} were prematurely terminated because of apparent discrepancies between measured water inflow and theoretical maximum water content. It can therefore not be excluded that those tests are compromised as well, and it must be conceded that even less long running tests might have been affected.

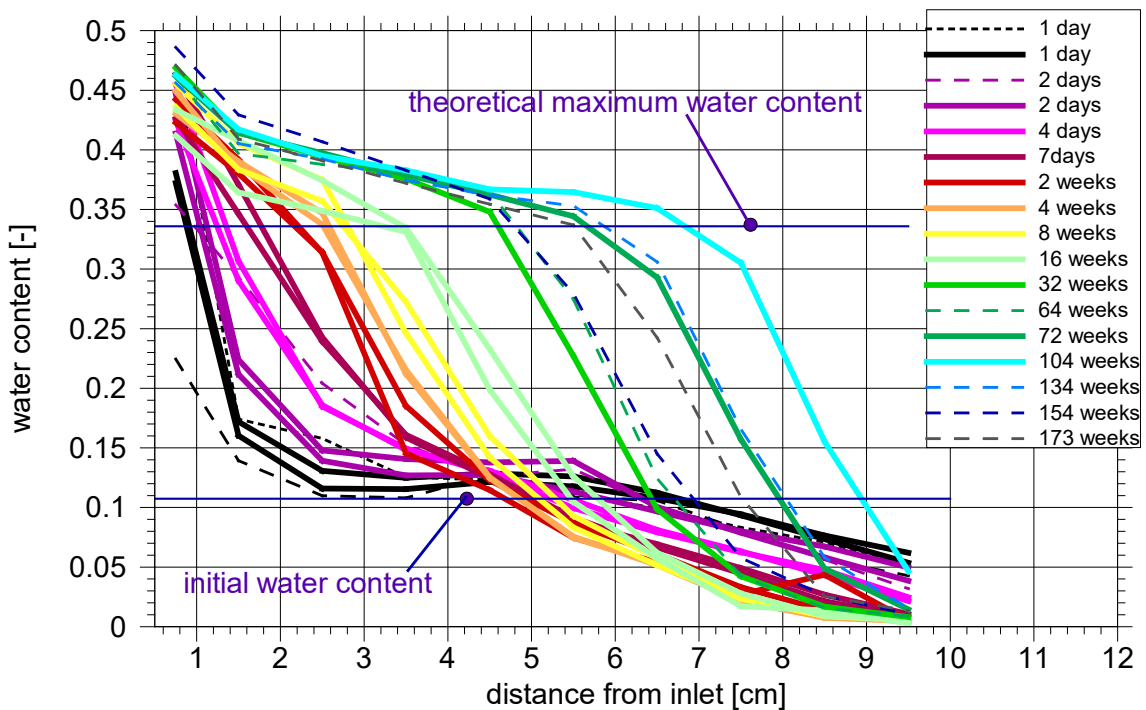


Fig. 3.8 Dynamics of the water content distribution with the original cell design

Reproducibility of the tests

Several tests were repeated to check the uncertainty to the derived water content distributions. In order to minimize the resulting effort this was done for tests up to a running time of 16 weeks. The results from tests with the same running time were averaged and plotted in Fig. 3.9. To indicate the difference between the original curves an uncertainty bar is included at the location of the data point.

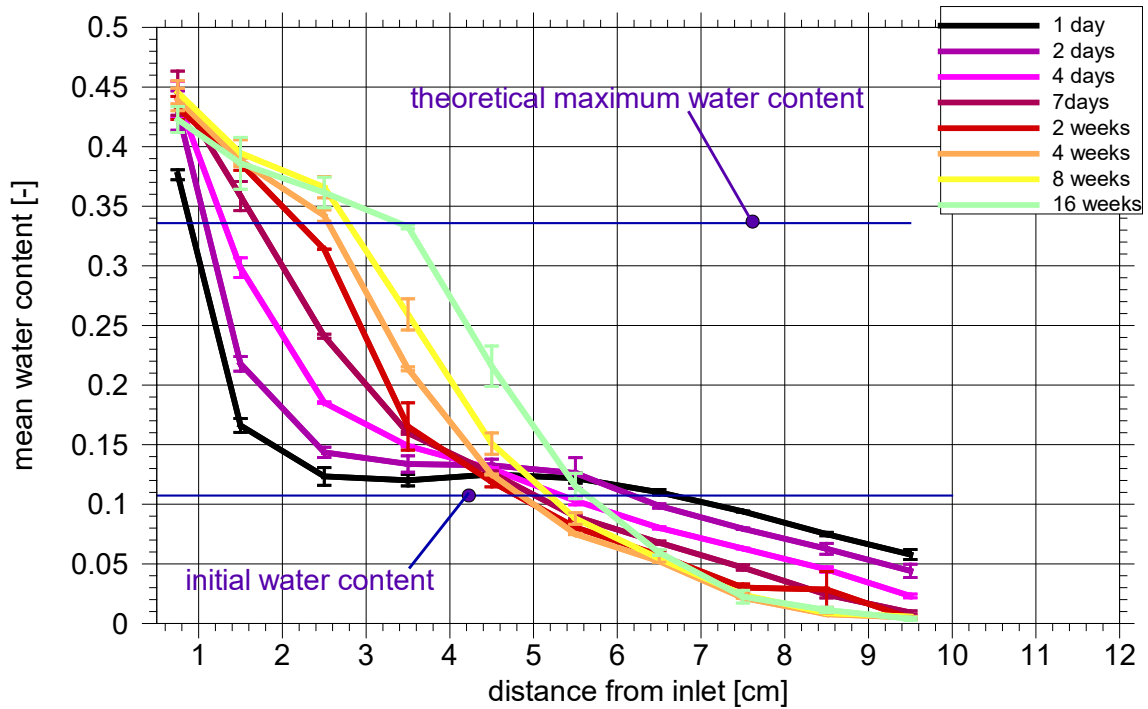


Fig. 3.9 Dynamics of the water content distribution; mean and deviations

A comparison of the related 160 data points yields the following statistics concerning the deviations Δw from the mean value:

- 2 cases with $\Delta w > 2\%$ ¹²
- 12 cases with $1\% < \Delta w < 2\%$
- 146 cases with $\Delta w < 1\%$

Based on these statistics the tests are considered to be fairly well reproducible. Further control tests were therefore not deemed necessary.

Water content at the water inlet

As discussed already in section 2 and in Appendix B it is expected that the water content at the water inlet reaches quickly full saturation. A theoretical maximum water content based on the initial dry density can be calculated. Taking the mean values for the dry

¹² Both cases were found in the tests with a running time of 16 weeks. In hindsight this might have already indicated an issue with the tightness of the cells.

density in the experiment from Tab. 3.2 yields a theoretical maximum water content of 33.6 %.

Measured, though, were water contents ranging from 41 % to 47 %, not counting the test results for just one day running time which agree very well with each other but show at the water inlet only a water content of 37 % and 38 %, respectively. As discussed in section 2, local swelling within the confinement of the test cell and thus increasing the local water uptake capacity is suspected to be the reason.

With a view to the somewhat lower water content values for tests {1 D b} and {1 D d} it has to be kept in mind that the referring water content is derived as a mean over a bentonite disc with a thickness of 5 mm. The data from /KRÖ 04/, however, leads to the conclusion that the thickness of the saturated zone is less than 4 mm. From the discussion in Appendix B it appears that it takes time in the order of a two weeks to reach a comparable saturation in the vicinity of the fully saturated zone. It is therefore assumed that the somewhat lower water content from tests {1 D b} and {1 D d} is the result of averaging over a domain that contains a completely saturated zone which has not yet reached the other side of the sample.

Development of the water content distribution with the original test set-up

The initial phase of water uptake and moisture re-distribution is illustrated by Fig. 3.10 where the mean water content distribution for running times of 1, 2 and 4 days are depicted. Clearly there is already some, if little, interaction of the drying and wetting processes even after only one day. The water content curve for one day is lowered at the hot end due to drying as expected and it intersects the level of the initial water content at 6 to 7 cm distance from the inlet. But anywhere inside these 6 to 7 centimetres it is increased above the initial water content by something like at least 2 %. Drying thus seems to affect essentially the whole sample in a very short period of time.

After 2 and 4 days running time, the intersection of the measured water content curves with the initial water content moves towards the inlet, indicating an increasing amount of vapour being produced by drying and driven towards the cool end of the sample. It has to be noted that in case of isothermal tests under similar conditions the wetting front did not reach more than 4 cm into the sample after 4 days /KRÖ 04/. In the present test, by

contrast, the wetting and the drying front are merged to an essentially continuous diffusion-like decreasing profile after 4 days.

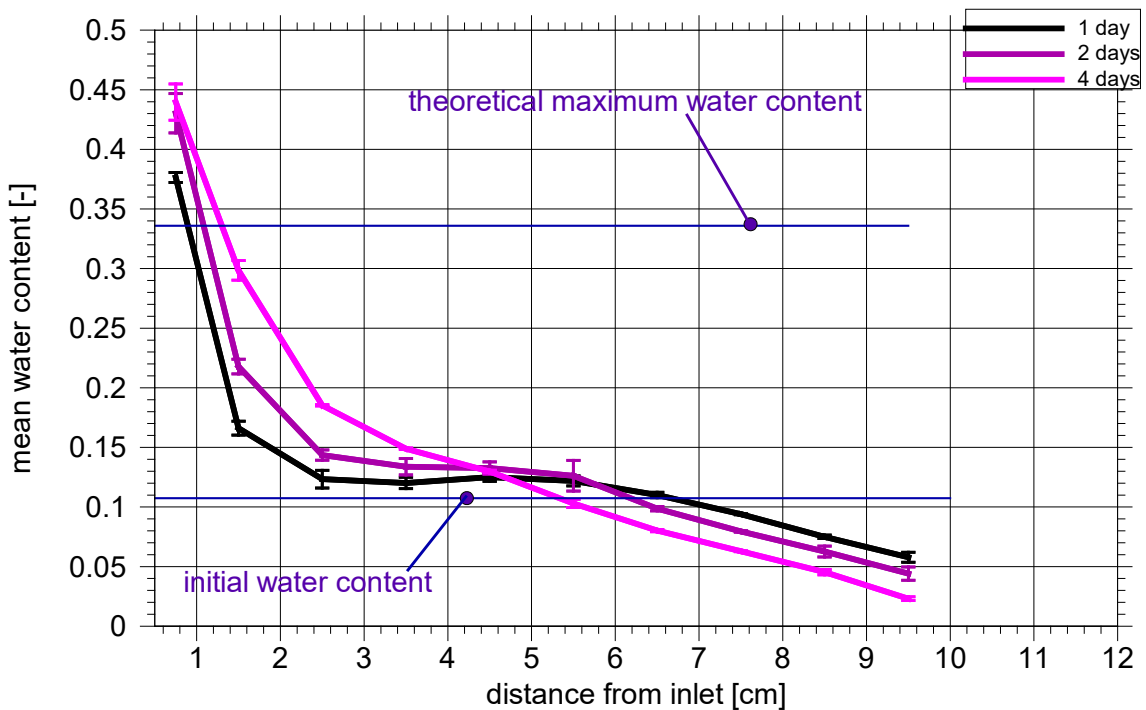


Fig. 3.10 Mean water content distributions for running times of 1, 2 and 4 days

After 7 days, however, the water content distribution begins to develop an inflection point leading to a considerable steepening of the wetting front as shown in Fig. 3.11. After 16 weeks the front has a length of only about 2 cm covering a drop from 35 % down to 10 % water content. Meanwhile, the water content in the dried part of the sample does not change significantly.

A compilation of all water content curves (mean distributions where applicable) is given in Fig. 3.12. Most prominent is the fact that the steep wetting front developed between 2 and 8 weeks running time is preserved over the rest of the test series. The upper end of the front relates in all cases closely to the theoretical maximum water content. After about 100 weeks the wetting front affects the heated side of the sample and begins to increase the water content even there.

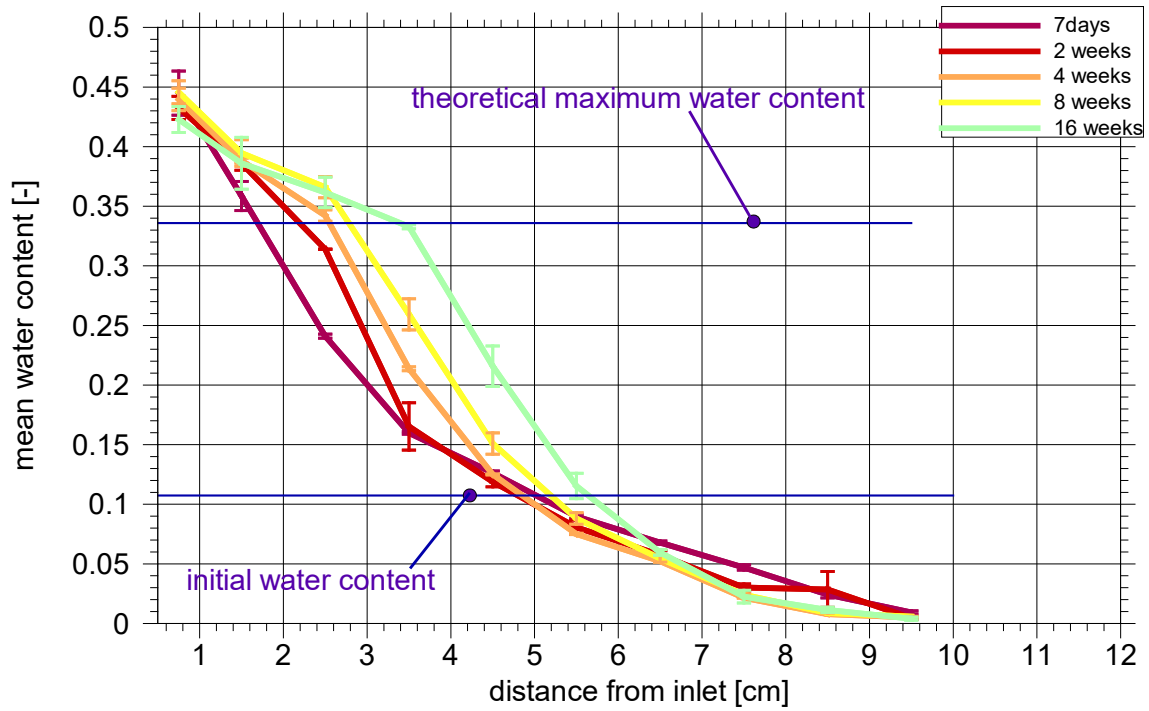


Fig. 3.11 Mean water content distributions for running times of 1 to 16 weeks

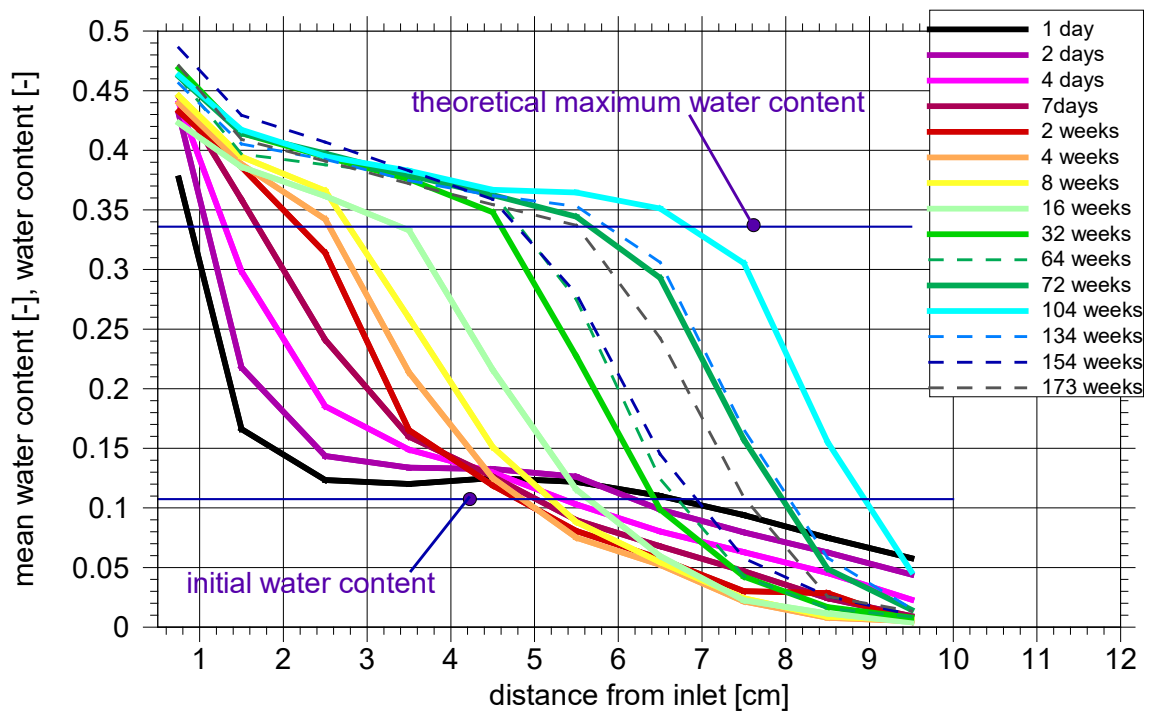


Fig. 3.12 (Mean) water content distributions for all running times

Also remarkable is the spreading of the zone with water contents exceeding the theoretical maximum value. This is in clear contrast to the isothermal tests where this zone was restricted to the first 4 mm over the whole experimental period covering 186 days (~26 weeks) /KRÖ 04/. Measurement errors as indicated in Fig. 3.10 and in Fig. 3.11 are too low to explain this phenomenon. Furthermore, it has to be noted that the water content distribution appears to converge in the range of very high values.

Results for the improved test set-up

Tests {8 W c}, {16 W d}, {32 W b}, {96 W}, {104 W b}, {156 W b}, and {160 W} were performed with the improved test set-up. Fig. 3.13 shows the determined water content distributions.

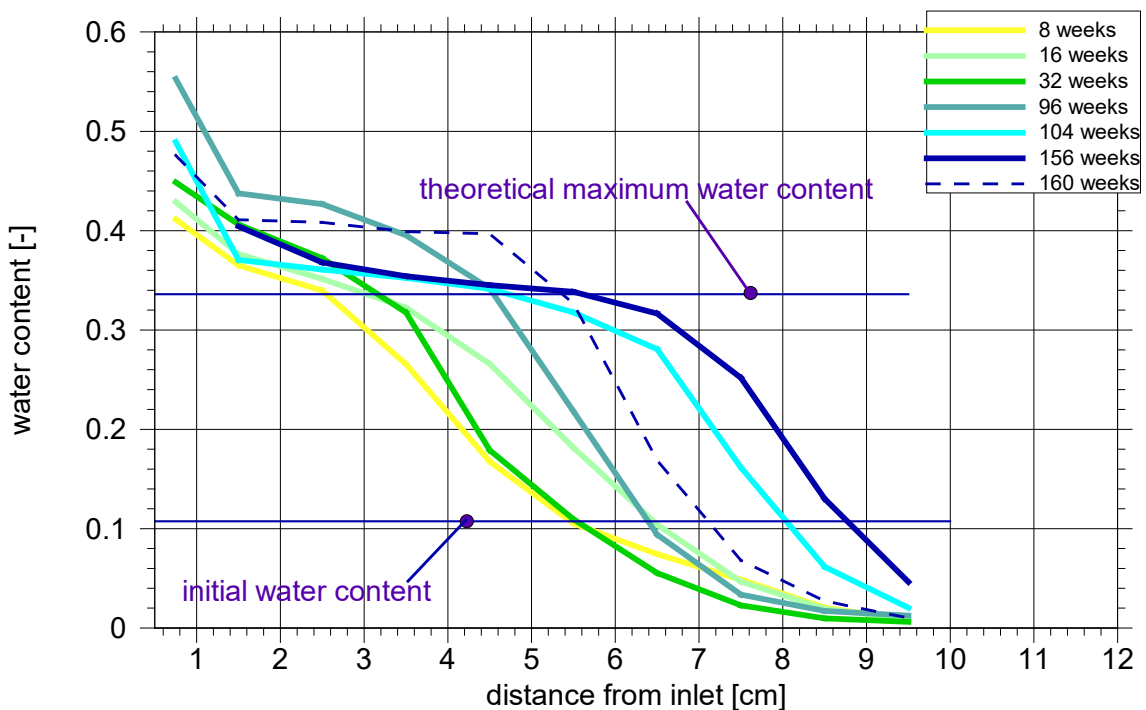


Fig. 3.13 Dynamics of the water content distribution with the strengthened cells

The water content curves for the shorter running times, namely 8 to 32 weeks, look qualitatively different from the longer running tests in that they show a wetting front with a lower angle of slope. The others have again the steep wetting front of the longer running tests with the original design and show in general the same characteristics (see Fig. 3.12). It can thus be speculated that the improved set-up withstood the developing

swelling pressure better than the original set-up but possibly only to a certain extent. After development of a certain swelling pressure, leakage apparently occurred again. This view is corroborated by the fact that the water content distribution of test {156 W} reaches significantly less deep into the sample than that of test {104 W}.

Comparison

Comparable water content distributions obtained with the old and the new cell design are compiled in Fig. 3.14 and discussed in the following.

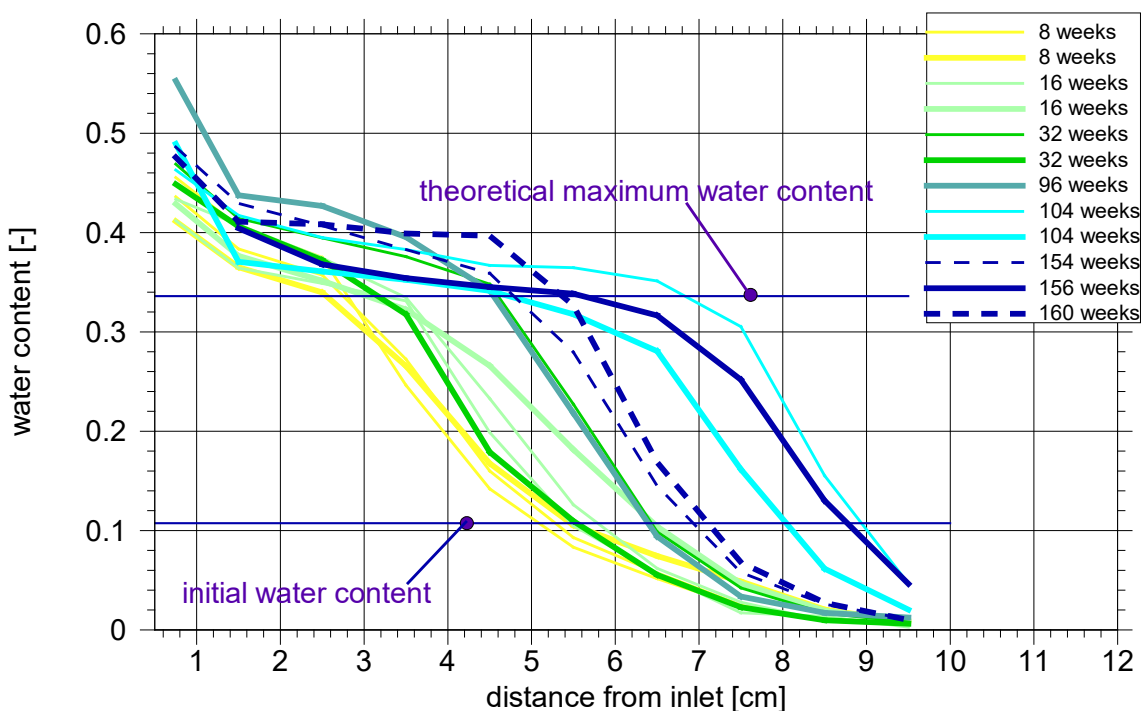


Fig. 3.14 Comparison of results with different cell types; thin lines – original design, thick lines – strengthened cells, dashed lines – obviously compromised tests

8 weeks running time (yellow lines): The obtained curves are basically the same.

16 weeks running time (light green lines): The results with the strengthened cell are also rather close to those of the original design but the wetting front shows a significantly lower slope.

32 weeks running time (green lines): While similar in slope, the wetting front in new test lies much closer to the inlet. Leakage has thus to be suspected.

96 weeks running time (turquoise line; strengthened cell only): Below the level of the theoretical maximum the curve is almost identical to the distribution obtained after 32 weeks with the original cell. Again, leakage has thus to be suspected.

104 weeks running time (cyan lines): The newly acquired distribution is lagging behind the curve from the original cell design by a quite similar shift as in the test over 32 weeks, indicating leakage again.

156 weeks running time (dark blue lines): By comparison to the 104-weeks curve the wetting front has consistently moved to right after 156 weeks. It also appears to be an improvement over the old 154- and 160-weeks curves as it exceeds them by far. However, the new 104-weeks curve has already been identified to be faulty and the new 156-weeks curve is also lagging behind the old 104-weeks curve suggesting leakage also in this case.

Further points to note are:

- Independent of the cell design, the length of the over-saturated zone is directly related to the beginning of the wetting front.
- Shorter test with the new design (8 weeks and 16 weeks) show less steep wetting fronts than all later ones. All later ones have basically the same slope.
- A steep wetting front appears to be related to inconsistent results
- Assuming that the inconsistency stems from leakage it might be assumed that the steep wetting front is actually an indication for leakage

3.7.2 Mean water content at end of test

- Data scatter for shorter running times ($t < 110$ d) surprisingly low
- Serious scatter later on
- Fast increase at the beginning
- After 400 days seemingly reaching sort of a stationary value
- The switch to the strengthened cell had apparently little impact on the total water uptake

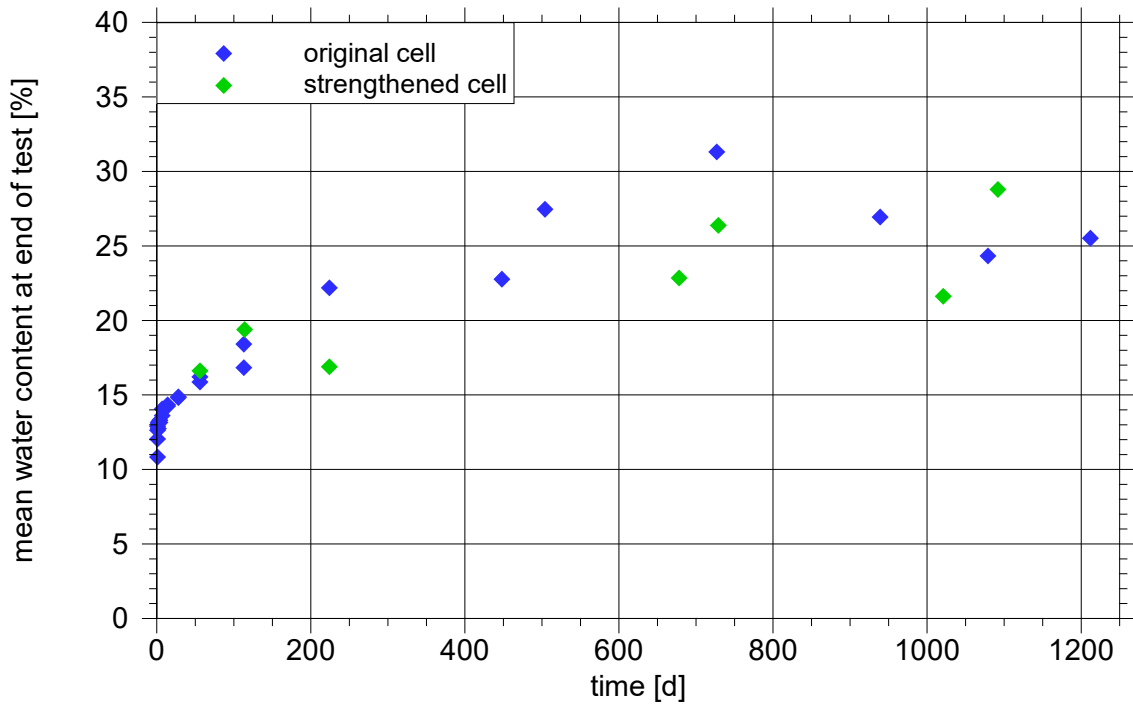


Fig. 3.15 Mean water content of the whole samples at end of test

3.7.3 Water uptake dynamics

While the individual time series of water uptake over time for each test show seemingly a clear trend, there is quite some scatter between the time series'. Fig. 3.16 shows the evolution of water uptake from the burette for the first 15 days of running time. The tests {1 T d}, {2 T c}, and {104 W a} are apparently off-trend and therefore marked in red in the graph. Data for the strengthened cells are marked in green showing that the switch in design had little impact on the total water uptake.

Except for the data marked in red, the evolution of data points appears to be qualitatively the same. But there seems to be a vertical random shift between the time series resulting in a bandwidth of about 8 cm³. Some time series actually started with an off set. Motivated by these observations it was attempted to shift the time series' in such a way that they formed a narrower band starting at the origin. The required shifts for each test are compiled in Tab. 3.4, the resulting plot is depicted in Fig. 3.17.

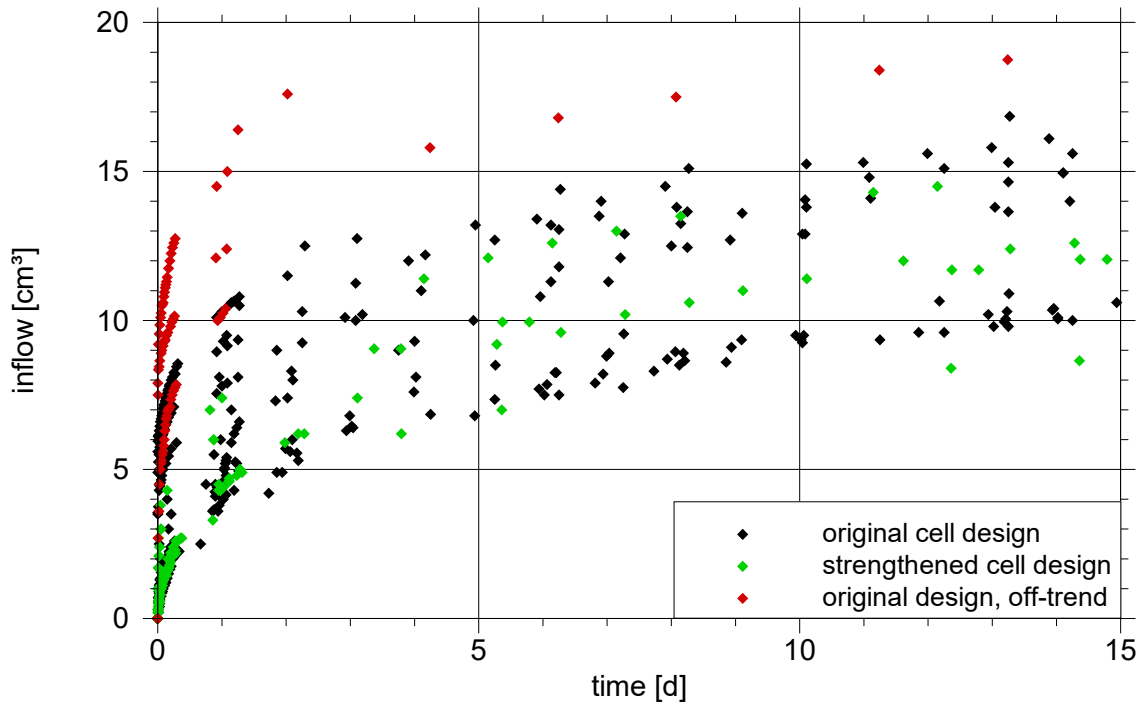


Fig. 3.16 Evolution of water uptake from the burette; run time < 15 d

Tab. 3.4 Vertical shift applied to the original inflow data

Duration	Run	Addend to inflow	Comment	Duration	Run	Addend to inflow	Comment
1 D	a	0	compromised	8 W	a	+1.5	
	b	-5			b	-3.5	
	c	-5	compromised		c	-3	strengthened
	d	-4					
2 D	a	-1	compromised	16 W	a	-3.5	
	b	-5.5			b	-2	
	c	-8			c	0	strengthened
4 D	a	-2		32 W	a	+2	
	b	0			b	0	strengthened
7 D	a	-2		64 W		+1	compromised
	b	0		72 W		+2.5	compromised
				96 W		0	strengthened
2 W	a	-4		104 W	a	-7	compromised
	b	+1			b	0	strengthened
4 W	a	+1.5		134 W		-5	compromised
	b	+2		154 W		-2	compromised
				156 W		0	strengthened
				160 W		+3	strengthened
				173 W		-1.5	compromised

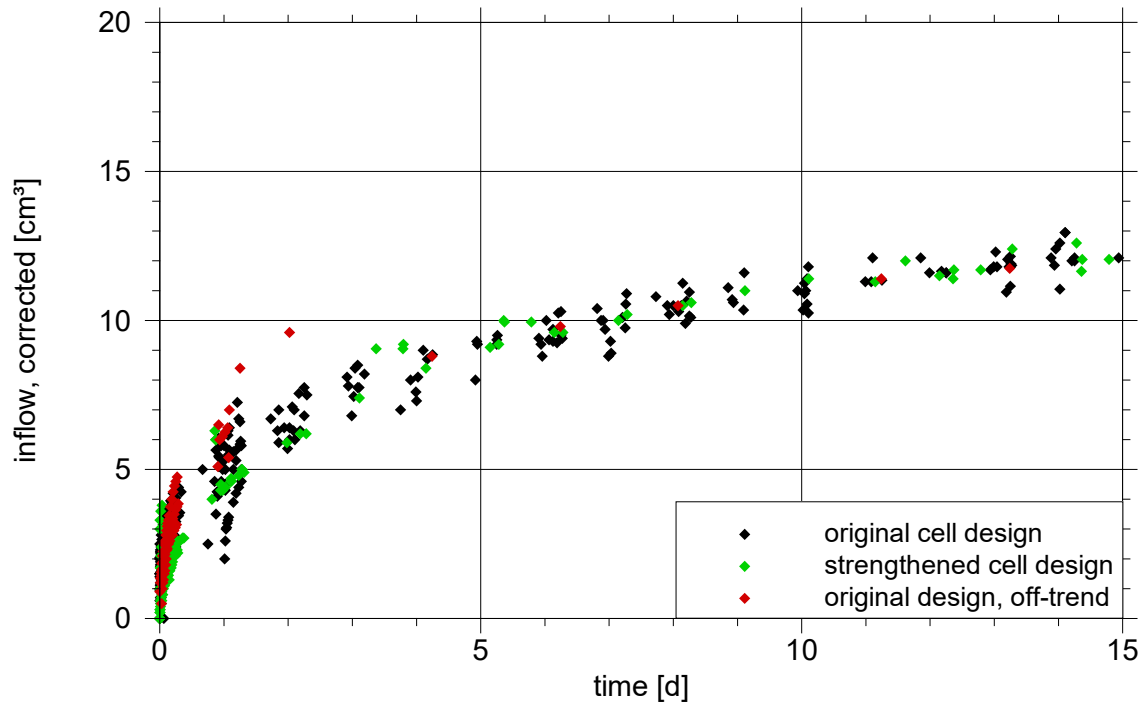


Fig. 3.17 Evolution of water uptake from the burette, corrected; run time < 15 d

Fig. 3.17 shows that a much higher degree of consistency can be achieved for the first 2 weeks as almost all curves fit into a much narrower bandwidth. The trends of {1 T d} and {2 T c} remain to be still off, though. Note that of the seven tests with strengthened cells only two required a correction.

Next, the inflow data over a period of 4 months were looked at. The uncorrected data are shown for up to 125 days in Fig. 3.18. The spread of about 8 cm³ between most curves as seen in the early data continues over this period.

Inexplicable jumps can be observed in two curves, namely {72 W} and {134 W}. Since the subsequent evolution of the curves seems to be in line with the other time series' these jumps indicate an unknown event rather than a single reading error.

While the uptake curves at early times are characteristic for a diffusion-like process they do not seem to converge later on. Instead, they increase more or less linearly. The resulting inflow rate has thus been essentially constant suggesting leakage from the test set-up

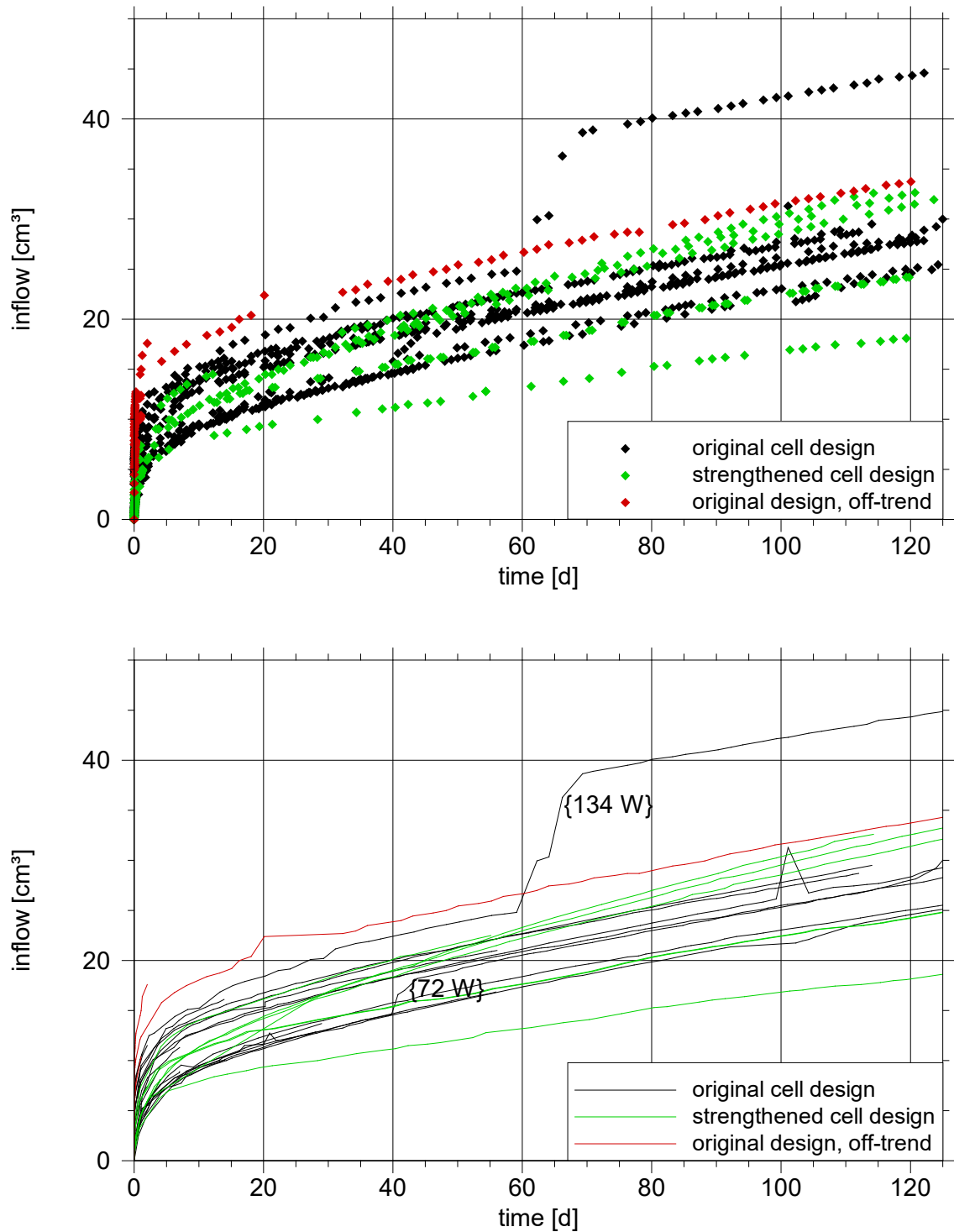


Fig. 3.18 Evolution of water uptake from the burette; run time < 125 d; symbols and lines

It had been the hope that the correction that had successfully applied to shift the time series' at early times inside a quite narrow band would do the same to the later data.

However, after about 20 days the subsequent course of the curves is divergent (see Fig. 3.19). The basically linear course of the curves can be tracked back to a point somewhere between 20 and 40 days. Tests with the original as well as the strengthened cell design are affected.

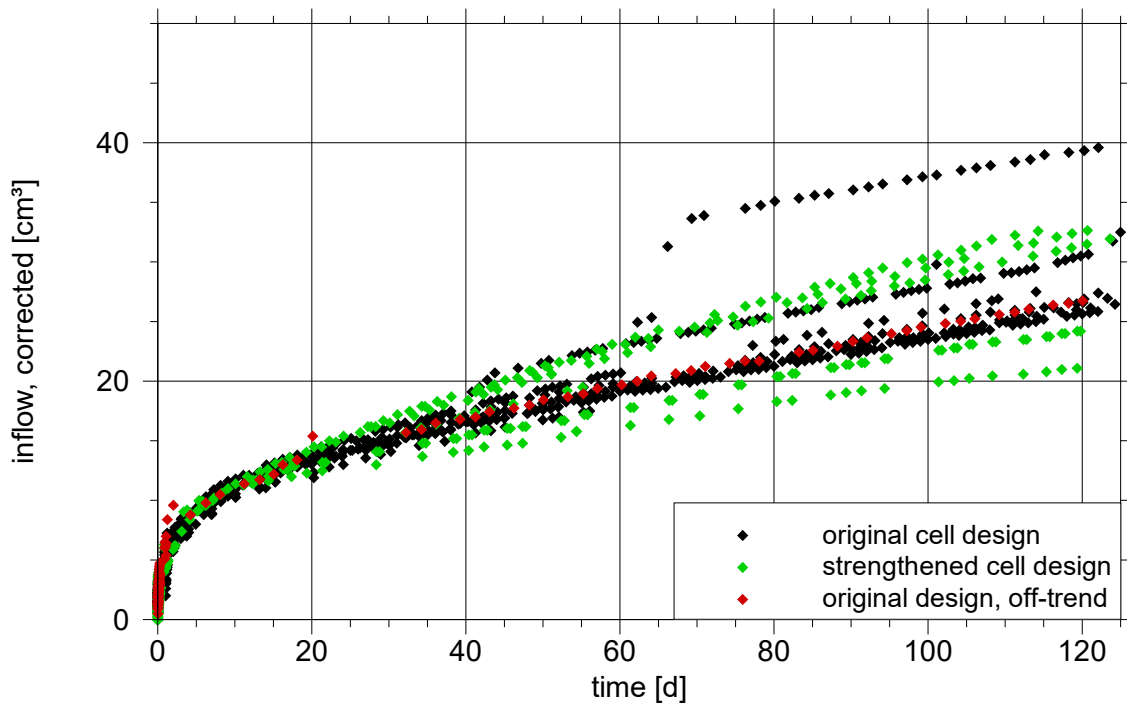


Fig. 3.19 Evolution of water uptake from the burette, corrected; run time < 125 d

Beyond about 400 days, the curves become increasingly divergent as shown in Fig. 3.20. Further even if very small jumps can also be seen in {154 W} and {173}. More important, though, may be the slight increase of the slope as for tests {104 W b}, {154 W}, {156 W} and {173} for there is no appreciable reason for this behaviour under a normal evolution of the test. Non-convergence and linear increase can be observed further on.

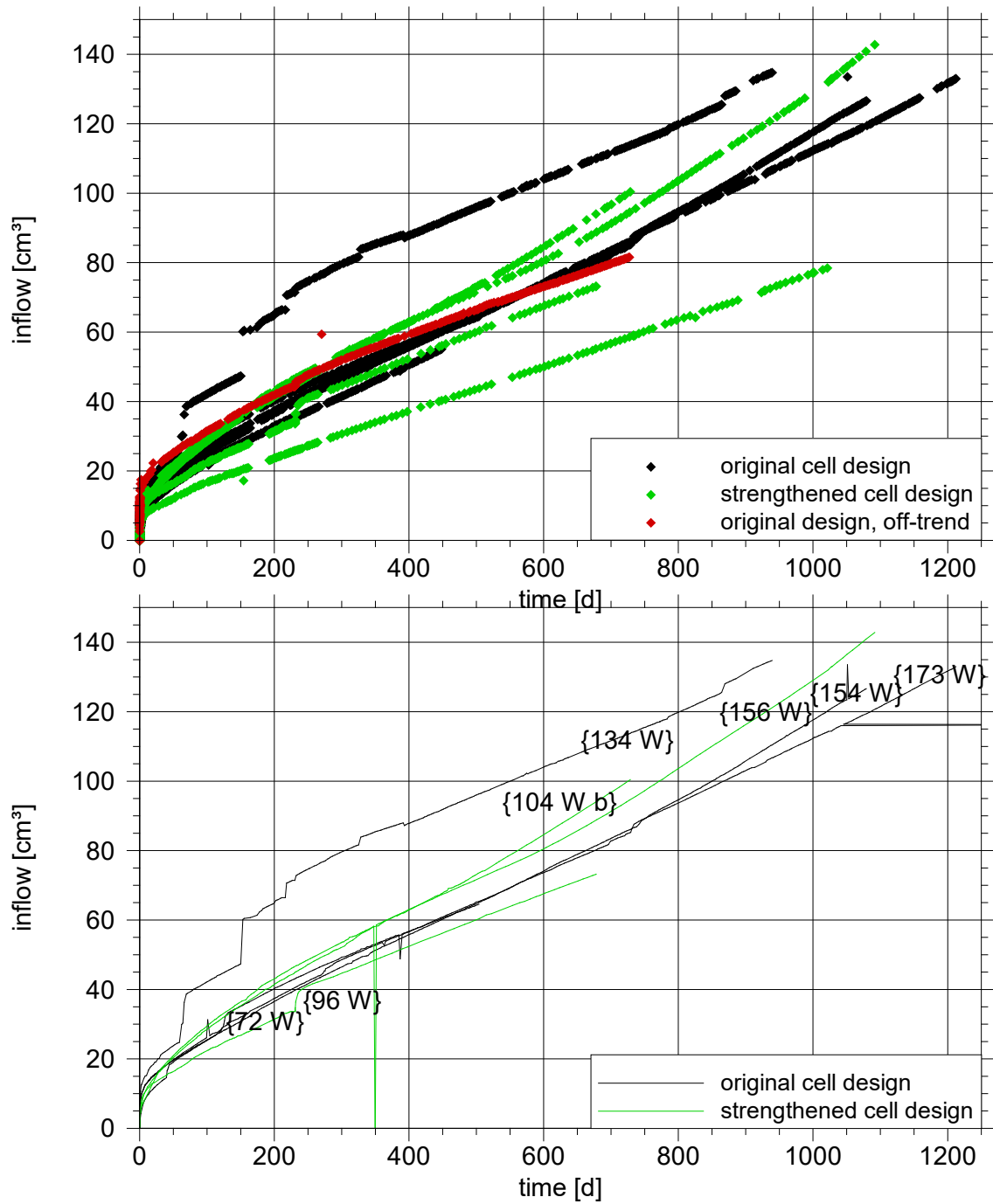


Fig. 3.20 Evolution of water uptake from the burette; run time < 1250 d

The correction of the time series' that helped to converge the inflow rates of different tests to a reasonably narrow bandwidth within a timeframe of 2 weeks has apparently very little impact in the long run. The data up to about 450 days or 64 weeks look slightly

more coherent in Fig. 3.21 than in the top plot in Fig. 3.20. For all longer running tests the resulting curves form basically the same pattern.

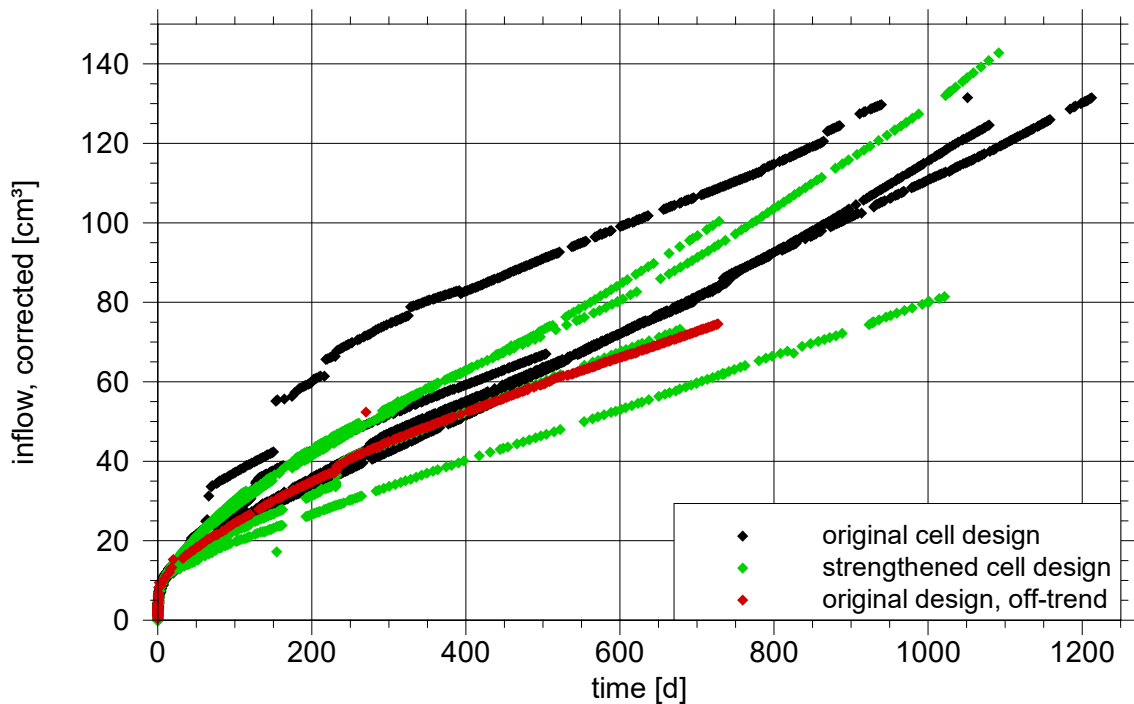


Fig. 3.21 Evolution of water uptake from the burette, corrected; run time < 1250 d

3.7.4 Total water uptake

The total amount of water taken up during a test is plotted in Fig. 3.22 over the running times of less than 250 days and in Fig. 3.23 for all tests. Quite some scatter can be observed in the data. An actual curve would probably appear to be bended in case of shorter-term tests. In the long run (running times ~ 100 to 200 d), however, the relation seems to be linear. The switch to the strengthened cell had apparently little impact on the total water uptake at that.

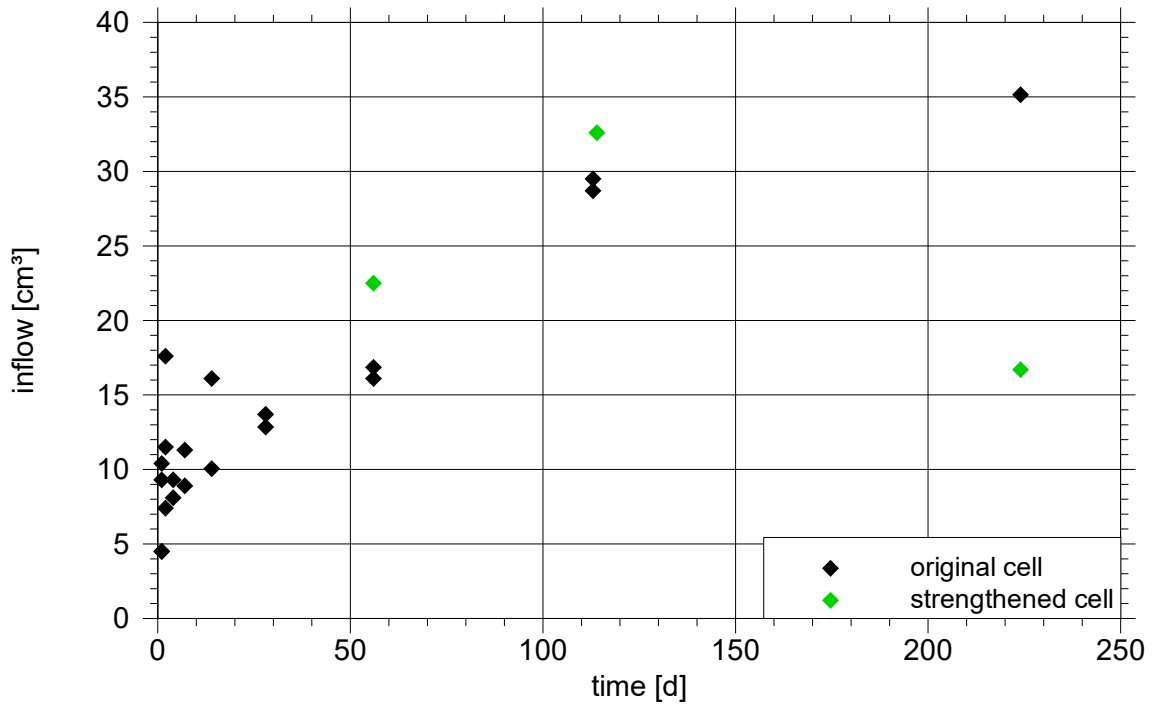


Fig. 3.22 Cumulated water outflow from the burette at the end of test; run time < 250 d

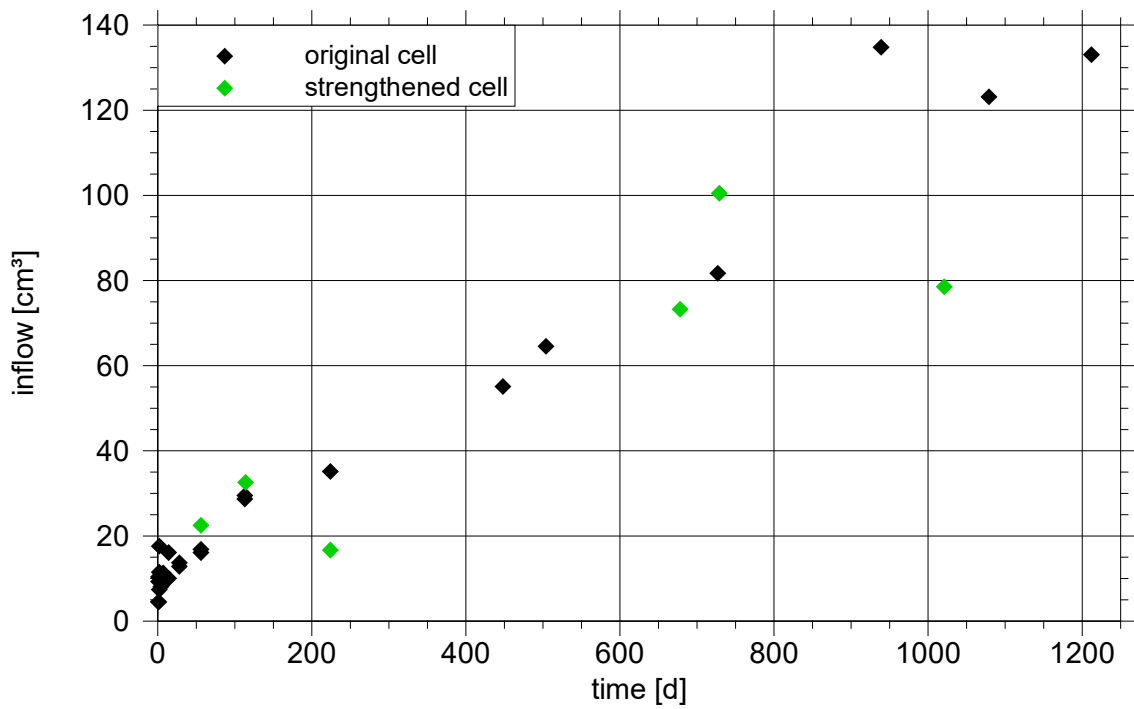


Fig. 3.23 Cumulated water outflow from the burette at the end of test; all run times

3.7.5 Dry density

Drying the bentonite discs of 1 cm thickness – 0.5 cm at the water inlet – allows for an estimation of the local dry density. Rather high uncertainties are introduced, however, by cutting off the discs because, firstly, cutting needs to be fast and is, secondly, done quite roughly with a scraper. The range of the individually derived dry densities can therefore be expected to be rather high as shown in Fig. 3.24.

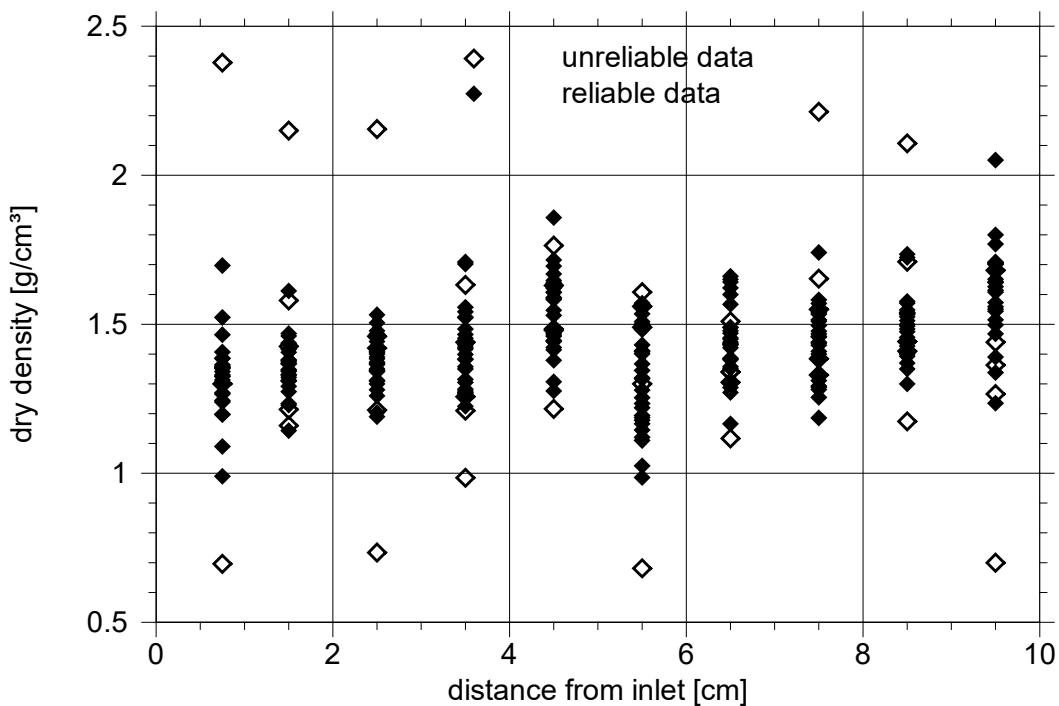


Fig. 3.24 Dry density distribution of all tests

A much clearer picture can be derived by averaging all dry density values for one particular location. The mean of all discs at a specific location are depicted in Fig. 3.25. A jump in density between 4.5 to 5.5 cm from the water inlet can be observed in this figure covering the contact area between the two blocks that form the whole sample. Averaging the density at the contact using the two neighboring values fits nicely in the overall trend, though. The density is increasing with distance to the water inflow as in isothermal tests indicating swelling at the inlet. However, the thickness of the swelling zone is much higher than in the isothermal tests.

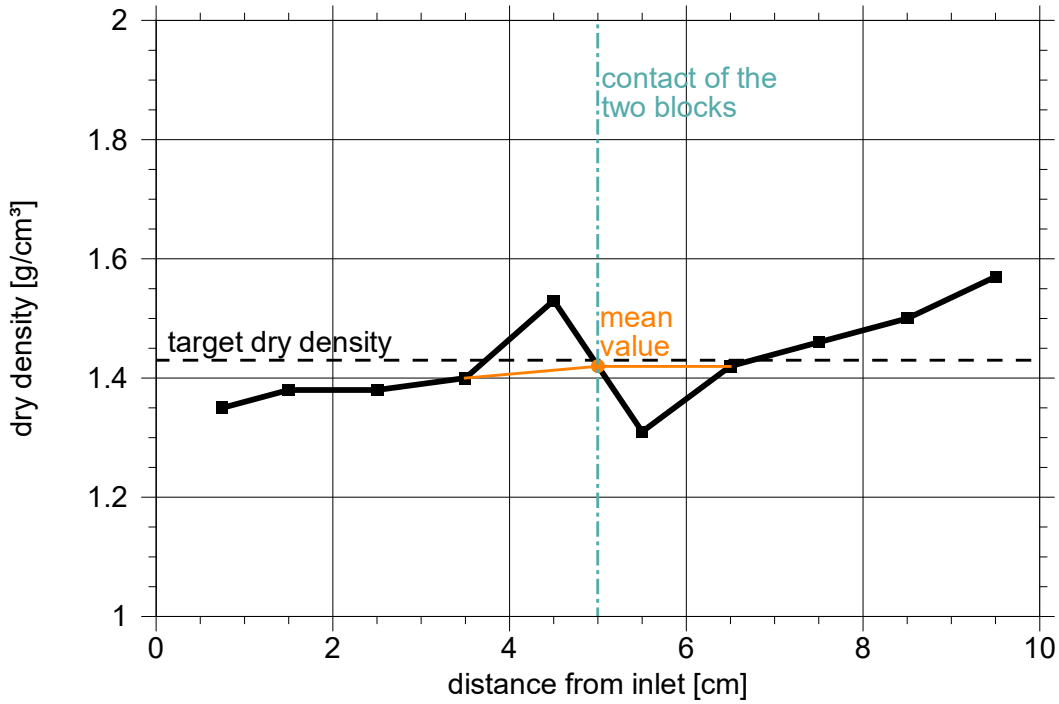


Fig. 3.25 Mean dry density distribution

3.7.6 Checking consistency of water uptake data

There are two ways of checking the measured and derived data for water uptake at the end of a test (see Appendix B) for internal consistency. The first check is a simple balance of mass saying that the amount of water entering the bentonite m_{in} sample must be equal to the mass of water Δm gained by the sample.

$$m_{in} = \Delta m \quad (3.1)$$

m_{in} - amount of water entering the bentonite [kg]

Δm - mass of water gained by the sample [kg]

The amount of water entering the bentonite is obviously the difference between the mass of water leaving the burette $m_{burette}$ and the mass of water m_{loss} contained in the volume between burette and sample, i.e. tubing, sinter plate and filter paper.

$$m_{in} = m_{burette} - m_{loss} \quad (3.2)$$

$m_{burette}$ - amount of water water leaving the burette [kg]

m_{loss} - mass of water mass of water between burette and sample [kg]

The amount of water gained by the sample ensues from the initially present amount of water m_{w0} in the sample and the amount of water at the end of the test m_{we} :

$$\Delta m = m_{we} - m_{w0} \quad (3.3)$$

m_{w0} - initial amount of water [kg]

m_{we} - amount of water at the end of the test [kg]

In terms of measurable quantities, the balance equation (3.1) can be written as

$$m_{w0} + m_{burette} - m_{loss} - m_{we} = 0 \quad (3.4)$$

Ideally, the summands on the left-hand side of eq. (3.4) should add up to 0. A positive value in eq. (3.4) means that inflow outweighs the amount of water determined at the end of test or in other words leakage from the test cell. Checking consistency by means of condition (3.4) is possible only a posteriori. The results for each test are compiled in Tab. 3.5. Results within a margin of ± 5 g are highlighted in green, above 5 g in red and below -5 g in blue.

By and large, the original test cells seem to work nicely up to running times of 32 weeks even if the deviation of the values at 16 weeks appears to be a little bit large. The impression is somewhat better with the data from the strengthened test cells but as in the tests with the original design something seems to happen after 32 weeks. Violation of eq. (3.4) is considerable for tests between 64 and 104 weeks with the original cells but increases significantly for longer running times. With the strengthened cells it is already strong beginning with 96 weeks. Evaluation of eq. (3.4) thus indicates that the

strengthened cells have performed somewhat better but apparently all tests with running times of 96 weeks and more have experienced considerable leakage.

Tab. 3.5 Evaluation of eq. (3.4) for all tests

test		time	eq. (3.4)
original test design			
1 T	a	1	-24,1
	b	1	1,7
	c	1	-3,7
	d	1	2,2
2 T	a	2	18,0
	b	2	-1,5
	c	2	7,3
4 T	a	4	-1,1
	b	4	-2,5
7 T	a	7	-2,3
	b	7	-3,1
2 W	a	14	2,9
	b	14	-3,9
4 W	a	28	-3,0
	b	28	-0,9
8 W	a	56	-1,7
	b	56	-2,6
16 W	a	113	7,9
	b	113	8,3
32 W	a	224	0,5
64 W	a	448	18,3
72 W		504	14,2
104 W	a	727	19,2
134 W		939	85,5
154 W		1079	87,4
173 W		1212	82,1
strengthened test cells			
8 W	c	56	1,7
16 W	d	114	-0,3
32 W	b	224	-2,7
96 W		678	65,9
104 W	b	729	52,0
156 W		1091	90,3
160 W		1120	39,8

The second check involves the maximum amount of water $m_{w\max}$, that can be accommodated by the sample. This value is simply a function of the mean dry density $\bar{\rho}_d$ and must always be larger or equal to the amount of water at the end of the test.

$$m_{w\max}(\bar{\rho}_d) \geq m_{we} \quad (3.5)$$

$m_{w\max}$ - maximum amount of water [kg]

$\bar{\rho}_d$ - mean dry density of the sample [kg/m³]

The ratio of both values yields the mean degree of saturation

$$S_{mean} = \frac{m_{we}}{m_{w\max}(\bar{\rho}_d)} \quad (3.6)$$

S_{mean} - mean degree of saturation [-]

which – according to eq. (3.5) – should not exceed a value of 1. Subtracting the initial amount of water m_{w0} in the sample on both sides of eq. (3.5) says that the inflowing mass of water m_{in} should not exceed the remaining available space for water

$$m_{w\max} \geq m_{w0} + m_{in} \quad (3.7)$$

Condition (3.5) in the form of eq. (3.7) is most useful to check for leakage without terminating the test, as in case of leakage condition (3.7) will be violated with time. Had it been applied earlier it might have led to a second modification of the test cells and would at least have saved a lot of testing time.

4 Conclusions and recommendations

4.1 Re-saturation under limited access to water

Detailed data about the water uptake dynamics of compacted bentonite at the bentonite-rock contact under a limited water supply rate from the rock (LWSR-conditions) have been gathered experimentally. The evolution of the water content was measured varying the inflow rate over a fixed period of time as well as varying the running time of the tests at a fixed inflow rate. The obtained water content distributions are characteristic for diffusive water migration.

The evolution of the water content distribution under LWSR-conditions is decidedly different from the water content evolutions previously explored in other tests under unimpeded access of the bentonite to water (UA-conditions) or to vapour-saturated air. Forming of the narrow fully saturated zone at a bentonite-water contact is a hallmark for the re-saturation under UA-conditions as discussed in detail in this work. By contrast, this phenomenon had not been observed when vapour-saturated air re-saturates the bentonite.

The fully saturated and locally swollen zone observed under UA-conditions does not appear during early stages of the present tests with water uptake under LWSR-conditions. The theoretical approach assumes a switch from LWSR- to UA-conditions after reaching saturation at the inflow boundary concomitant with a quick development of the fully saturated zone. The observed evolution of a peak in the water content curves at the inflow boundary in the longer running tests is therefore most interesting since it indicates the transition from the LWSR- to UA conditions that is expected according to the theoretical approach.

But apparently, the highly saturated zone starts to develop even before full saturation at the boundary is reached. The transition is not a quick switch as theoretically assumed but takes considerable time which indicates an additional effect or process close to the inflow boundary that is not yet identified. It can be speculated that the time that is required to develop the narrow saturated zone relates to the ratio of inflow to the flow rate at which the water is further distributed inside the bentonite. Investigating the phenomena concerning the fully saturated zone more closely might therefore increase the process

understanding in general and additionally help to explain why this zone, once developed, persists with time.

The EVD-approach for numerical modelling of water uptake by confined compacted bentonite, adopted and qualified for UA-conditions, has been advanced on a theoretical basis to cope also with LWSR-conditions. After calibration of the model, experimental and numerical results were compared. Matching numerical results and measurements to a reasonable degree was possible within acceptable parameter ranges and with one and the same parameter set, thereby backing up the assumptions of the EVD-concept in general and the considerations about the specific aspects of uptake under LWSR-conditions in particular. Conceptualisation, modelling and measurements thus provide a consistent framework for describing the re-saturation of a bentonite buffer at repository-relevant flow rates even if the some of the effects or processes close to the inflow boundary are not yet fully understood and thus not captured in the advanced framework of the EVD-model.

4.2 Final state of re-saturation under a thermal gradient

All in all, 33 uptake tests with varying running times up to 173 weeks against a high temperature gradient have been performed, 26 test in the originally devised set-up and seven tests in cells that had been strengthened against the swelling pressure exerted by the wetted bentonite samples. The experimental set-up was optimised towards a linear temperature gradient along the cell axis. Repeating all tests up to a running time of 16 weeks showed a good reproducibility of the measurements.

The target of finding out about the steady-state conditions at the end of re-saturation against a temperature gradient was missed, though. It had been expected that water uptake would have come to an end under these conditions, but an end of water uptake was not reached in any of the tests. Instead of converging towards zero, the observed uptake rate became even more or less constant after a few months.

In the longer running tests the amount of water entering the cells was exceeding the capacity of the bentonite for taking up water significantly while the samples proved to be far from fully saturated. This observation indicates leakage from the cells, probably in form

of water vapour. Such a leakage could have formed if the swelling pressure had been underestimated while constructing the cells and the rings had been separated.

Two unexpected features were found in the evolution of the water content distribution, firstly the forming of the steep moisture front, and, secondly, the apparently steady growing of the highly saturated zone at the water inlet. The latter is a clear indication of swelling which underpins the idea of a swelling pressure induced leakage.

Several measures were derived to encircle the time when leakage might have commenced:

- (1) the change from a smooth to a steep wetting front (section 3.7.1),
- (2) the change to a constant outflow rate from the burette (section 3.7.3),
- (3) the total amount of water leaving the burette (section 3.7.4), and
- (4) the a posteriori comparison of inflow and total water content (section 3.7.6).

Judging from criterion (1) leakage would have occurred between 2 and 8 weeks for the original cells and 16 to 32 weeks for the strengthened cells. Criterion (2) leads to 20 to 40 days (3 to 7 weeks), criterion (3) to 100 to 200 days (14 to 28 weeks), and criterion (4) to 8 to 16, possibly 32 weeks for the original cells and 32 and 96 weeks for the strengthened cells. While the spread of these data is considerable the criteria agree at least with the conclusion that essentially all tests exceeding a running time of 32 weeks were probably compromised by leakage. Note that the difference between data from the original test design and the strengthened cells confirms an increased effectiveness of the strengthened cell even if not to a satisfactory degree.

While the location(s) for such a leakage cannot be determined directly it seems to be likely that it would be rather in the zone of high swelling than in the dried-out zone since friction at the ring walls would be higher in the wet, swollen part. This would explain the steep moisture front because vapour would be drawn from the moisture front towards the leak(s).

Under such conditions the monitoring of the water uptake leads to the conclusion that a dynamic equilibrium between water uptake and water loss via leakage could have been reached when the uptake rate became constant. The measured water content profiles would then not be representing the uptake conditions at the time of test termination but at a much earlier and rather difficult to determine point in time. With some effort the ob-

tained water content profiles might at least be related to a certain time span with the help of the water uptake curves. However, since neither locations nor numbers of leaks are known this work would be rather pointless.

Further insight could have been gained by numerical modelling of this experiment. It has to be assumed, though, that the forming of leaks is rather a local phenomenon than an axisymmetric one. Modelling would therefore have required a fully three-dimensional treatment of the problem while the code VIPER /KRÖ 11/ which had been foreseen for modelling is not yet far enough developed to do so. Modelling the experiment was therefore abandoned.

The final conclusion from this exercise sounds a bit trivial but is to be taken seriously: the experimental effort to provide conclusive data about the end state of water uptake against a significant thermal gradient is considerable. Unfortunately, the work presented here has just added to several other not successful attempts. The construction of a fully operative test cell thus remains to be a challenge.

References

- /AKE 07/ Åkesson, M., Birgersson, M., Kristensson, O., Hökmark, H. (Clay Technology): Benchmark 2.1 ITT. Präsentation auf dem 5. Meeting der Task Force EBS in Weimar, 2007.
- /BÖR 84/ Börgesson L.: Water flow and swelling pressure in non-saturated bentonite based clay barriers. In: Clay Barriers for Isolation of Toxic Chemical Wastes, International Symposium, May 28–30, Stockholm. 1984.
- /DES 17/ Dessirier, B., Åkesson, M., Lanyon, B., Frampton, A., Jarsjö, J.: Reconstruction of the water content at an interface between compacted bentonite blocks and fractured crystalline bedrock. Applied Clay Science, Vol. 142, p. 145-152, 2017.
- /DIX 08/ Dixon, D., Guo, R.: Use of numerical simulations to aid in assessing field observations made during in-floor container emplacement simulations. Proceedings of the Workshop on “Long-term performance of smectitic clays embedding canisters with highly radioactive waste” held in Lund, 2007, Applied Clay Science (to be published), 2008.
- /DUE 04/ Dueck, A.: Hydro-mechanical properties of a water unsaturated sodium bentonite - Laboratory study and theoretical interpretation. Doctoral thesis, Department of Building and Environmental Technology, Lund University, Division of Soil Mechanics and Foundation Engineering, 2004.
- /DUE 07/ Dueck, A., Börgesson, L.: Model suggested for an important part of the hydro-mechanical behaviour of a water unsaturated bentonite. Engineering Geology 92, pp. 160–169, Elsevier, 2007. /FIN 95/ Finsterle, S. and Pruess, K.: Solving the estimation-identification problem in two-phase flow modeling. Water Resources Research, Vol. 31, NO. 4, pp. 913-924, 1995.

- /FRA 17/ Fransson Å, Åkesson M, Andersson L.: Bentonite Rock Interaction Experiment, Characterisation of rock and installation, hydration and dismantling of bentonite parcels. Report SKB R-14-11, Svensk Kärnbränslehantering AB, Solna, 2017.
- /HOK 06/ Hokr, M., Frydrych, D.: TH modelling BM 1.1. Präsentation auf dem 3. Meeting der Task Force EBS in Barcelona, 2006.
- /KAH 86/ Kahr, G., Kraehenbuehl, F., Müller-Vonmoos, M., Stoeckli, H. F.: Wasseraufnahme und Wasserbewegung in hochverdichtetem Bentonit. Nagra Technical Report NTB 86-14, 1986.
- /KRI 15/ Kristensson, O., Börgesson, L.: Canister Retrieval Test - Final report. Technical Report TR-14-19, Svensk Kärnbränslehantering AB, Stockholm, 2015.
- /KRÖ 04/ Kröhn, K.-P.: Modelling the re-saturation of bentonite in final repositories in crystalline rock. Final report, FKZ 02 E 9430 (BMWA), Gesellschaft für Anlagen- und Reaktorsicherheit (GRS) mbH, GRS-199, Köln, 2004.
- /KRÖ 05/ Kröhn, K.-P.: New Evidence for the Dominance of Vapour Diffusion During the Re-saturation of Compacted Bentonite. Engineering Geology, Volume 82, Issue 2, 2005.
- /KRÖ 08/ Kröhn, K.-P.: Simulating water uptake of compacted bentonite under non-isothermal conditions, decoupled from the mechanics and without feedback of hydraulics to heat transport. Proceedings of the Workshop on "Long-term performance of smectitic clays embedding canisters with highly radioactive waste" held in Lund, 2007, Applied Clay Science, Vol. 47, pp. 28-35, 2010; Online: <http://dx.doi.org/10.1016/j.clay.2008.06.004>, 2008; printed version: 2010.
- /KRÖ 11/ Kröhn, K.-P.: Code VIPER - Theory and Current Status. Status report, FKZ 02 E 10548 (BMW), Gesellschaft für Anlagen- und Reaktorsicherheit (GRS) mbH, GRS-269, Köln, 2011.

- /KRÖ 17/ Kröhn, K.-P.: Hydraulic Interaction of Engineered and Natural Barriers – Task 8b-8d,8f of SKB. Summary report, FKZ 02 E 10336, 02 E 10548, 02 E 10558, 02 E 11102, and 02 E 11213 (BMW), Gesellschaft für Anlagen- und Reaktorsicherheit (GRS) mbH, GRS-430, Köln, 2017.
- /KRÖ 18/ Kröhn, K.-P.: Re-saturation of compacted bentonite under repository-relevant flow conditions. FKZ 02 E 11102 (BMW). Geomechanics for Energy and the Environment, Elsevier, 2018. DOI:10.1016/j.gete.2018.09.003
- /NOS 18/ Noseck, U., Becker, D., Brasser, T., Buhmann, D., Fahrenholz, C., Flügge, J., Kröhn, K.-P., Meleshyn, A., Mönig, J., Moog, H., Rübél, A., Spießl, S., Wolf, J.: Scientific Basis for a Safety Case of Deep Geological Repositories. Final Report, FKZ 02E11102 (BMW), GRS-501, GRS Braunschweig, 2018.
- /PUS 01/ Pusch, R., Kasbohm, J.: Can the Water Content of Highly Compacted Bentonite be Increased by Applying a HighWater Pressure? SKB, Technical Report 01-33, 2001.
- /SAN 06/ Sánchez, M., Gens, A.: FEBEX Project. Final report on thermo-hydro-mechanical modelling. Technischer Bericht, 05-2/2006, ENRESA, 2006.
- /VID 17/ Vidstrand, P., Stigsson, M., Åkesson, M., Fransson, Å.: SKB Task Forces EBS and GWFTS. Modelling the interaction between engineered and natural barriers. A compilation of Task 8 descriptions. Report SKB P-16-05, Svensk Kärnbränslehantering AB, Solna, 2017.
- /VIL 05/ Villar, M.V., Martín, P.L., Barcala, J.M.: Infiltration test at isothermal conditions and under thermal gradient. Technical report CIEMAT/DMA/M2140/1/05, CIEMAT, Madrid, 2005.

Table of figures

Fig. 2.1	Flow situation after drilling a deposition hole.....	5
Fig. 2.2	Flow situation immediately after emplacement of canister and buffer	6
Fig. 2.3	Water reaching the buffer; a) moment of contact, b) shortly afterwards	8
Fig. 2.4	Water in a fully saturated granite under extremely low pressure	8
Fig. 2.5	Water re-distribution in the buffer at a limited water supply rate.....	9
Fig. 2.3	Principle of the three test set-ups.....	12
Fig. 2.4	Sketch of a test cell.....	13
Fig. 2.5	Granite porosities determined by sample and pore water weight.....	15
Fig. 2.6	Gas permeability as a function of the gas pressure.....	16
Fig. 2.7	Principle of the test via a rising water table	21
Fig. 2.8	Principle of re-saturation via rising water table.....	22
Fig. 2.9	Weighing arrangement for determination of the beginning of the test	23
Fig. 2.10	Whole test set-up (left) and close-up of the test cell and water bowl	24
Fig. 2.11	Marking of the bottom of the bentonite sample at the outside of the cell	25
Fig. 2.12	Principle of the final test configuration	27
Fig. 2.13	Final test configuration in the laboratory	28
Fig. 2.14	View of the cell from below after removing head end and sinter plate.....	28
Fig. 2.15	Visual inspection of water content distributions inside the sample	29
Fig. 2.16	Eventually used bronze sinter plate; total and close-up	30
Fig. 2.17	Water content distributions inside the sample using bronze sinter plates....	32
Fig. 2.18	Measured water content distributions varying the inflow rate	35
Fig. 2.19	Measured and calculated water content distributions varying the inflow rate.....	36
Fig. 2.20	Measured distributions of dry density varying the inflow rate	37
Fig. 2.21	Averaged distributions of dry density varying the inflow rate	37
Fig. 2.22	Measured water content varying running time of the tests at 0.02 ml/h.....	39
Fig. 2.23	Measured water content varying running time of the tests at 0.05 ml/h.....	40
Fig. 2.24	Measured and calculated water content distributions varying running time .	41
Fig. 2.25	Measured distributions of dry density varying the running time	42
Fig. 2.26	Averaged distributions of dry density varying the running time.....	42
Fig. 3.1	Sketch of the test cell.....	46
Fig. 3.2	Photo of the test cell without thermal insulation	47

Fig. 3.3	View from below the head peace	47
Fig. 3.4	Test cell with inner and outer thermal insulation	48
Fig. 3.5	Complete test set-up.....	48
Fig. 3.6	Pressing a bentonite disc out of a ring after cutting.....	49
Fig. 3.7	Temperatures from the short-term tests at specific locations	53
Fig. 3.8	Dynamics of the water content distribution with the original cell design.....	54
Fig. 3.9	Dynamics of the water content distribution; mean and deviations	55
Fig. 3.10	Mean water content distributions for running times of 1, 2 and 4 days	57
Fig. 3.11	Mean water content distributions for running times of 1 to 16 weeks	58
Fig. 3.12	(Mean) water content distributions for all running times	58
Fig. 3.13	Dynamics of the water content distribution with the strengthened cells.....	59
Fig. 3.14	Comparison of results with different cell types	60
Fig. 3.15	Mean water content of the whole samples at end of test.....	62
Fig. 3.16	Evolution of water uptake from the burette; run time < 15 d	63
Fig. 3.17	Evolution of water uptake from the burette, corrected; run time < 15 d	64
Fig. 3.18	Evolution of water uptake from the burette; run time < 125 d	65
Fig. 3.19	Evolution of water uptake from the burette, corrected; run time < 125 d	66
Fig. 3.20	Evolution of water uptake from the burette; run time < 1250 d	67
Fig. 3.21	Evolution of water uptake from the burette, corrected; run time < 1250 d....	68
Fig. 3.22	Cumulated water outflow from the burette at the end of test	69
Fig. 3.23	Cumulated water outflow from the burette at the end of test; all run times ..	69
Fig. 3.24	Dry density distribution of all tests.....	70
Fig. 3.25	Mean dry density distribution	71
Fig. B.2	Water content evolution at uptake of water vapour; from /KRO 04/	94
Fig. B.3	Dry density evolution at uptake of liquid water; from /KRO 04/.....	95
Fig. B.4	Dry density evolution at uptake of water vapour; from /KRO 04/	95
Fig. B.5	Degree of saturation at the inflow boundary after inflow of Äspö-solution ...	97
Fig. B.6	Degree of saturation at the inflow boundary after inflow of vapour.....	98

List of tables

Tab. 2.1	Volume and bulk dry density of the seven granite discs.....	12
Tab. 2.2	porosity: measured, maximum, minimum, mean and deviations	12
Tab. 2.3	Composition of synthetic Äspö-solution (e.g. /KRÖ 04/).....	17
Tab. 2.4	Mean degree of saturation in the granite discs after 5 weeks.....	18
Tab. 2.5	Data for determination of the initial water content	33
Tab. 2.6	Test specific input data	34
Tab. 2.7	Input data valid for all numerical models	34
Tab. 3.1	Characteristic values for the Experiment.....	50
Tab. 3.2	Characteristic values after removal of tests {1 D a}, {1 D c}, and {2 D a}.....	51
Tab. 3.3	Test labels, cell design, and running times	52
Tab. 3.4	Vertical shift applied to the original inflow data.....	63
Tab. 3.5	Evaluation of eq. (3.4) for all tests.....	73

A Appendix: Analysis of data

A.1 Measured data

All directly measured data can be classed as one of the following four groups:

- sample characteristics
 - d sample diameter [cm]
 - h sample height [cm]
 - M_0 initial mass of the sample [g]
- water uptake of the sample
 - m_B mass of the weighing pan [g]
 - m_{Be} mass of pan and saturated material (one disc) [g]
 - m_{Bd} mass of pan and dried material (one disc) [g]
- measured inflow
 - V_{wi} volume of in flown water [cm³]
 - V_{wp} water taken up by filter paper [cm³]
 - V_{wf} water taken up by the frit [cm³]
- Temperature distribution
 - T temperature [C°]

Some quantities are given as a function of a spatial coordinate, like the water content of a single sample distribution; some – like inflow - are given as a function of time. And the dynamics of the water content distribution or the temperature distribution depend on time as well as on space.

A.2 Derived data

Dry sample

(A.1)

$$m_d = m_{Bd} - m_B$$

m_d - mass of a dry disc [g]

$$M_d = \sum_{i=1}^n m_{d_i} + \Delta m \quad (\text{A.2})$$

M_d - total mass of the dry sample [g]¹³

Δm - mass loss due to cutting [g]

n - number of discs [-]

$$V = \frac{1}{4} \pi d^2 h \quad (\text{A.3})$$

V - volume of the dry sample [cm³]

$$\rho_d = \frac{M_d}{V} \quad (\text{A.4})$$

ρ_d - dry density of the sample [g/cm³]

$$\Phi_d = 1 - \frac{\rho_d}{\rho_s} \quad (\text{A.5})$$

Φ_d - porosity of the dry sample [g/cm³]

ρ_s - grain density; $\rho_s = 2,78$ [g/cm³]

$$V_d = \Phi_d \cdot V \quad (\text{A.6})$$

V_d - pore volume of the dry sample [g/cm³]

State at end of test

$$m_e = m_{Be} - m_B \quad (\text{A.7})$$

m_e - mass of a disc at the end of test [g]

$$M_e = \sum_{i=1}^n m_{e_i} + \Delta m \quad (\text{A.8})$$

M_e - total mass of the sample at the end of test [g]

¹³ The mass of a single disc should be correct save for weighing errors. However, there is an additional error summing up the mass values to get the total sample mass because of the little loss of material during cutting off the discs. This error may amount to about 1 g or approximately 0.35 % of the initial sample mass. This loss has not been measured in all tests. In these cases, the loss was estimated to reduce this error.

$$m_{we} = m_{Be} - m_B \quad (\text{A.9})$$

m_{we} - mass of water in a disc at the end of test [g]

$$M_{we} = \sum_{i=1}^n m_{we_i} \quad (\text{A.10})$$

M_{we} - total mass of water at the end of test [g]

$$w_e = \frac{m_{we}}{m_d} \quad (\text{A.11})$$

w_e - water content of a disc at the end of test [-]

Initial state

$$M_{w0} = M_0 - M_d \quad (\text{A.12})$$

M_{w0} - initial mass of water in the sample [g]

$$w_0 = \frac{M_{w0}}{M_0} \quad (\text{A.13})$$

w_0 - initial water content in a disc¹⁴ [-]

$$\Phi_0 = \Phi_d - \frac{\rho_d}{\rho_h} \cdot w_0 \quad (\text{A.14})$$

Φ_0 - initial porosity of the sample [g/cm³]

ρ_h - density of the hydrated water; $\rho_h = 1,0$ [g/cm³] (assumed)

$$V_0 = \Phi_0 \cdot V \quad (\text{A.15})$$

V_0 - initial volume of the pore space [g/cm³]

$$\rho_0 = \frac{M_0}{V} \quad (\text{A.16})$$

ρ_0 - initial density of the sample [g/cm³]

¹⁴ The water content is assumed to be equally distributed over the sample.

Theoretical maximum water uptake

$$V_{ws} = V_{wi} - V_{wp} - V_{wf} \quad (\text{A.17})$$

V_{ws} - additional water in the sample at the end of test [g]

$$V_{wh} = V_{ws} \cdot \frac{\rho_w}{\rho_h} \quad (\text{A.18})$$

V_{wh} - volume of the hydrated water [g]

ρ_w - density of free water; $\rho_w = 1,0$ [g/cm³]

$$V_{w\max 0} = V_0 \cdot \frac{\rho_h}{\rho_w} \quad (\text{A.19})$$

$V_{w\max 0}$ - water uptake capacity at begin of test (initial state) [cm³]

$$V_{w\max d} = V_0 \cdot \frac{\rho_h}{\rho_w} \quad (\text{A.20})$$

$V_{w\max d}$ - water uptake capacity at dry-state [cm³]

$$w_{\max} = \frac{\rho_h}{\rho_d} - \frac{\rho_h}{\rho_s} \quad (\text{A.21})$$

w_{\max} - maximum water content [-]

$$m_{w\max} = V_d \cdot \rho_h \quad (\text{A.22})$$

$m_{w\max}$ - maximum mass of water [g]

A.3 Compilation of derived data

- dry sample
 - M_d total mass of the dry sample
 - V volume of the dry sample
 - ρ_d dry density of the sample
 - Φ_d porosity of the dry sample
 - V_d pore volume of the dry sample
- sample at begin of test (initial state)
 - M_{w0} initial mass of water in the sample
 - w_0 initial water content
 - V_0 initial volume of the pore space
 - $m_{w\max}$ maximum mass of water
- sample at end of test
 - M_e total mass of the sample at the end of test
 - M_{we} total mass of water at the end of test
 - $w(x)$ water content distribution at the end of test
 - $\rho_d(x)$ dry density distribution at the end of test
 - $\Phi_d(x)$ porosity distribution at the end of test

B Appendix: Revisiting data from earlier uptake experiments

B.1 Final porosity

The final porosity at steady-state after re-saturation is a parameter that is hard to come by, experimentally as well as theoretically. It is nevertheless of importance in the framework of the extended vapour diffusion (EVD) model where it denotes an air-filled porosity at the end of re-saturation (water transport is assumed to essentially take place via water vapour). In the EVD-approach the final porosity thus controls the final water content. In the past this parameter has been treated like a fudge factor in the range between 2 and 10 %. However, revisiting data based on water uptake experiments with MX-80 bentonite where one experiment was performed with liquid water and one with vapour saturated air under otherwise same conditions /KRÖ 04/ can help here.

The measured evolution of the water content is depicted in Fig. B.1 and Fig. B.2 for uptake via water and uptake via vapour, respectively. Both experiments have been running for about half a year and they show interesting similarities as well as differences. Both show after a few days basically the same penetration depth and at the end a similar water content gradient.

The most obvious difference is a peak in water content right at the inflow boundary that has been found for liquid water but not for water vapour. Next to this peak the absolute value of the water content reaches locally a steady-state value of 29 % within 2 weeks at inflow of liquid water while it takes about 2 months until a much lower water content of about 22 % is reached using water vapour (see also Fig. B.5 and Fig. B.6).

Related to the initial dry density of 1500 kg/m^3 in both experiments is a maximum water content of 30.7 %. In case of uptake of liquid water, next to the peak where a steady-state value of 29 % had been found, the dry density was on the average a bit elevated above the initial value to about 1515 kg/m^3 as observable in Fig. B.3. In case of uptake from vapour, the dry density at the inflow boundary was by contrast a little decreased to about 1490 kg/m^3 (see Fig. B.4). From these data an estimate of the final porosity can be derived. For uptake of liquid water this translates into a final porosity value of 1.6 % and for the uptake from water vapour into 13.6 %. However, these values are related to the

specific cases discussed above. Transfer of these numbers to other dry densities or types of bentonite should thus be considered with appropriate care.

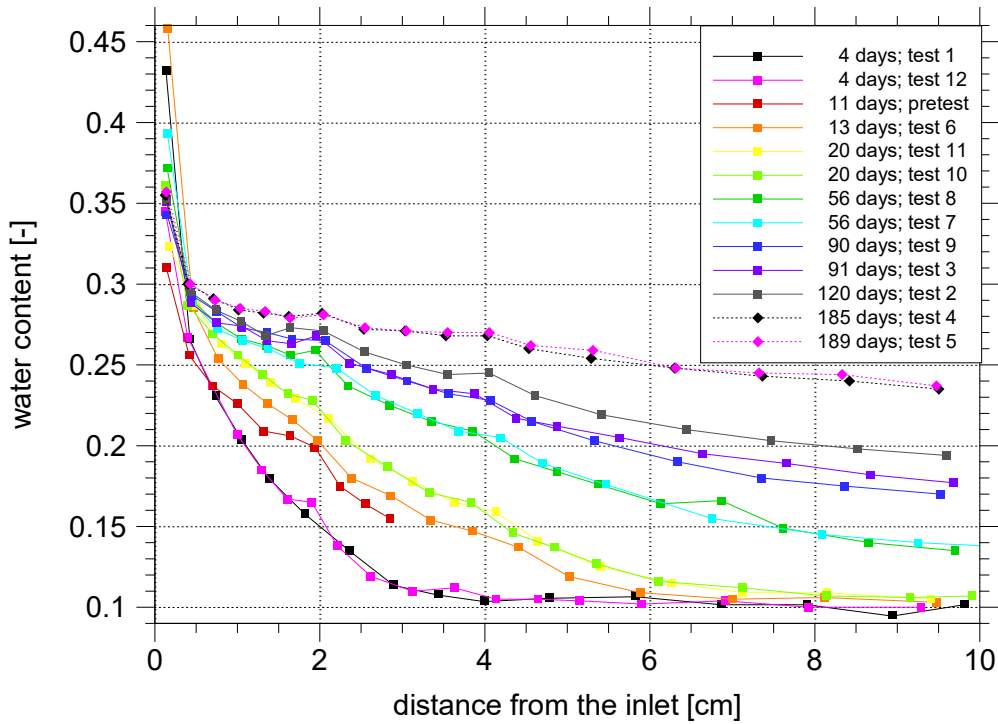


Fig. B.1 Water content evolution at uptake of liquid water; from /KRO 04/

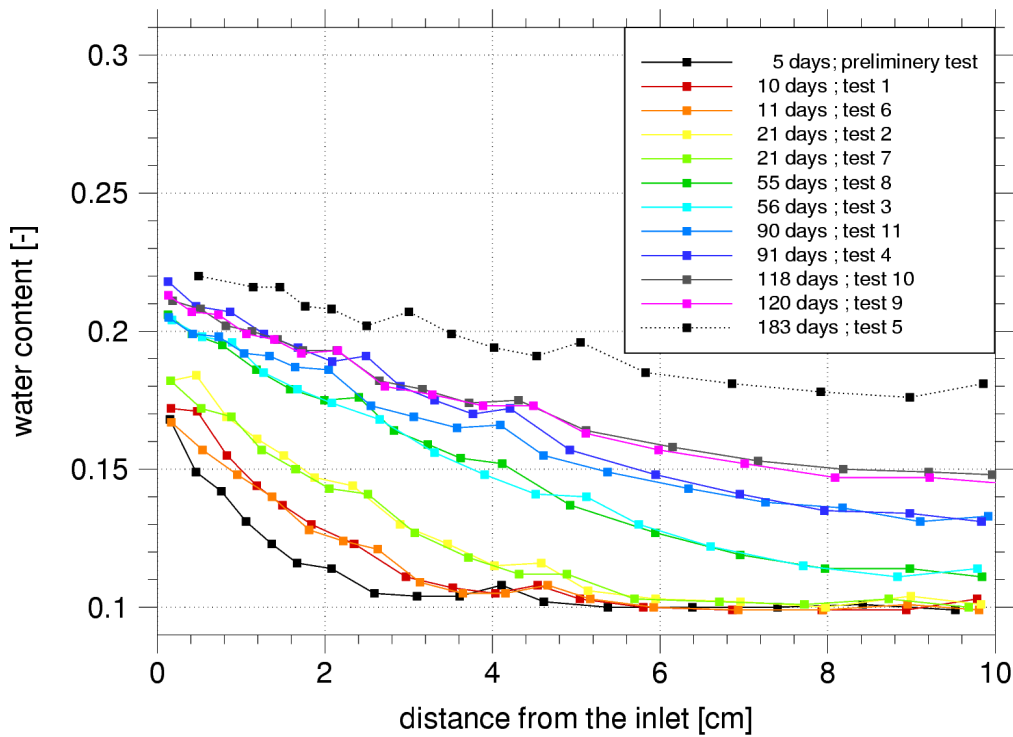


Fig. B.2 Water content evolution at uptake of water vapour; from /KRO 04/

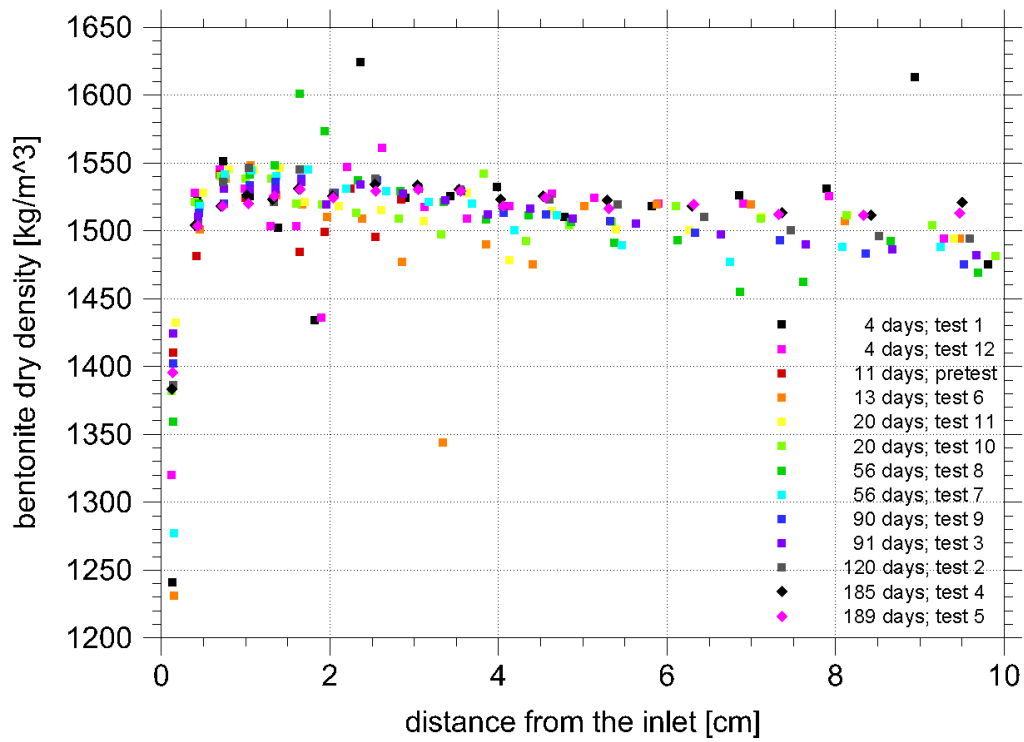


Fig. B.3 Dry density evolution at uptake of liquid water; from /KRO 04/

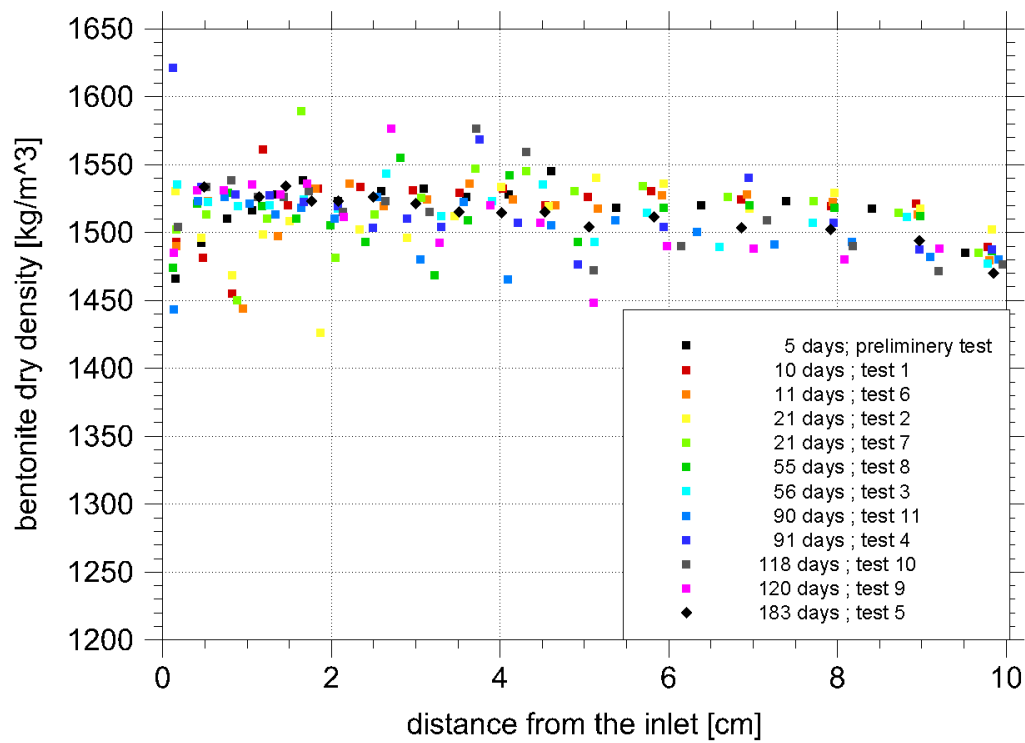


Fig. B.4 Dry density evolution at uptake of water vapour; from /KRO 04/

In the uptake experiment with restricted access to liquid water, the final porosity cannot be as clearly defined as in the previously discussed cases. The data presented in section 2.5.6 indicate the forming of a fully saturated zone as in water uptake under UA-conditions (see next subsection). But in the present tests this process takes much more time and as long as the nature of this zone is not fully understood, some differences in the properties of this zone cannot be excluded. Moreover, switching from LWSR- to UA-conditions in the present version of the code VIPER simply does not take the fully saturated zone into account. Thereby, the shift of the inflow boundary from the actual inlet under LWSR-conditions to the point at the inner end of the highly saturated zone under UA-conditions is ignored.

There is a principal difference between the present uptake experiment and the two earlier experiments as well as a difference in the dry density. Direct transfer of the final porosity derived from the earlier experiments to the present experiment thus appears to be questionable. Instead, the final porosity for the numerical model was fitted to the results. Starting point had been the final porosity derived from uptake with vapour since it had been expected that water re-distribution under LWSR-conditions would not allow for a stable zone containing free liquid water. It turned out, though, that a much better fit could be gained by reducing the final porosity to 9 %. This value was then chosen for modeling.

B.2 Degree of saturation in the narrow zone of peak water content

The effect of a narrow highly saturated zone at the bentonite-water contact is clearly visible in Fig. B.1. Since such a zone had not been expected when designing the experiment, it was only interpreted as such in hindsight. A better spatial resolution as well as more focus on the early dynamics would have been foreseen otherwise.

Combining the data for water content and for dry density, the degree of saturation can be derived for each data point. This is of particular interest in the vicinity of the inflow boundary in order to assess the state of re-saturation. The degree of saturation is depicted in Fig. B.5 and Fig. B.6 for uptake of water and vapour, respectively, focussing on the domain next to the inflow boundary.

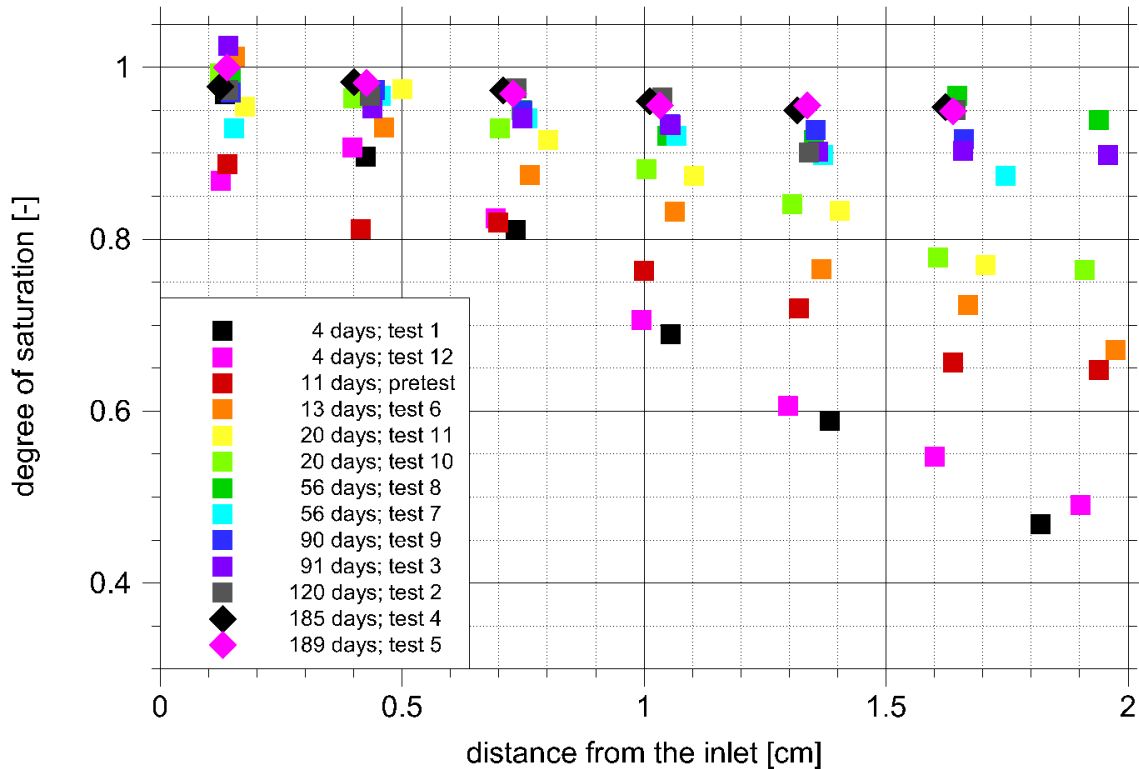


Fig. B.5 Degree of saturation at the inflow boundary after inflow of Äspö-solution

The saturation data for the first discs at the inflow boundary plotted in Fig. B.5 are actually scattered around a value of 1, thereby indicating full saturation. By contrast, the saturation in the second discs from the inlet is clearly just close to 1, despite the fact that steady-state had been reached here after 14 days. It thus appears that the zone in the range of the first disc had indeed been fully saturated while a residual air-filled porosity remains in the rest of the bentonite sample.

In case of water uptake via vapour the situation is quite different. In the first disc next to the inlet, the degree of saturation apparently increases over the first two months of the experiment. Later data points basically scatter around a value of 65 %. In the next disc this value is slightly higher amounting to about 70 %. The final saturation in case of water uptake via vapour is thus significantly lower than in case of uptake via liquid water.

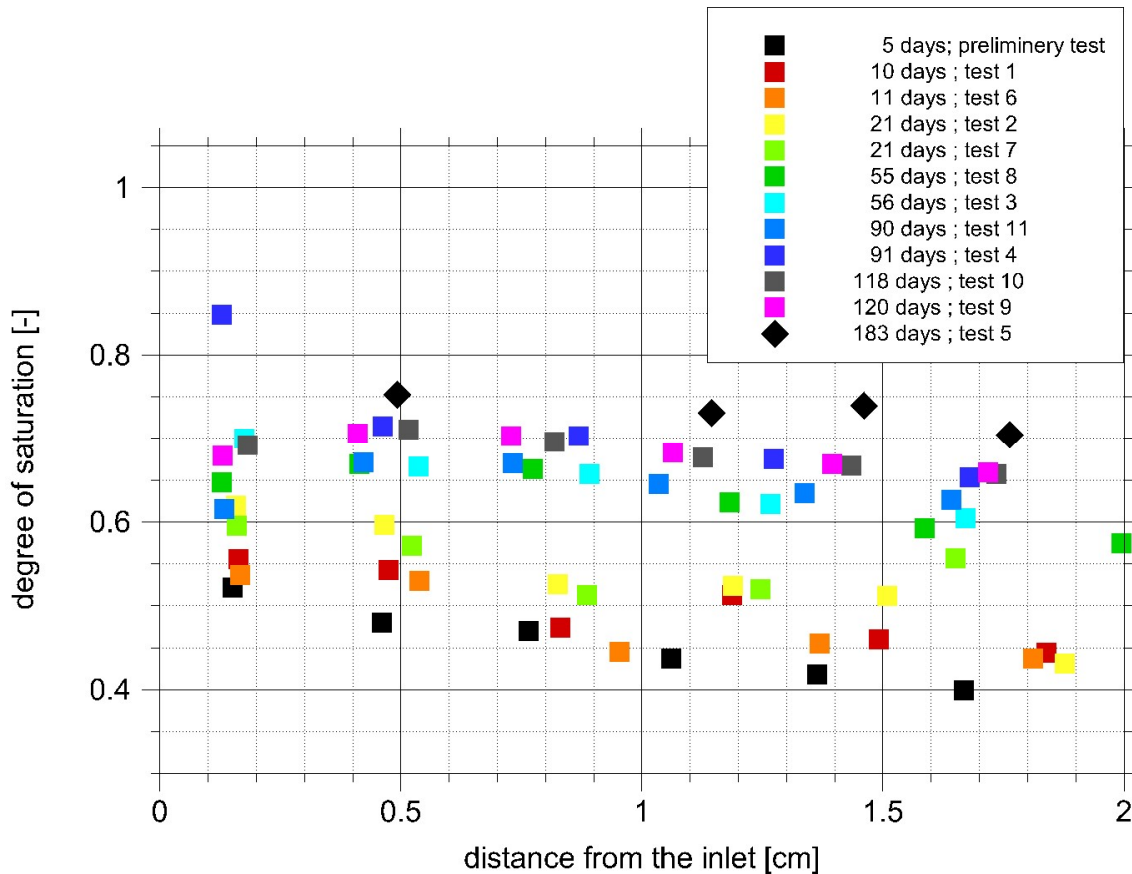


Fig. B.6 Degree of saturation at the inflow boundary after inflow of vapour

Several conclusions can be drawn from this observation:

- Despite the assumptions underlying the early vapour diffusion models (eg. /KRÖ 05/ and /KRÖ 08/) the uptake of water does not involve vapour diffusion alone but also another diffusive process. However, the same conclusion had already been drawn when certain shortcomings in explaining results from the ITT-experiment at the URL in Canada had been encountered. Accordingly, the diffusion of interlamellar water was identified as likely candidate for the missing process, included in the re-saturation code VIPER, and confirmed by improving the model results considerably /KRÖ 11/. A detailed discussion of the process dynamics at a microscopic level close to full water saturation is still pending.
- The final water content at the bentonite-water contact depends on the state of the source, liquid or gaseous, and is lying at about 1 to 2 % below theoretical maximum water content in case of water and at 8 to 9 % below in case of vapour. However,

these values are related to the case discussed above. Transfer of these numbers to other dry densities or types of bentonite should thus be considered with appropriate care.

- Further investigations about the re-saturation state at advanced stages of re-saturation including the narrow fully saturated zone at the bentonite-water contact appear to be advisable.

**Gesellschaft für Anlagen-
und Reaktorsicherheit
(GRS) gGmbH**

Schwertnergasse 1
50667 Köln
Telefon +49 221 2068-0
Telefax +49 221 2068-888

Forschungszentrum
Boltzmannstraße 14
85748 Garching b. München
Telefon +49 89 32004-0
Telefax +49 89 32004-300

Kurfürstendamm 200
10719 Berlin
Telefon +49 30 88589-0
Telefax +49 30 88589-111

Theodor-Heuss-Straße 4
38122 Braunschweig
Telefon +49 531 8012-0
Telefax +49 531 8012-200

www.grs.de